

UNCLASSIFIED

AD NUMBER
AD808787
NEW LIMITATION CHANGE
TO Approved for public release, distribution unlimited
FROM Distribution authorized to U.S. Gov't. agencies and their contractors; Administrative/Operational Use; NOV 1966. Other requests shall be referred to Air Force Flight Dynamics Lab., AFSC, Wright-Patterson AFB, OH 45433.
AUTHORITY
AFFDL ltr, 25 Jun 1971

THIS PAGE IS UNCLASSIFIED

**THE CYCLIC STATE OF MATERIALS
AND THE RELATIONSHIP TO
MECHANICAL PROPERTIES AND FATIGUE**

DEWEY G. YOUNGER

*AERONUTRONIC DIVISION OF PHILCO CORPORATION
FORD MOTOR COMPANY*

TECHNICAL REPORT AFFDL-TR-66-125

NOVEMBER 1966

This document is subject to special export controls and each transmittal to foreign governments or foreign nationals may be made only with prior approval of AFFDL (FDTR), Wright-Patterson Air Force Base, Ohio 45433.

**AIR FORCE FLIGHT DYNAMICS LABORATORY
RESEARCH AND TECHNOLOGY DIVISION
AIR FORCE SYSTEMS COMMAND
WRIGHT-PATTERSON AIR FORCE BASE, OHIO**

20071217481

AD-808787

NOTICES

When Government drawings, specifications, or other data are used for any purpose other than in connection with a definitely related Government procurement operation, the United States Government thereby incurs no responsibility nor any obligation whatsoever; and the fact that the Government may have formulated, furnished, or in any way supplied the said drawings, specifications, or other data, is not to be regarded by implication or otherwise as in any manner licensing the holder or any other person or corporation, or conveying any rights or permission to manufacture, use, or sell any patented invention that may in any way be related thereto.

Copies of this report should not be returned to the Research and Technology Division unless return is required by security considerations, contractual obligations, or notice on a specific document.

**THE CYCLIC STATE OF MATERIALS
AND THE RELATIONSHIP TO
MECHANICAL PROPERTIES AND FATIGUE**

DEWEY G. YOUNGER

This document is subject to special export controls and each transmittal to foreign governments or foreign nationals may be made only with prior approval of AFFDL (FDTR), Wright-Patterson Air Force Base, Ohio 45433.

FOREWORD

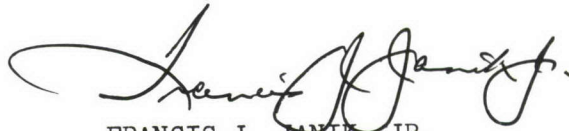
This report was prepared by the Advanced Structures Development Department, Aeronutronic Division of Philco Corporation, Ford Road, Newport Beach, California 92663 under United States Air Force Contract No. AF 33(615)-2539, Task 146704 of Project 1467. The work was administered under the direction of the Theoretical Mechanics Branch, Structures Division, Air Force Flight Dynamics Laboratory, Research and Technology Division. Mr. Vincent E. Kearney was the Task Engineer for the Laboratory.

Mr. D. G. Younger of the Aeronutronic Division was responsible for both the experimental and theoretical aspects of the work performed. The contributions of the following personnel are gratefully acknowledged: Dr. H. M. Berkowitz for the "Relationship Between Diametral and Axial Strains" appearing in the Appendix, Messrs. L. E. Marler and R. L. Rahe for assistance in conducting tests, and Mr. G. Santantonio for preparation of specimens. The author, further, gratefully acknowledges the efforts of Mrs. M. A. Anderson for typing and assembling this report.

The Aeronutronic Division of Philco Corporation has assigned Publication No. U-3670 to this report.

This report covers work performed during the period 15 April 1965 to 15 August 1966. This manuscript was released by the author August 1966 for publication as an RTD Technical Report.

Publication of this report does not constitute Air Force approval of the report's findings or conclusions. It is published only for the exchange and stimulation of ideas.



FRANCIS J. JANIK, JR.

Chief, Theoretical Mechanics Branch
Structures Division

ABSTRACT

This report contains the results of an experimental and theoretical study relating to the stabilized cyclic state of materials. The objectives accomplished in the program were (a) the experimental verification of the important role played by the cyclic state in fatigue. (b) The correlation of virgin material properties with the cyclic stress-strain curve for four materials (2024-0 and 2024-T351 aluminum alloy plus annealed and hard OFHC copper), and (c) the application of the cyclic stress-strain curve to fatigue analysis. Both constant load-range and constant strain-range fatigue tests up to fatigue-lives of 10^4 cycles were performed under axial loading conditions at speeds of 3 to 15 cycles/minute. Specimens were of circular cross-section with a one-inch gage length and longitudinal strain measurements were made with a dual-range mechanical extensometer. Power-law relationships were developed from the elastic and plastic components of stabilized strains, and these were related to true fracture stress, fracture ductility, and failure strain. Both cyclic stress-strain envelope curves and cyclic stress-strain curves were developed and employed in fatigue analyses to predict the effect of mean stresses on the fatigue life. A brief series of dual-level cumulative fatigue tests were performed in the low-life fatigue region and the validity of the Palmgren-Miner rule was questioned.

TABLE OF CONTENTS

SECTION		PAGE
I	INTRODUCTION	1
II	MATERIAL AND SPECIMEN DETAILS	3
	2.1 Materials	3
	2.2 Specimen Details	4
III	TEST EQUIPMENT AND PROCEDURE	7
	3.1 Testing Machine	7
	3.2 Strain Instrumentation	7
	3.3 Temperature-Rise Instrumentation	11
IV	EXPERIMENTAL RESULTS AND RELATED DISCUSSIONS	12
	4.1 Static Test Results	12
	4.2 Test Results During Cycles of Constant Load Range	20
	4.3 Test Results During Cycles of Constant Strain Range	38
V	CORRELATION OF PHENOMENOLOGICAL BEHAVIOR	58
	5.1 Fundamental Relationships	58
	5.2 Fatigue Life Correlations	62
VI	CYCLIC STATE RELATIONSHIPS	
	6.1 Microscopic and Macroscopic Viewpoints and a Hypothesis	79
	6.2 Hysteresis Components and the Envelope Curve	82
	6.3 Cyclic Stress-Strain Curve or Locus Curve	85
VII	PREDICTION OF MEAN STRESS EFFECT FROM CYCLIC STRESS-STRAIN CURVE	89
	7.1 Mean Value Effects at Short-Life	89
	7.2 Mean Value Effects at Long-Life	90
VIII	EFFECTS OF VARIABLE AMPLITUDE STRAINING	102
	8.1 Response to Dual Level Strain Amplitudes	102
	8.2 Cumulative Fatigue Damage During Multi-Level Loadings	108

TABLE OF CONTENTS (Continued)

SECTION	PAGE
IX CONCLUSIONS	110
9.1 Experimental Procedures	110
9.2 Phenomenological Observations	110
9.3 Data Correlations and Fundamental Relationships .	112
REFERENCES	114
APPENDIX	
A RELATIONSHIP BETWEEN DIAMETRAL AND AXIAL STRAINS . . .	118
B PROCEDURE FOR USING THE CYCLIC STRESS-STRAIN CURVE TO ESTABLISH THE EFFECT OF STRESS RATIO IN LONG- LIFE FATIGUE	126

LIST OF ILLUSTRATIONS

FIGURE		PAGE
1	Test Specimen for Static and Cyclic Axial Loads	5
2	Testing Machine and Experimental Setup	8
3	Dual-Range Mechanical Extensometer Mounted for Test . . .	10
4	Standard Stress-Strain Curves for Test Materials	13
5	Poisson's Ratio Variations During Tensile Test of Aluminum and Copper Materials	15
6	True Stress-True Strain Relationships for 2024-T351 and 2024-0 Aluminum Alloy	17
7	True Stress-True Strain Relationships for Soft and Hard Copper	18
8A	Reproduced Recording of Hysteresis and Cyclic Creep Typical of 2024-0 Aluminum Alloy During Constant Load- Range Tests	22
8B	Recording of Hysteresis and Cyclic Creep Typical of 2024-T351 Aluminum Alloy During Constant Load-Range Testing	23
9	Cyclic Creep of 2024-0 During Cycles of Constant Load Range	24
10	Strain Limit Variations for 2024-0 During Cycles of Constant Load Range ($R_p = -1$)	25
11	Strain Limit Variations for 2024-T351 During Cycles of Constant Load Range ($R_p = -1$)	27
12	Strain Limit Variations for 2024-T351 During Cycles of Constant Load Range ($R_p = 0$)	28
13	Strain Limit Variations for 2024-T351 During Cycles of Constant Load Range ($R_p = -1$)	29
14	Typical Recording During Cyclic Loading of Hard Copper .	31
15	Strain Variations for Hard Copper During Cycles of Constant Load Range ($R_p = -1.0$ AND -0.82)	32

LIST OF ILLUSTRATIONS (Continued)

FIGURE		PAGE
16	Strain Variations for Hard Copper During Cycles of Constant Load Range ($R_p = 0.0$)	33
17	Strain Variations for Hard Copper During Cycles of Constant Load Range ($R_p = +0.4$)	34
18	Strain Variations for Soft Copper During Cycles of Constant Load Range ($R_p \approx -0.8$)	35
19	Strain Variations for Soft Copper During Cycles of Constant Load Range ($R_p = 0.0$)	36
20	Strain Variations for Soft Copper During Cycles of Constant Load Range ($R_p = 0.4$)	37
21	Drum-Recordings of Stress (Load) Variations During Cycles of Constant Strain Range	41
22	Stress Limit Variations for 2024-0 During Cycles of Constant Strain Range ($R_{\epsilon} \approx -1$)	42
23	Stress Limit Variations for 2024-0 During Cycles of Constant Strain Range ($R_{\epsilon} \approx 0$)	43
24	Stress Limit Variations for 2024-0 During Cycles of Constant Strain Range ($R_{\epsilon} > 0$)	44
25	Stress Limit Variations for 2024-T351 During Cycles of Constant Strain Range ($R_{\epsilon} \approx -1$)	45
26	Stress Limit Variations for 2024-T351 During Cycles of Constant Strain Range ($R_{\epsilon} \approx 0$)	46
27	Stress Limit Variations for 2024-T351 During Cycles of Constant Strain Range ($R_{\epsilon} > 0$)	47
28	Drum-Recordings Showing Stress (Load) Variations for Hard and Soft Copper During Cycles of Constant Strain Range	48
29	Stress Limit Variations for Annealed Copper During Cycles of Constant Strain Range ($R_{\epsilon} \approx -1$)	50

LIST OF ILLUSTRATIONS (Continued)

FIGURE		PAGE
30	Stress Limit Variations for Annealed Copper During Cycles of Constant Strain Range ($R_{\epsilon} \approx 0$)	51
31	Stress Limit Variations for Annealed Copper During Cycles of Constant Strain Range ($R_{\epsilon} > 0$)	52
32A	Stress Limit Variations for Hard Copper During Cycles of Constant Strain Range ($-1 < R_{\epsilon} < 0$)	53
32B	Stress Limit Variations for Hard Copper During Cycles of Constant Strain Range ($-1 < R_{\epsilon} < 0$)	54
33	Stress Limit Variations for Hard Copper During Cycles of Constant Strain Range ($R_{\epsilon} \approx 0$)	55
34	Stress Limit Variations for Hard Copper During Cycles of Constant Strain Range ($R_{\epsilon} \gg 0$)	56
35	Definition of Cyclic Stress and Strain Components for Stable Hysteresis Conditions	63
36	Relationship Between Strain Range Components and Fatigue Life (2024-0 Aluminum Alloy)	64
37	Relationship Between Total Strain Range and Fatigue Life (2024-0 Aluminum Alloy)	65
38	Relationship Between Strain Range Components and Fatigue Life (2024-T351 Aluminum Alloy)	68
39	Relationship Between Total Strain Range and Fatigue Life (2024-T351 Aluminum Alloy)	69
40	Relationship Between Strain Range Components and Fatigue Life (Annealed OFHC Copper)	71
41	Relationship Between Total Strain Range and Fatigue Life (Annealed OFHC Copper)	72
42	Relationship Between Strain Range Components and Fatigue Life (Hard OFHC Copper)	74
43	Relationship Between Strain Range and Fatigue Life (Hard OFHC Copper)	75

LIST OF ILLUSTRATIONS (Continued)

FIGURE		PAGE
44	Macro-Micro Fatigue Analog	81
45	Power-Law Relationships Between Strain Components of the Cyclic State and Fatigue Life	83
46	Cyclic Stress-Strain Envelope and Locus Curves	84
47	Comparison Between Hypothesized Cyclic State Using Long- Life Fatigue Data and the Theoretical Cyclic State	86
48	The Relationship Between the Envelope Curve and the Cyclic Stress-Strain Curve.	88
49	The Cyclic Stress-Strain Curve and Related Strains	92
50	Fatigue Curves for 2024-T3 Aluminum Alloy	95
51	Fatigue Curves for Normalized SAE 4130 Steel	97
52	Components of Total Strain Range During Fatigue of Hard AISI 4130 Steel	98
53	Fatigue Curves for SAE 4340 Steel	99
54	Components of Total Strain Range During Fatigue of Hard AISI 4340 Steel	100
55	Normalized Cyclic Stress-Strain Curves	101
56	Stress Limit Variations for Annealed Copper During Cycles of Low-High Magnitudes of Constant Strain Range ($R_{\epsilon} \approx 0$)	103
57	Stress Limit Variations for Annealed Copper During Cycles of High-Low Magnitudes of Constant Strain Range ($R_{\epsilon} \approx 0$)	105
58	Stress Limit Variations for Hard Copper During Cycles of Low-High Magnitudes of Constant Strain Range ($R_{\epsilon} \approx 0$)	107

SYMBOLS

- A = material constant related to strain at tensile fracture
- A_f = area at final fracture in tensile test
- A_o = original area of tensile specimen
- A_T = true or instantaneous cross-sectional area
- a = radius of the cross-section at the neck
- C = column end-fixity coefficient (Euler's column equation)
- C_1 = material constant related to strain at tensile fracture
- C_2 = material constant related to true fracture stress
- D_f = fracture ductility, $\ln (A_o/A_f)$, from tensile test
- D_o = original diameter
- D_T = true or instantaneous diameter
- E = modulus of elasticity, tension or compression
- E_{tan} = tangent modulus
- F = flow stress at surface
- $(F)_f$ = flow stress at fracture in tensile test
- k = exponent of Manson-Coffin equation
- m = exponent of elastic term in Manson equation
- N = number of applied cycles
- N_B = number of cycles to buckling failure
- N_f = number of cycles at failure in fatigue
- N_{fi} = number of cycles that will cause eventual failure at the i -th level in a multilevel fatigue test
- n = exponent equal to $-k$
- n_i = number of cycles applied at the i -th level in a multilevel fatigue test
- P = load
- P_{max} = maximum load (corresponding to ultimate strength)
- p = exponent in mean-stress equation
- q = exponent in mean-stress equation
- R = profile or surface radius; also, stress or strain ratio
- R_B = Rockwell "B" hardness reading
- R_F = Rockwell "F" hardness reading
- R_p = load ratio

SYMBOLS (Continued)

- R_{ϵ} = strain ratio
- R_{σ} = stress ratio
- γ = damage index; also exponent of the order of $1/n$
- ϵ = conventional engineering strain
- ϵ_f = conventional engineering strain at fracture in tensile test
- ϵ_{ln} = true strain (natural strain)
- ϵ_{max} = maximum strain in cycle
- ϵ_{min} = minimum strain in cycle
- ϵ_o = mean engineering strain
- ϵ_{Tot} = total of strain (limiting strain); total cyclic strain, $\Delta\epsilon$, plus cyclical permanent set, ϵ_U
- $\Delta\epsilon$ = range of total cyclic strain
- $\Delta\epsilon_e$ = range of cyclic elastic strain
- $\Delta\epsilon_{end}$ = range of strain at endurance limit ($R_{\epsilon} = -1$)
- $\Delta\epsilon_p$ = range of cyclic plastic strain
- σ = nominal stress (based on original area)
- σ_a = amplitude of alternating stress
- σ_c = peak compression stress
- σ_{cy} = yield strength in compression
- σ_e = endurance limit stress (single amplitude at $R_{\sigma} = -1$)
- σ_f = true fracture stress in tensile test
- σ_m = mean stress
- σ_{max} = maximum stress in cycle
- σ_{min} = minimum stress in cycle
- σ_T = true stress or average true stress
- σ_{ty} = yield strength in tension
- σ_U = unidirectional strain or cyclical permanent set
- σ_{ult} = ultimate tensile strength
- σ_z = axial stress (longitudinal axis)
- $\Delta\sigma$ = range of cyclic stress (nominal)
- $\Delta\sigma_T$ = range of cyclic true stress
- μ = Poisson's ratio

SECTION I

INTRODUCTION

Experimental evidence supports the view that two different types of microscopic deformation occur in fatigue depending on which of the two extremes of the life range is involved. A static-like (coarse-slip) deformation is known to predominate at low life (high stress) and a pure fatigue (fine slip) deformation is found at long life (low stress); therefore, within the present state of the art, it has been considered rather doubtful that both deformation types could be explained by a single theory.

A number of very refined attempts have been made by other investigators to develop theories (or empirical equations) that are valid over the complete fatigue range, but each of these has met with only limited success. By far the majority of theories on fatigue failure are very limited in their range of validity in that they are generally based on very limited failure information and/or virgin material properties. Furthermore, the simple theories give little or no insight as to the basic processes that cumulate to produce failure and, as such, they offer little more than "curve-fitting" correlations with questionable utility in predicting failure under realistic cyclic load spectrums of varying magnitude, mean values, etc.

As displayed by the more refined theories, fatigue damage should be described in the fundamental terms of dislocations, slip mechanisms, crack initiation, crack propagation, and final failure. Studies of these fundamentals are currently progressing; but, it is not clear that these individual studies will yield, in the near future, a simple model upon which to base a theory of fatigue failure.

Nevertheless, recently a very promising new avenue for studies in fatigue has been brought into focus. Attention was directed by the author, (Reference 1) in 1958, to the stabilized cyclic state of materials, and it was suggested at that time that the resulting cyclic stress-strain relationships offered a basic tool for fatigue analysis. More recently, additional evidence has supported these views. The cyclic stress-strain relationship is now known to be virtually independent of pre-test conditions as well as independent of loading parameters known to be critical in fatigue (i.e., load cycles, strain cycles, range, and mean values). This, of course, implies that such a cyclic state or relationship is apparently independent of damage, and may well establish an important base-line from which fatigue damage can be assessed.

The potential that the stabilized state in materials offers to an understanding of fatigue has been considered very great; therefore, a comprehensive

experimental and analytical study of the cyclic state at the phenomenological level has been undertaken in the present program. During the course of the study, however, wherever pertinent, observations from other investigations at both the macroscopic and microscopic levels have been introduced to support the arguments of the present author. Particular emphasis is placed on the power-law relationships which are now being widely used in fatigue correlations. From these relationships the cyclic stress-strain curve can be easily generated and then employed in fatigue analyses.

The cyclic stress-strain curve, as envisioned in Reference (1), was considered to be attained at the microscopic level, and it did not appear that the cyclic state could be accurately revealed at the macroscopic level of measurement for all materials. However, it became evident during the course of this study that when the proper balance exists between elastic and plastic strains in a given cycle, the gross effects of microscopic straining processes can be fully revealed and the cyclic curve can be accurately identified at the macroscopic level.

SECTION II

MATERIAL AND SPECIMEN DETAILS

2.1 MATERIALS

The four materials tested in this program consisted of two basic types; namely, an age-hardenable aluminum alloy (2024) and a work-hardenable pure copper (OFHC*). The aluminum alloy was tested in both the as-received T351 condition for wrought round rod and in the O-condition developed through a softening heat-treatment. The pure copper was tested in the as-received cold-work condition (3/4-hard) as well as in an annealed condition. The two hardnesses of the two basic materials provided, therefore, four distinct material responses during the test series.

2.1.1 ALUMINUM ALLOY

The aluminum alloy was received in the 2024-T351 condition in the form of round rods 12-foot in length and 1-1/16 inch in diameter which were wrought from the same heat of material. The other elements comprising the composition of the aluminum alloy were expressed as percent of weight as follows:

Si(0.50), Fe(0.50), Cu(3.8-4.9), Zn(0.25)

Mn(0.3-0.9), Mg(1.2-1.8), Cr(0.10), other (0.15)

Approximately one-hundred specimens were machined from the rod stock and half of these were softened to the 2024-O condition by heat treating at 650°F for two hours followed by air cooling. The threaded areas of the specimens were protected by dipping in plating stop-off. This heat treatment provided 100 percent removal of strains from prior cold work.

2.1.2 PURE COPPER (OFHC)

The copper material was also supplied in the form of round rods 12-foot in length and 1-1/16 inches in diameter with the cold-work hardness specified as 3/4-hard. Half of the one-hundred specimens machined from the OFHC copper were annealed in accordance with the following heat-treatment schedule:

- . Degrease, and place in sand retort
- . Purge with nitrogen for 15 minutes
- . Charge in furnace at 750°F for 1 hour
- . Furnace cool to below 200°F

*Oxygen-free, High-conductivity

It is important in the above procedure to keep the material free from the effects of oxidation while at elevated temperatures. The threaded areas were lightly buffed after the anneal procedure.

2.2 SPECIMEN DETAILS

2.2.1 CONFIGURATION

All experimental results (static and cyclic testing) were obtained from specimens having the configuration shown in Figure 1. The dimensions of the specimen were selected so as to be compatible with the SR-4 Baldwin-Emery testing machine (tension-compression, axial load) and also have sufficient length at the constant-diameter test section to permit the mounting of either electric-wire strain gages and/or a one-inch mechanical extensometer.

The contour of the specimen between the reduced section and the threaded ends was selected to provide a transition which is free of stress concentration effects. The controlled profile as noted in Figure 1 consists of an elliptical joining at the test section and a parabolic joining at the threaded ends. The two described surfaces are smoothly joined at their point of tangency which is positioned near the mid-region of the fillet. Specimens having the above fillet contour were employed very successfully by Dubuc, Reference (2), in low-cycle fatigue tests and his preliminary experiments verified the effectiveness of the fillet in eliminating stress concentrations at the ends of the test section. The elliptical joining provides a close approximation to the hydrodynamic contour of a free jet of water which was proposed by Baud, Reference (3), as a contour for a fillet free of "stress-raiser" effects. The parabolic section was selected as a convenient transition surface which is well outside the critical test-section region.

2.2.2 SPECIMEN FABRICATION

Automatic control was required in the machining operation in order to combine rapid machining with the required dimensional accuracy along the transition contour. This was accomplished by performing the final machine operation in a contour lathe equipped with a precision ground contour-template.

The machining sequence for all test specimens was as follows:

- (1) Round bar stock was cut to lengths leaving approximately 1/16 inch on the overall finished dimension.
- (2) Parts were finished to overall length removing approximately .030 inch from each end.
- (3) Centers were machined in each end and held to the same depth to insure constant registering in the different machining operations to follow.

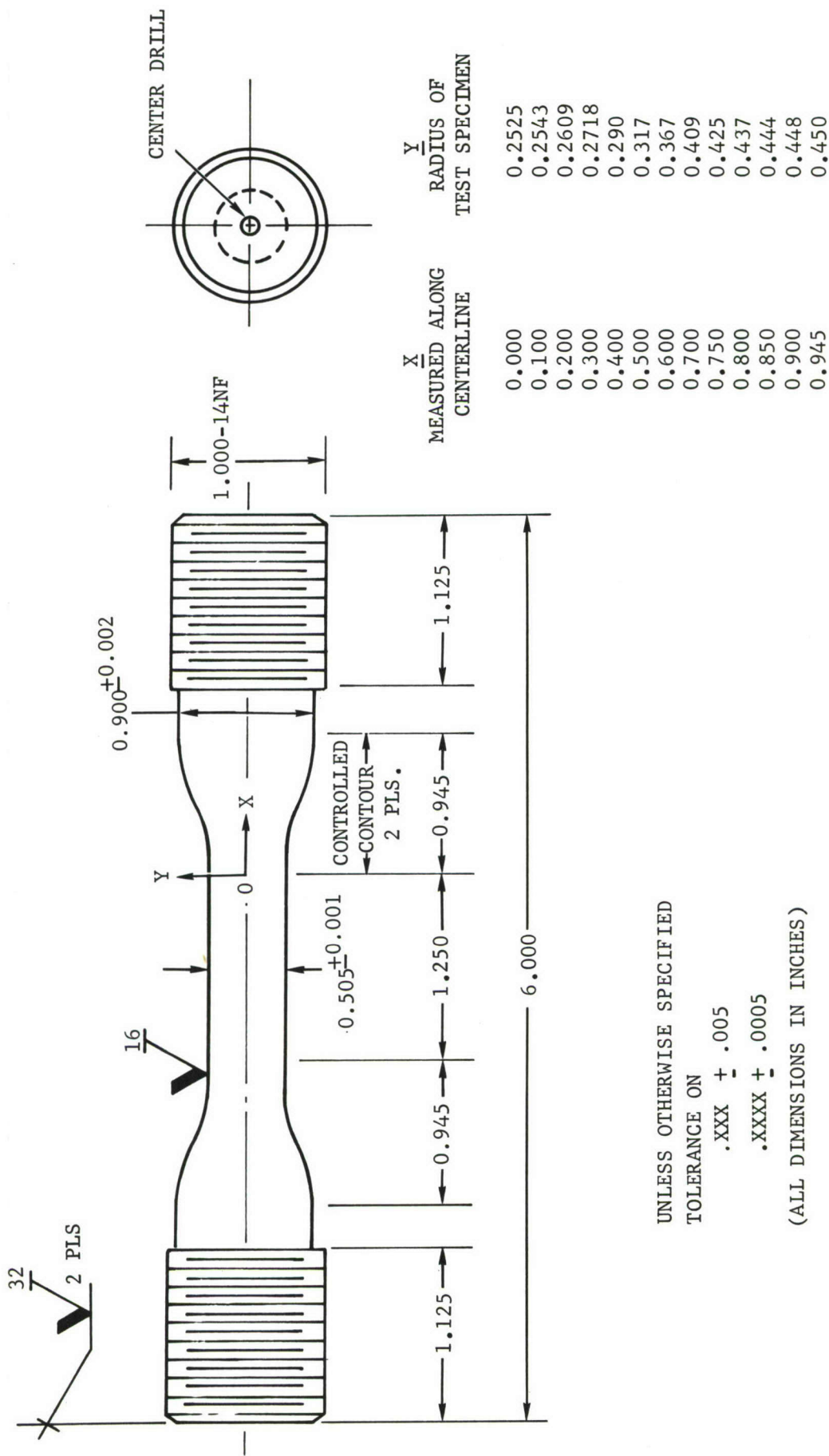


FIGURE 1. TEST SPECIMEN FOR STATIC AND CYCLIC AXIAL LOADS

- (4) A 1-inch section at approximately the center of each specimen was removed for stress relief purposes to a rough O.D. dimension of .530. This leaves .025 on the diameter to be removed to attain the .505 diameter when contouring the test section.
- (5) The .900 diameter was roughed to .910 diameter leaving stock for the contour operation to bring the 1.125 inch thread length to print callout.
- (6) Specimens were turned to .995-.998 inch O.D. for threading.
- (7) Specimens were threaded (single pointed) to a 2-3 class fit using a 1-inch, 14 ring-gauge set at a pitch diameter of .9536 inch.
- (8) Specimens were then transferred to the contour lathe taking cuts from .030 to .060 inch per pass to within .005 inch of the finished diameter. A final pass of .005 inch was taken to maintain the best machined finish possible.
- (9) All of the above listed operations were constantly being cooled with a soluble coolant solution being sprayed at the point of contact between the tool and the work.
- (10) The 16 micro-finish was obtained by light polish using 400 followed by 600 3M wet or dry emery paper.

SECTION III

TEST EQUIPMENT AND PROCEDURE

3.1 TESTING MACHINE

All of the tests, static and cyclic, were performed in a Baldwin-Emery SR-4 Testing Machine (Model FGT). This is a very sturdy, compact machine of the screw-gear type designed for the automatic application of tension-compression axial loads. Mechanical and electrical provisions in the form of cams and limit switches are contained within the load sensing (Console) and strain sensing (MA-7 Recorder) equipment to afford accurate automatic control of either load or strain limits during a test. The load capacity for the machine is $\pm 50,000$ pounds with a maximum cycling speed at about 10 to 15 cycles per minute depending on the range of loading. The speeds used during the program rarely exceeded 6 or 7 cycles per minute and in a few large strain-range tests the speed was held near 3 cycles per minute. At these speeds the machine was capable of maintaining the limits of load or strain within ± 1 percent of the set value.

The massive specimen holders of the testing machine were adaptable to either pinned-end or fixed-end loading of the test specimen. Careful alignment of these holders assured true axial loading as well as flat-and-parallel surfaces for applying compressive loads. The accuracy of the holder alignment was confirmed at the outset of the program by means of a specially prepared hard-aluminum specimen. On the specimen three wire strain gages were mounted axially and spaced at 120 degree intervals around the circumference of the one-inch gage length. During several compression-tension cycles below the elastic limit of the specimen, no significant variation in the gage outputs were noted. Also, during the course of the test program, the fatigue cracks were found to have initiated at points on the specimen surface which were randomly oriented around the circumference of the gage-section, thus indicating no preferential high-stress region that might be associated with poor machine alignment.

In Figure 2 are shown the SR-4 machine and a typical test setup in which a mechanical extensometer is used. The MA-7 Drum Recorder is shown mounted to the right side of the console. Continuous or intermittent recording of stress-strain hysteresis loops was afforded by the high-magnification recorder. For the constant strain-range tests the rotation of the drum actuated microswitches which in turn reversed the loading of the machine.

3.2 STRAIN INSTRUMENTATION

Post-yield electric wire strain gages and a dual-range mechanical extensometer were used in the static tests to record virgin tension and compression stress-strain data. The wire strain gages were capable of measuring unidirectional strains up to 8 percent. Each static-test

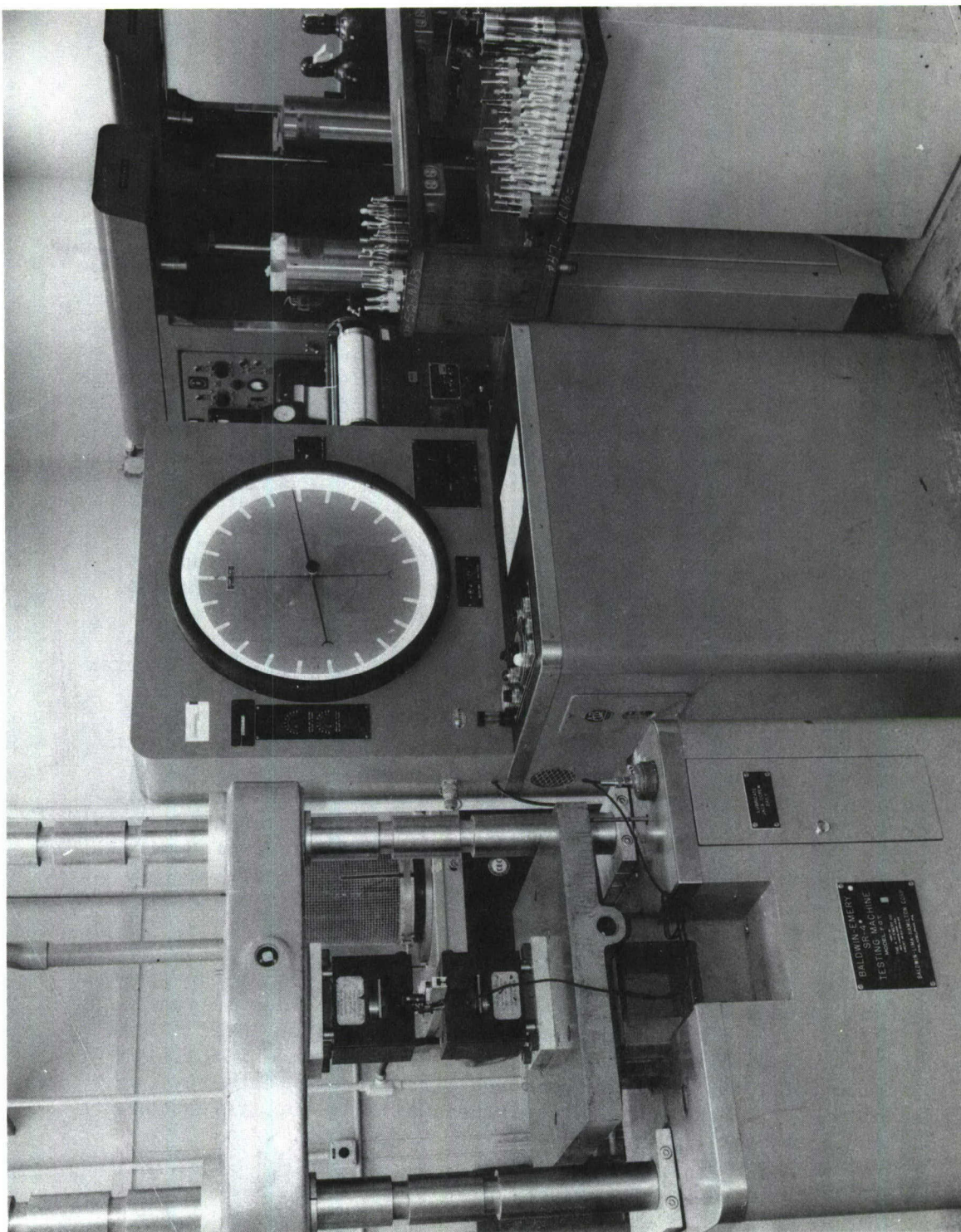


FIGURE 2. TESTING MACHINE AND EXPERIMENTAL SETUP

specimen was provided with two diametrically opposite longitudinal gages (3/4-inch length) and two diametrically opposite transverse gages (1/8-inch length). Each set of two gages was connected into a standard bridge circuit so as to give an average strain response. A mechanical extensometer was simultaneously mounted on the static-test specimens to check the correspondence between longitudinal strains as measured by wire-gages and by the mechanical device. Strains for a given stress recorded on an X-Y plotter and the drum recorder were found to be duplicated within 2 or 3 percent. The "electrical noise" superimposed on the output of the X-Y plotter limited the ability to read strains more accurately from the wire-gages.

The mechanical extensometer employed in the static and cyclic tests was a Riehle dual-range extensometer of one-inch gage length. The existing microformer in the extensometer was replaced, however, with a Baldwin microformer so as to match the strain response to the Baldwin recorder. The hybrid extensometer is shown in Figure 3. It was initially calibrated and periodically checked to ascertain the magnification ratio operative during both the high and low magnification range of application. The two magnification ratios were found to consistently hold at a value of 164.3 and 17.14 with the switch-over occurring at approximately 3 percent strain. At the low magnification the extensometer can measure strains up to 100 percent.

Available data on wire and foil strain gages indicated that their survival and accurate response under the large alternating and creep strains of interest in this program was very doubtful. This was borne out by an initial series of tests in which 3/4-hard copper specimens were subjected to cyclic loads. In these tests the superposition of cyclic creep and alternating strains exceeded the limits that could be handled without failure by the gages. A relatively new type of wire grid gage mounted on a phenolic glass base was tried along with the post-yield gages. Although the new type gages were superior to the post-yield gages, neither was successfully used under these severe conditions. In view of the difficulties encountered in the initial constant-load-range tests, no further attention was given to the application of wire strain gages in the program. All strain measurements, therefore, were relegated to the mechanical extensometer during the cyclic stress and strain tests. Nevertheless, in the constant-strain-range tests in which cyclic creep was absent, the wire strain gage may have proven more successful.

The mechanical extensometer proved to be a reliable and accurate device for sensing the cyclic strains. Also, during a given test, periodic diameter measurements could be made with a micrometer placed between the knife-edges of the extensometer. During the final stages of a test, the extensometer could be easily removed, thus permitting observation of crack propagation.

Premature failure was found to occur in several of the early fatigue specimens due to the small knife-edge marks made by the extensometer. A simple solution to the problem was found, however, by placing a drop or two

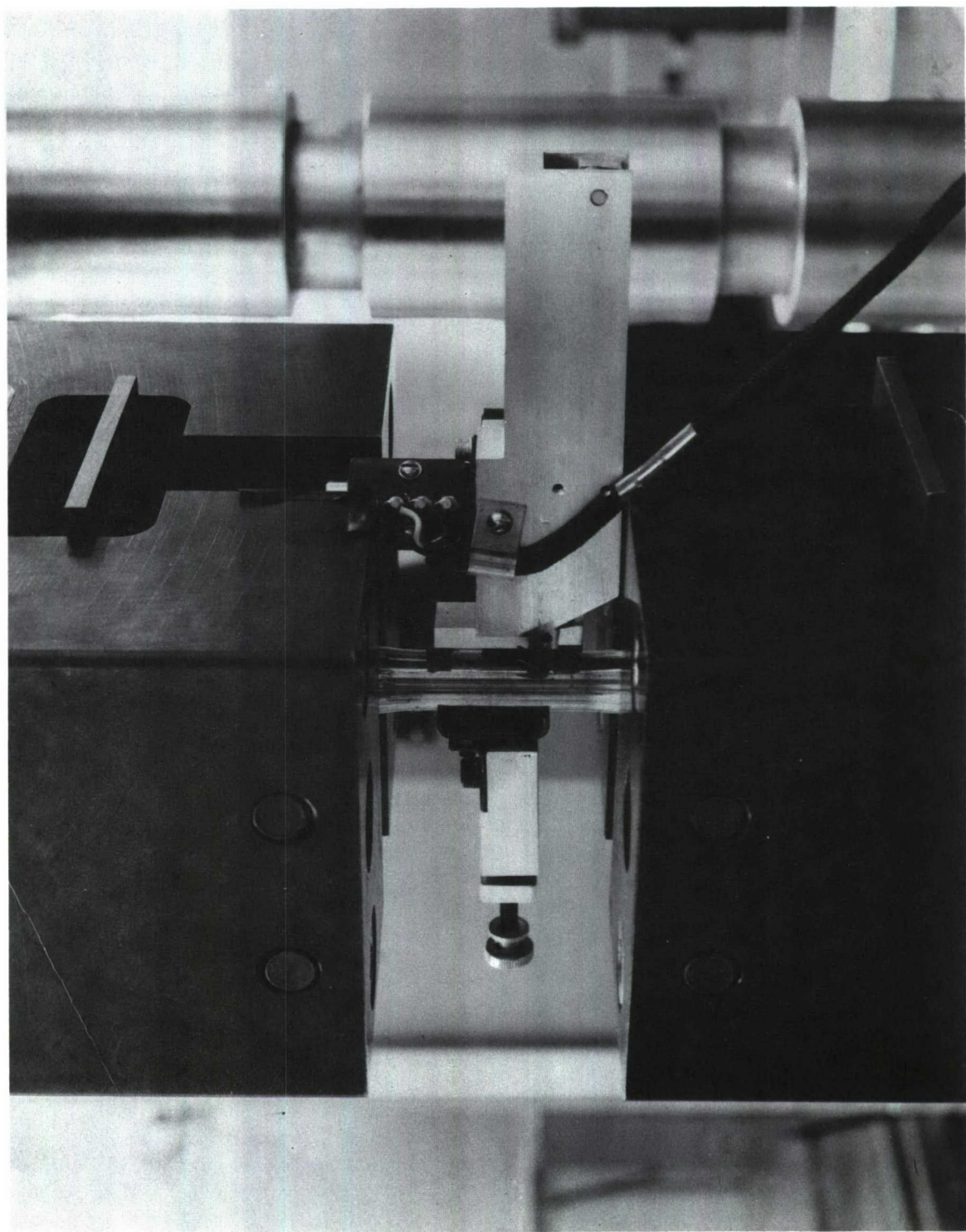


FIGURE 3. DUAL-RANGE MECHANICAL EXTENSOMETER MOUNTED FOR TEST

of a commercially available adhesive at the one-inch gage-mark locations on the specimen. The adhesive cured sufficiently in one hour at room temperature to form a very tough little pad beneath the knife-edge and thus prevent the localized damage. The size of the small pads of adhesive were controlled through the use of masking tape. The pad dimensions were approximately $1/8 \times 1/8$ inch in planform with a thickness of about .010 inch. Even under high surface strains near 5 percent the pads showed no tendency toward unbonding.

3.3 TEMPERATURE-RISE INSTRUMENTATION

Three specimens, one hard copper and two soft copper, were instrumented with thermocouples in an attempt to determine if a temperature rise offered an explanation for the cyclic creep noted for the materials during cycles of constant load-range. Copper-Constantan thermocouples were employed and temperatures were sensed with a potentiometer-type instrument capable of sensing $\pm 1/2^{\circ}\text{F}$ temperature variations. The thermocouples were attached to the specimen at two surface locations, at the center and at one end of the gage length. On the first soft copper specimen the thermocouples were held tightly against the surface and bonded with an adhesive. On the second soft copper and the single hard copper specimen the thermocouples were attached mechanically. That is, a sharp knife was used to slice and lift up a short sliver of the surface, and after laying the thermocouple underneath, the sliver was peened down again, so as to mechanically clamp the thermocouple in place. The results of the measurements are discussed in Section 4.2.4.

SECTION IV

EXPERIMENTAL RESULTS AND RELATED DISCUSSIONS

The experimental phases of the program were primarily directed toward obtaining data which appeared necessary to the study of the stabilized cyclic condition of materials and its possible correlation with virgin material properties and fatigue failure. The test series included static tests, cyclic tests under conditions of constant stress-range or load-range, and cyclic tests under conditions of constant strain-range. A short series of tests were also performed to determine the extent of temperature-rise effects in copper during cyclic stressing and the effect of dual-level strain cycles on the stabilized cyclic state.

4.1 STATIC TEST RESULTS

Six to ten specimens of each condition of the 2024 aluminum alloy and OFHC copper were used to obtain virgin material property data. Standard properties such as modulus of elasticity, yield strength, ultimate strength, percent elongation, hardness, etc., were recorded for each of the materials. In addition, transverse strains and neck-down profile radii were measured in the tensile test to enable the determination of Poisson's ratio, true stress-true strain relations, and the flow stress correction factors.

4.1.1 STRESS-STRAIN CURVES AND POISSON'S RATIO

Static stress-strain data and Poisson's-ratio variations were obtained from specimens instrumented with longitudinal and transverse wire strain gages. These gages were described in Section 3.2. The resulting tension and compression curves as obtained from two or more specimens of each material are shown in Figure 4. A summary of the mechanical properties derived from the tension and compression tests is given in Table I.

Values of Poisson's ratio were determined from the tensile load-strain plots produced on the X-Y plotter by the longitudinal and transverse gages. The variation of Poisson's ratio* between the elastic and plastic value are presented in Figure 5. The transition from a value near $1/3$ to the plastic value of $1/2$ occurs in the knee-region of the tension stress-strain curve. The range of stress over which the transition takes place was found to be related to the sharpness of the "knee" and the transition is far from being abrupt. Although variations in Poisson's ratio did not directly enter into the data reduction or material parameters employed in this program, they are of fundamental importance to those studies in which longitudinal strains are theoretically derived from diametral strain measurements.

*Although Poisson calculated the ratio only for elastic action, it is convenient to retain his term in the inelastic range of strains.

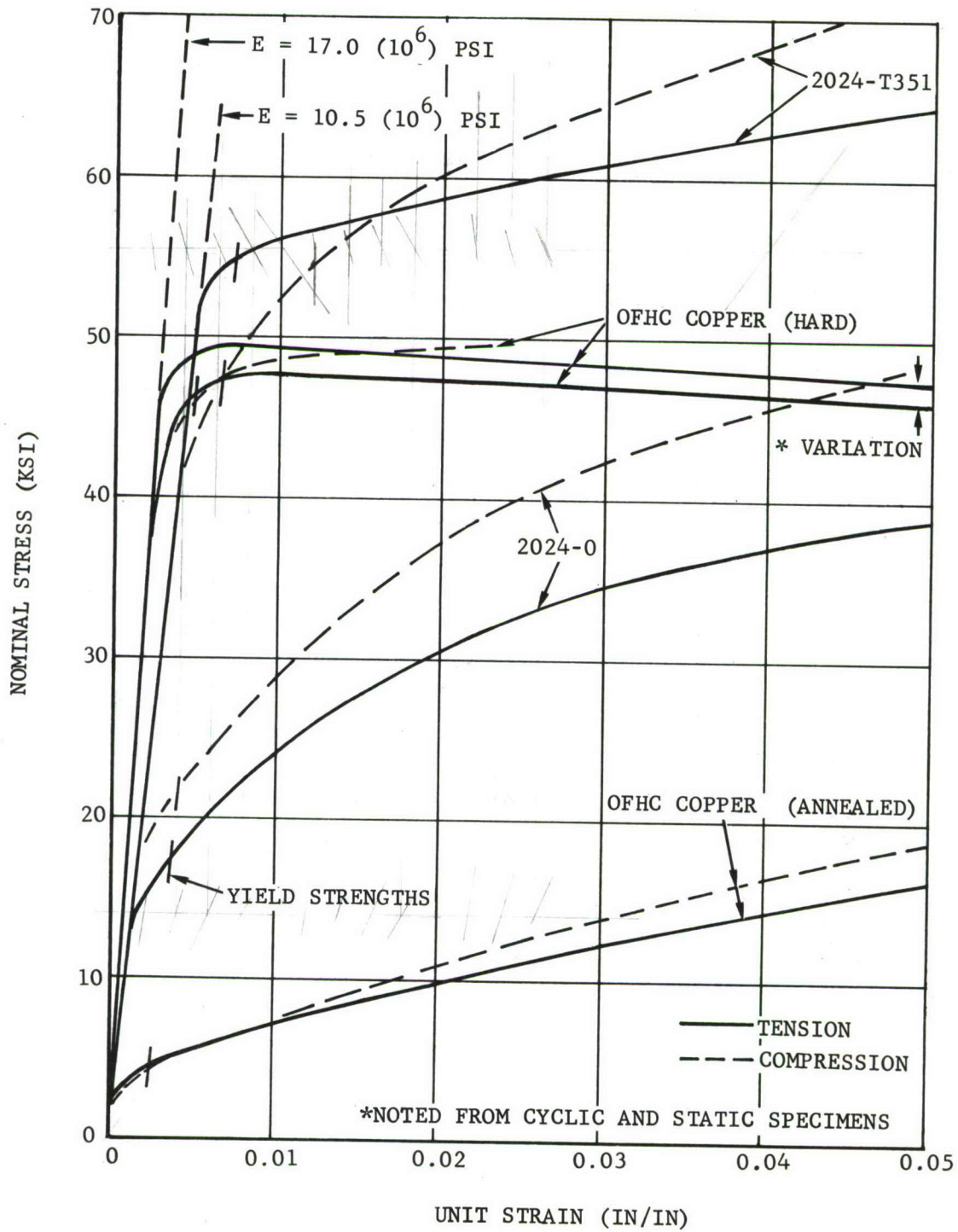


FIGURE 4. STANDARD STRESS-STRAIN CURVES FOR TEST MATERIALS

TABLE I. SUMMARY OF MECHANICAL PROPERTIES
AS DERIVED FROM STATIC TESTS

PROPERTY	2024 ALUMINUM ALLOY		OFHC COPPER	
	-0	-T351	Annealed	Work Hardened
σ_{ty} , PSI	17,300	54,800	4,300	46,300 to 48,500
σ_{cy} , PSI	21,700	47,300	4,000	46,000
σ_{ult} , PSI	42,500	73,000	31,500	47,400 to 49,000
E, PSI	$10.5(10^6)$	$10.5(10^6)$	$17.0(10^6)$	$17.0(10^6)$
Percent Elongation (in one inch)	21.0	29.0	80.8	38.3
Percent Reduction in Area	30.3	34.3	86.0	76.8
Hardness Readings*	77-78 R_F 35-37 R_B	102-103 R_F 79-81 R_B	13-20 R_F	79-83 R_F 40-45 R_B

*The comparison between R_F and R_B values is not clearly defined for aluminum and copper materials.

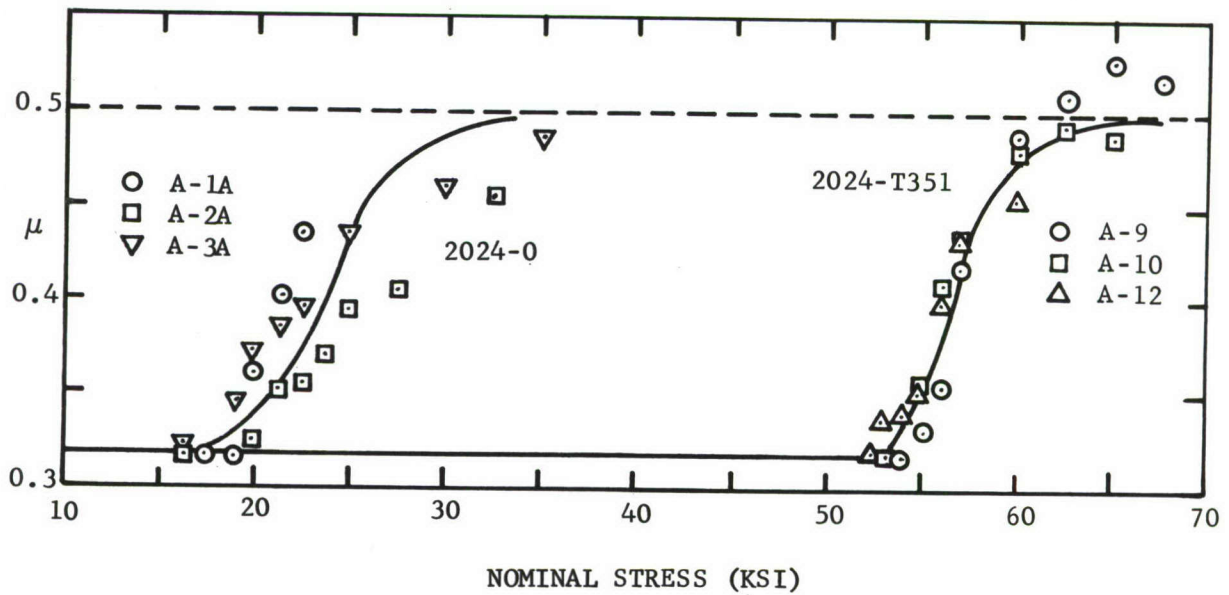
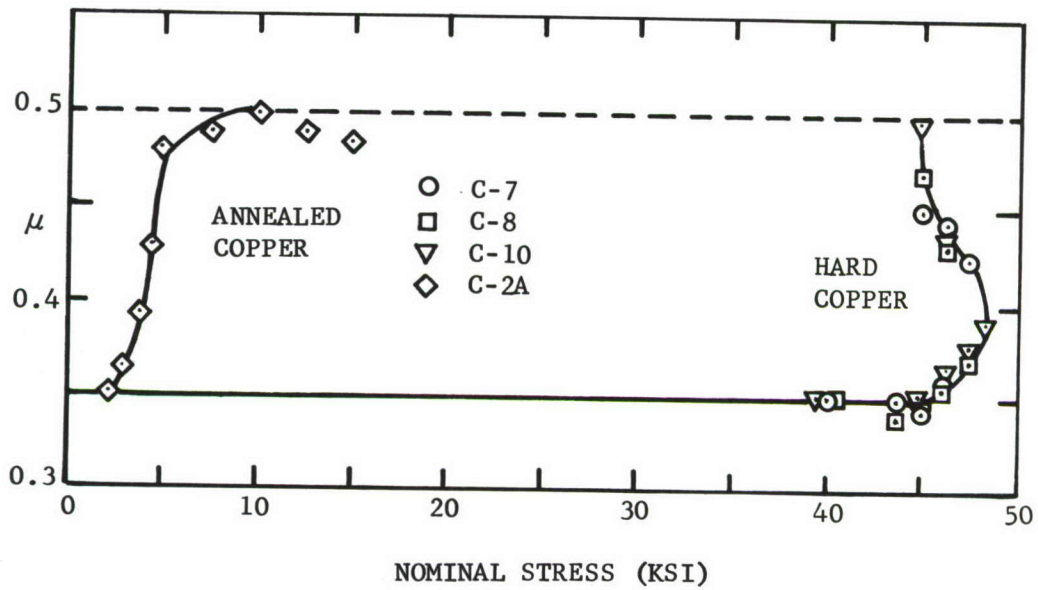


FIGURE 5. POISSON'S RATIO VARIATIONS DURING TENSILE TEST OF ALUMINUM AND COPPER MATERIALS

The manner of introducing Poisson's ratio into the relationship between diametral and axial strains is given in Appendix A.

4.1.2 TRUE STRESS-TRUE STRAIN RELATIONSHIPS

Data for use in the development of true stress-true strain relationships were obtained from specimens which were carried to fracture in the tension test. The necessary data consisted of applied loads and instantaneous diameters with emphasis being placed on those measurements taken after ultimate load and during the neck-down process. Specimens employed in the stress-strain tests and additional specimens (minus the strain instrumentation) were used to obtain the data. The strain-rate in the specimens was not held constant during the tests, but the machine head-travel was held between 0.060 and 0.002 inches per minute. The former speed corresponded closely with that used in the three-cycle-per-minute tests at 2% total strain, and the latter speed was that employed in the standard tensile tests. The data did not show a strain-rate effect over this speed range. The minimum diameters were measured manually using pointed- and ball-anvil micrometers.

The data points corresponding to the recordings of load and diameter are shown in Figures 6 and 7 where true stresses versus true strains (natural strains) have been plotted. The true strain is related logarithmically to the ratio of original and instantaneous cross-sectional areas. These stresses and strains are defined as follows:

$$\sigma_T = \sigma \left(\frac{A_o}{A_T} \right) = \sigma \left(\frac{D_o}{D_T} \right)^2 \quad (1)$$

$$\epsilon_{ln} = \ln \left(\frac{A_o}{A_T} \right) = \ln \left(\frac{D_o}{D_T} \right)^2 \quad (2)$$

The relationship between true strain and engineering strain, ϵ , under constant volume deformation is

$$\epsilon_{ln} = \ln(1 + \epsilon) \quad (3)$$

As noted by the curves in Figure 6, fracture occurred abruptly for the aluminum alloys while the power law relationship between stress and strain was applicable. This was not the case for the two copper materials. As indicated by the curves of Figure 7 for the highly ductile coppers, a

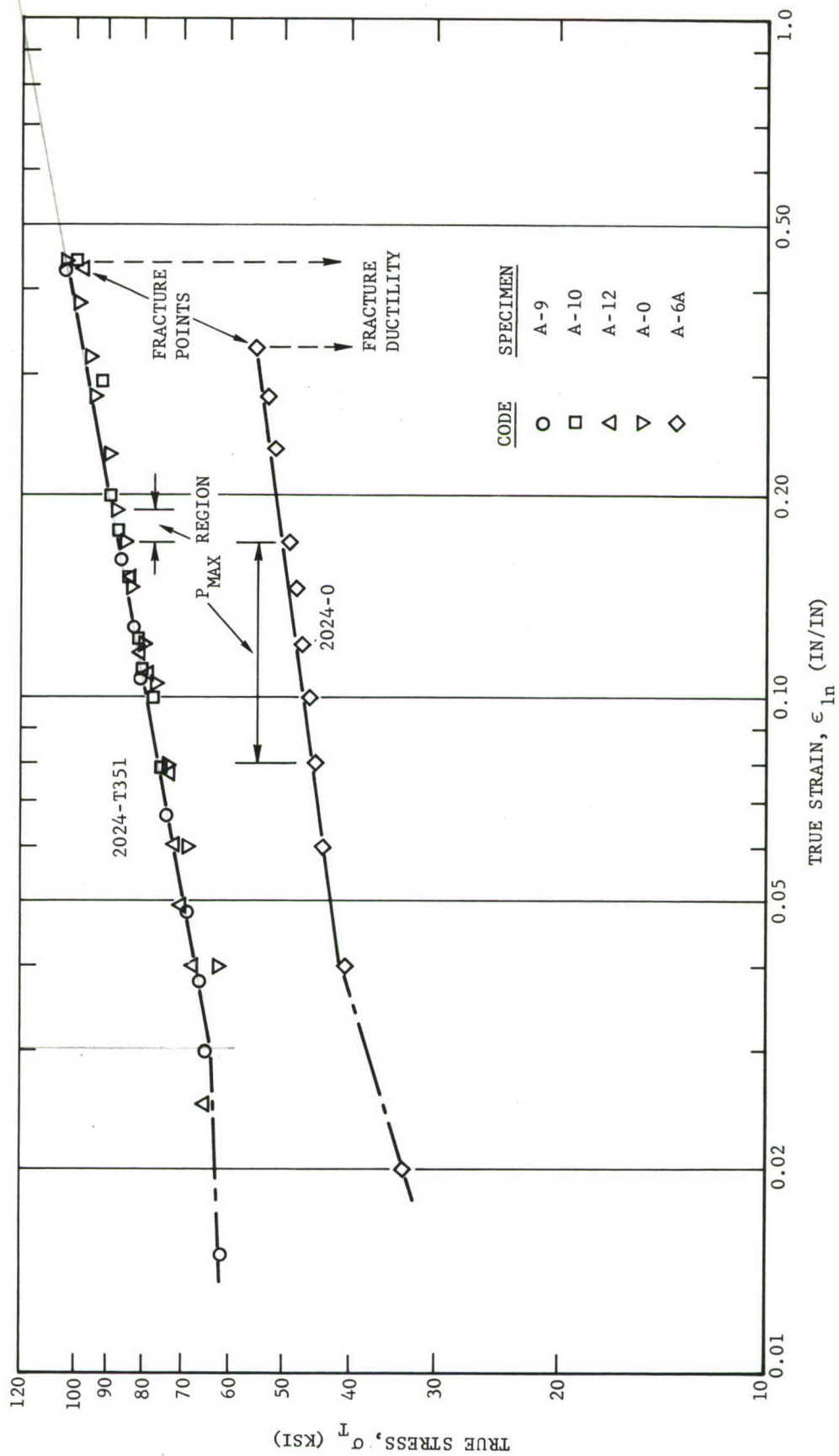


FIGURE 6. TRUE STRESS-TRUE STRAIN RELATIONSHIPS FOR 2024-T351 AND 2024-0 ALUMINUM ALLOY

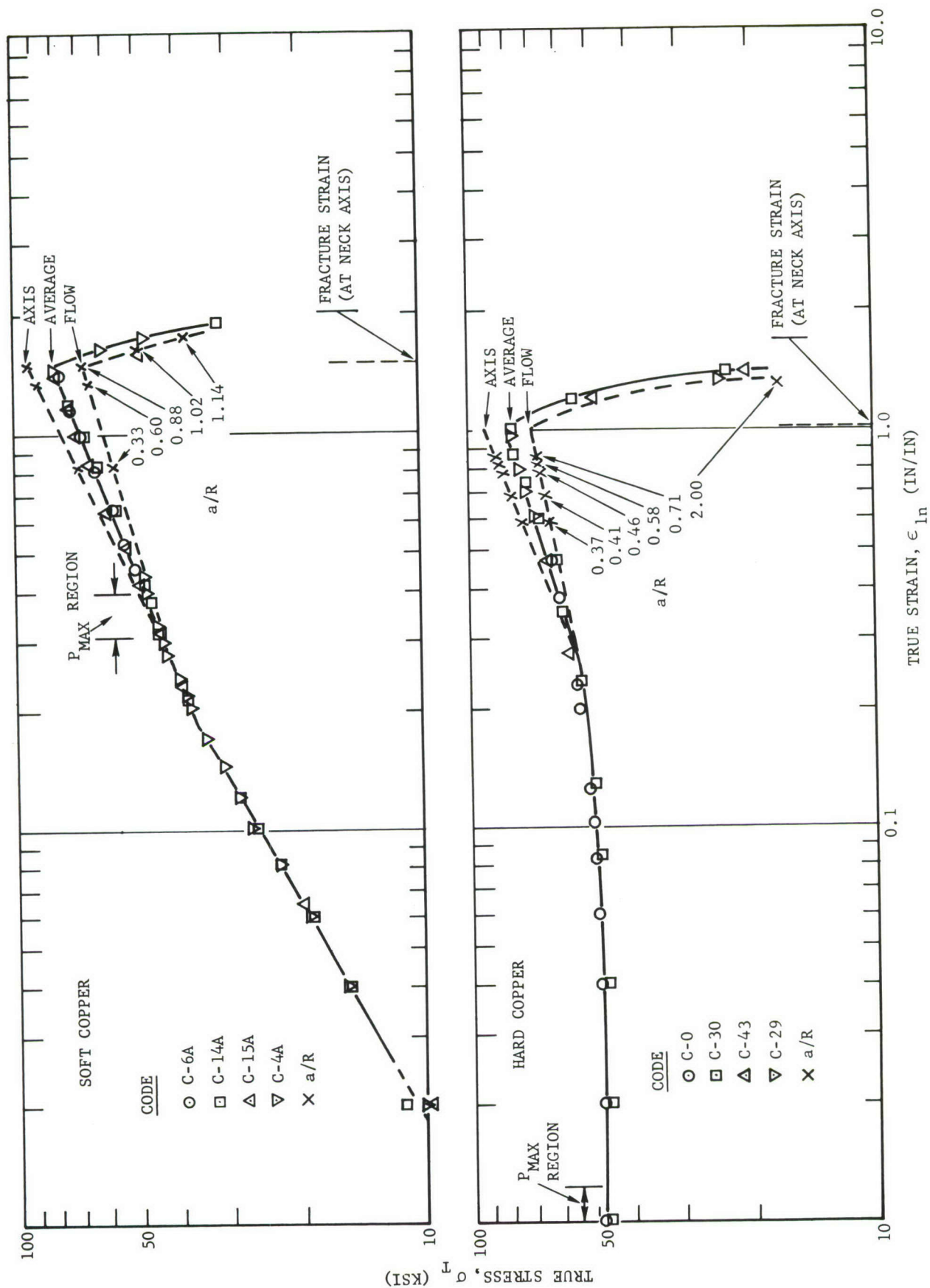


FIGURE 7. TRUE STRESS-TRUE STRAIN RELATIONSHIPS FOR SOFT AND HARD COPPER

definite drop in the value of true stress occurred well before the specimen finally fractured into two parts. It was evident from the final appearance of the fracture that failure had actually occurred on the axis of the neck cross section at the time the peak true stress was reached. The two ends of the failed specimen showed a cup-cup relationship instead of the more familiar cup-cone. These findings are in accord with the theoretical predictions of Bridgman, Reference (4), in which he showed that failure should be expected at the axis where ductility has been decreased by the maximum hydrostatic tension. Bridgman further pointed out that in specifying the stress conditions under which fracture occurs it is obvious that the stress on the axis should be specified and not the average across the neck. In terms of stress, these refinements in determining the applicable stress level may not be large for most metals; however, in terms of fracture strain, large errors can be introduced if the strain at first fracture on the axis is ignored. That is, for highly ductile materials true fracture strains determined solely from measurements of final fracture diameter can be in error by 50 percent. Such would be the case for either of the copper materials studied herein. The final diameters of these specimens would have indicated true fracture strains much larger than the true strain at which fracture actually occurred on the neck axis.

The corrections for the stress levels which take into account the stress distribution at the neck of the copper tensile specimens are included in Figure 7. Similar corrections for the aluminum alloys were unnecessary due to the small degree of necking that preceded fracture. The "correction" formulas derived by Bridgman, Reference (5), required that profile radius data, R , at the neck be obtained as well as the usual data relating loads and neck-diameters, $2a$.

The formulas for flow stress, F , at the surface and stress, σ_z , at the longitudinal axis are as follows:

$$F = \frac{\sigma_T}{\left(1 + \frac{2R}{a}\right) \ln \left(1 + \frac{a}{2R}\right)} \quad (4)$$

$$\sigma_z = \frac{\sigma_T \left[1 + \ln \left(1 + \frac{a}{2R}\right)\right]}{\left(1 + \frac{2R}{a}\right) \ln \left(1 + \frac{a}{2R}\right)} \quad (5)$$

The above corrections are shown as dashed lines in the figure. The lines were determined by a number of specific points for which the a/R values had been recorded. The uppermost line gives the stress at the neck axis and the lowermost line gives the flow stress at the neck surface.

The convergence exhibited by the curves for hard and soft copper is of interest. The cold work introduced into the soft copper during the tensile test causes this material to approach closely that of the previously hardened copper. The difference between the failure strains of the two

conditions of copper is related to the amount of pre-strain in the hard copper as applied in the initial hardening process. It is not surprising, therefore, to find that the true stress levels at maximum load are almost identical for the two hardnesses of copper.

4.1.3 HARDNESS READINGS

Rockwell hardness readings were taken on all specimens that were eventually softened through heat-treatment. These readings were taken before and after the softening treatment with all indentations being made on the shoulder region just outside the threads. The spread in the recorded values have been given in Table I.

Hardness readings were also taken from the majority of failed specimens following both the cyclic-stress and cyclic-strain tests. These readings were taken on the reduced section (gage length) approximately 1/4-inch from the failure region. Although the time delay in taking readings after failure was not expected to be of consequence, all readings were made within two hours after failure. The post-fatigue failure values indicated no hardness change in the hard aluminum alloy. The soft aluminum alloy showed a measurable hardness increase, the soft-copper showed a very large hardness increase, and the hard-copper showed a definite softening; however, the scatter of readings did not permit correlation with the severity of the fatigue cycle.

4.2 TEST RESULTS DURING CYCLES OF CONSTANT LOAD RANGE

4.2.1 GENERAL FEATURES

Fatigue failures in less than 10^4 cycles without the superimposed effects of cyclic creep or compression instability were difficult to obtain under constant load-range testing. The 2024-0 aluminum alloy and the two conditions of copper were particularly susceptible to cyclic creep. The 2024-T351 aluminum alloy was less susceptible to creep; but nevertheless, this effect could only be prevented through careful selection of load ranges and mean values.

In order to experience low-life fatigue it was necessary to subject the specimens to large excursions of strain. Strains were not controlled in the constant load-range tests; therefore, the required magnitudes of strain could only be induced by applying a high peak stress in combination with a large range of stress. These stringent requirements led to stress magnitudes that either extended the specimen well into the range of inelastic tensile strains or beyond the level that would cause buckling of the specimen. When buckling was found to occur, it was observed to be a very slow but continuous process of lateral deflection during cyclic loading. Once the lateral deflection reached a value near 0.050-inch, the test was terminated.

If a range of load were selected that did not induce buckling instability, then high tensile stresses were generally operative and cyclic creep was imminent. A predominant feature of the cyclic creep process was the slow contraction of the specimen area. Under constant loading the slow reduction in area produced ever-increasing values for the true stress. Thus, a type of tensile instability took place in which creep strain increased the true stress, and the increased stress accelerated the creep. The cyclic creep proceeded rather slowly in a cycle-dependent rather than time-dependent manner and appeared to reflect the second-order, irreversible, deformation phenomena discussed in Reference 40. The true strains and true peak stresses active during the cyclic creep were found to approach the true stress-true relationship shown in either Figure 6 or 7. The values of stress and strain then followed this relationship until the true strain at P_{max} was reached. At this strain level the cyclic creep accelerated, the specimen began to slowly neck down, and the peak load limit could not be precisely maintained. The cyclic load testing was generally carried somewhat beyond this point until the tensile instability became unmanageable. A tensile neck-down test was then performed.

4.2.2 ALUMINUM ALLOY RESULTS

A tracing of a typical record obtained during the constant load-range testing of a 2024-0 aluminum alloy specimen is shown in Figure 8A. The load limits applied during this test were +7000 and -3000 pounds. The drum-recorder produced a continuous record of the hysteresis response extending to failure, but only the initial few cycles are shown in the figure. As indicated by the record, a definite cyclic creep began at the outset of the constant load-range test. The creep continued to final failure with some acceleration of the creep occurring during the later cycles. The complete creep history for this specimen (A-62A), as well as that of several other soft-aluminum specimens, are shown in Figure 9.

The cyclic creep histories shown in Figure 9 are representative of the results obtained during load cycles having a ratio, R_p , between -1 and 0. The load range is noted on each graph. The lower right-hand graph depicts a manner of plotting the creep data that better shows the constancy of the cyclic engineering strain, $\Delta\epsilon$, upon which the cyclic creep is superposed. For each of these tests it was found that the hysteresis loop reach a near stable shape but slowly crept along the strain axis.

In Figure 10 a similar set of strain histories are shown. Here, however, the loads are completely reversed ($R_p = -1$) and the creep effects are considerably reduced, if not eliminated. Since very little creep was experienced in this series of tests, the true stress limits were found to remain essentially constant after the first cycle of static yielding.

The fracture surface of each of the specimens depicted in Figures 9 and 10 ranged between that of a typical tensile failure with no evidence of a fatigue surface (specimens A-62A and A-65A) to that showing considerable fatigue (specimens A-63A, A-64A, and A-71A). At the end of 10,685 cycles, specimen A-64A had not failed and the cyclic load test was stopped. The specimen was pulled, as in a tensile test, to failure with an ultimate strength of 47,250 psi being achieved. This strength was approximately

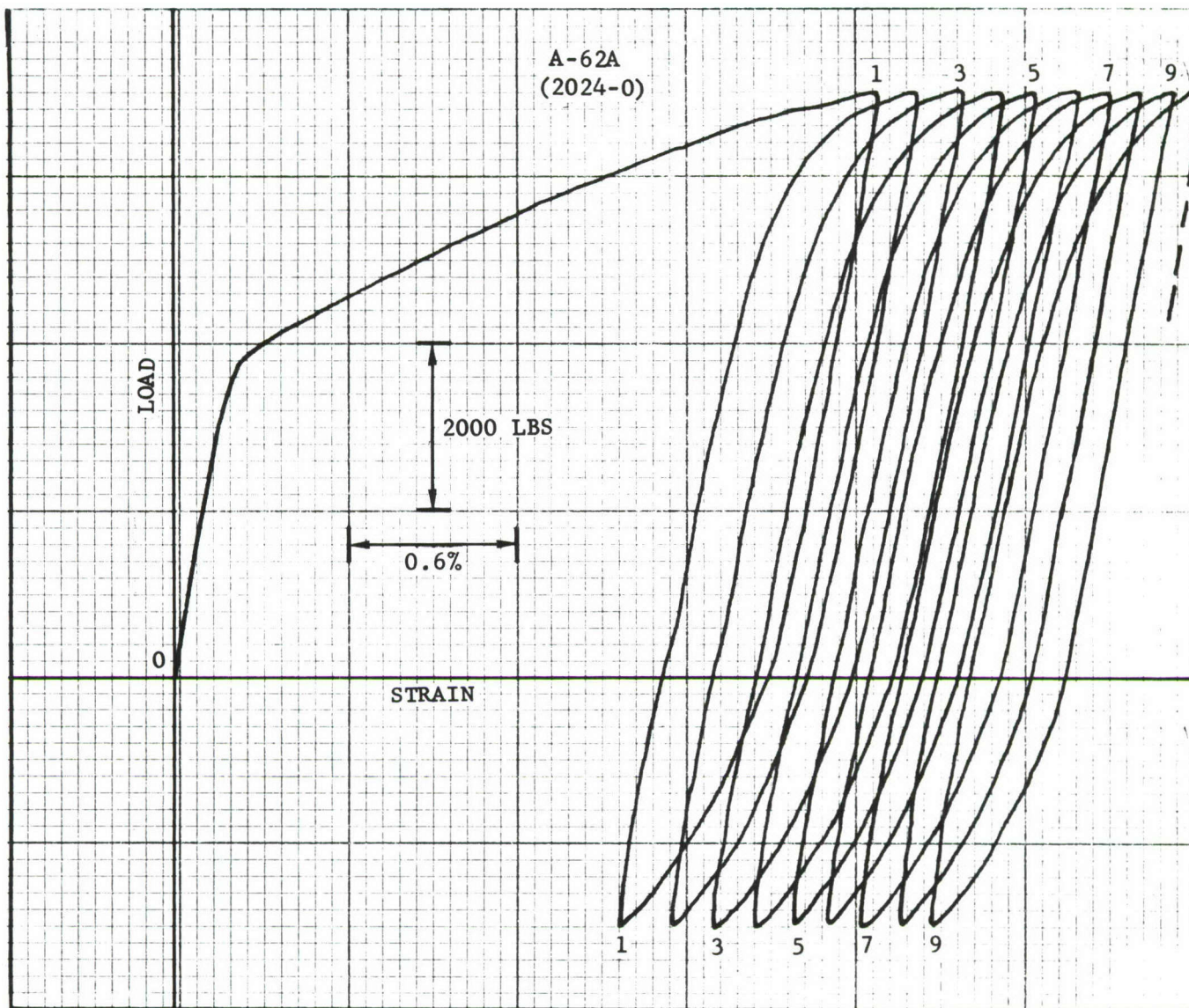


FIGURE 8A. REPRODUCED RECORDING OF HYSTERESIS AND CYCLIC CREEP
TYPICAL OF 2024-0 ALUMINUM ALLOY DURING CONSTANT
LOAD RANGE TESTS

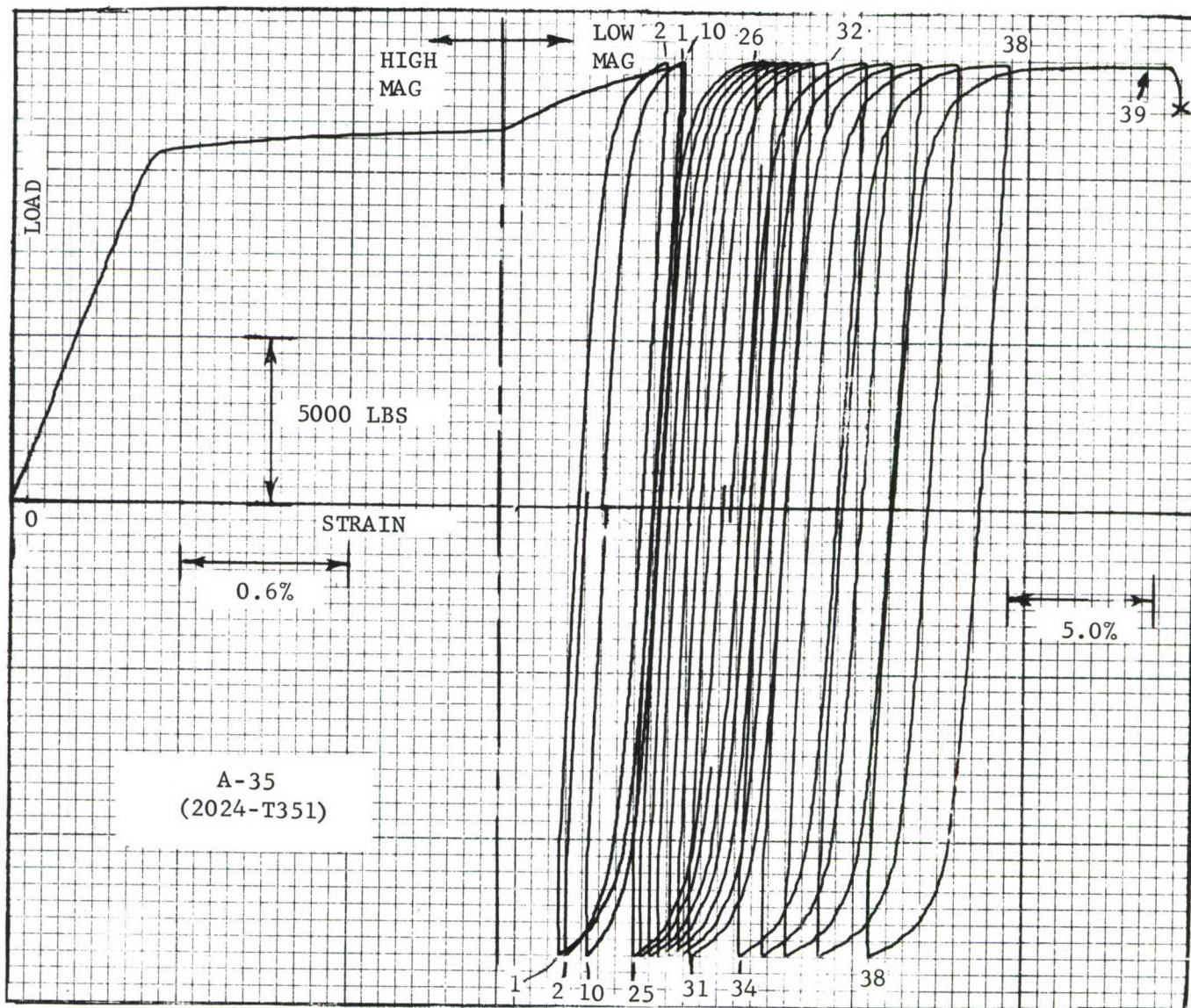
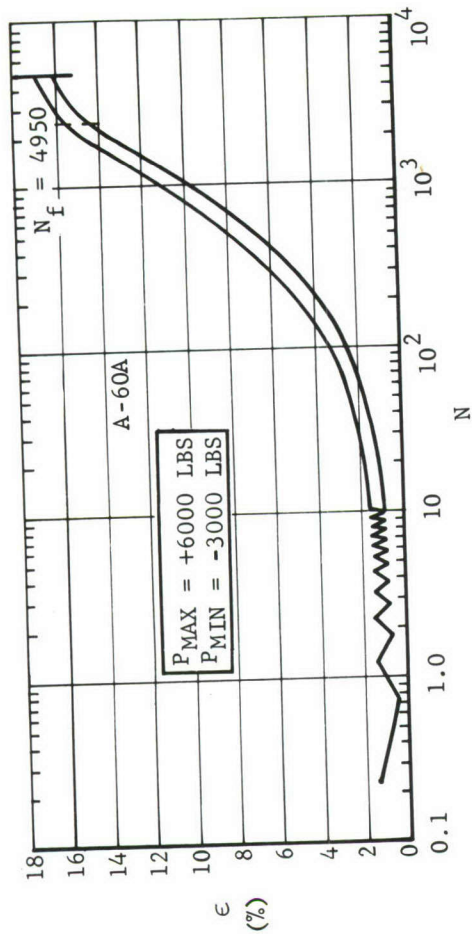
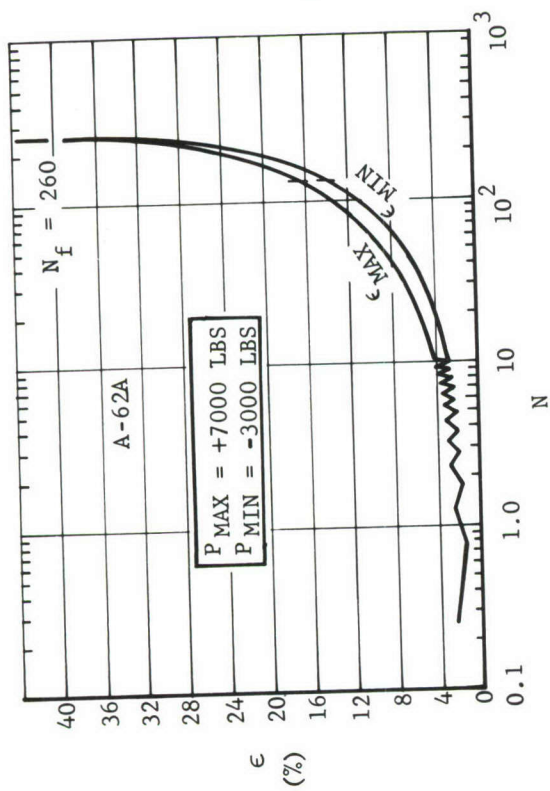


FIGURE 8B. RECORDING OF HYSTERESIS AND CYCLIC CREEP TYPICAL OF 2024-T351 ALUMINUM ALLOY DURING CONSTANT LOAD-RANGE TESTING



24

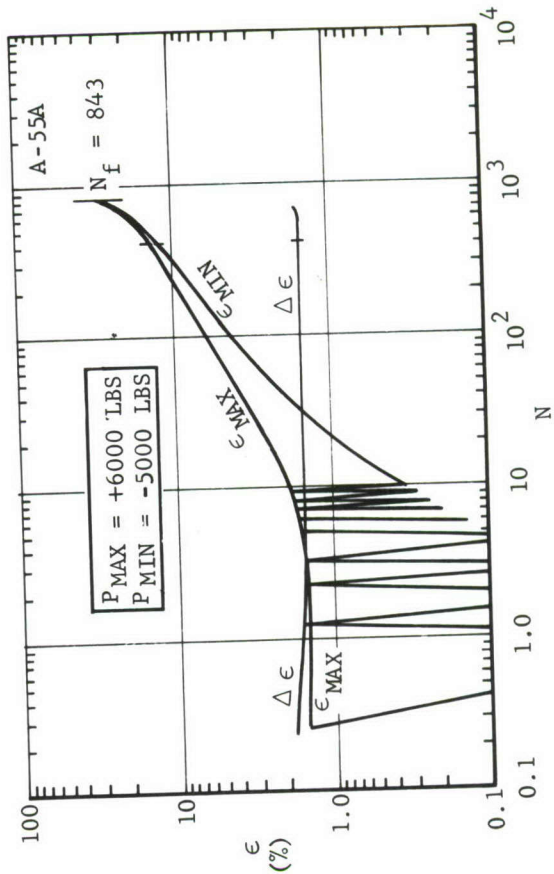
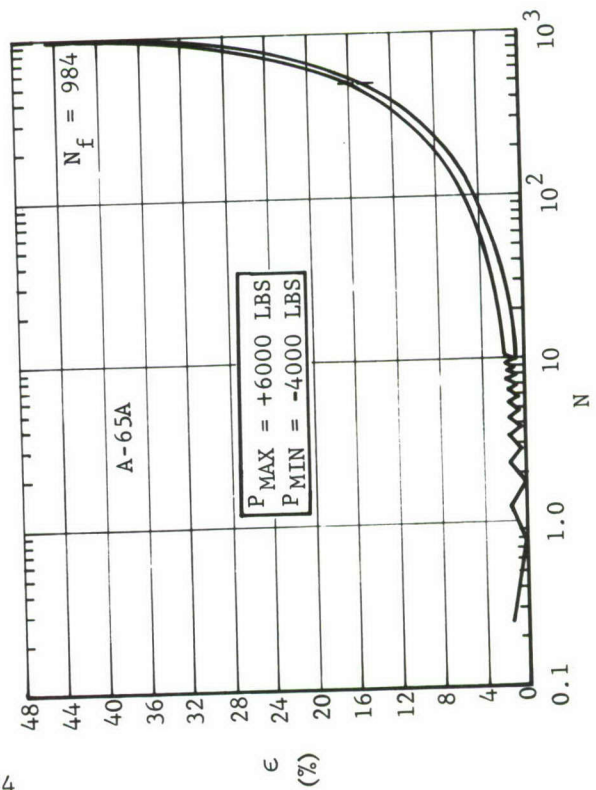


FIGURE 9. CYCLIC CREEP OF 2024-0 DURING CYCLES OF CONSTANT LOAD RANGE

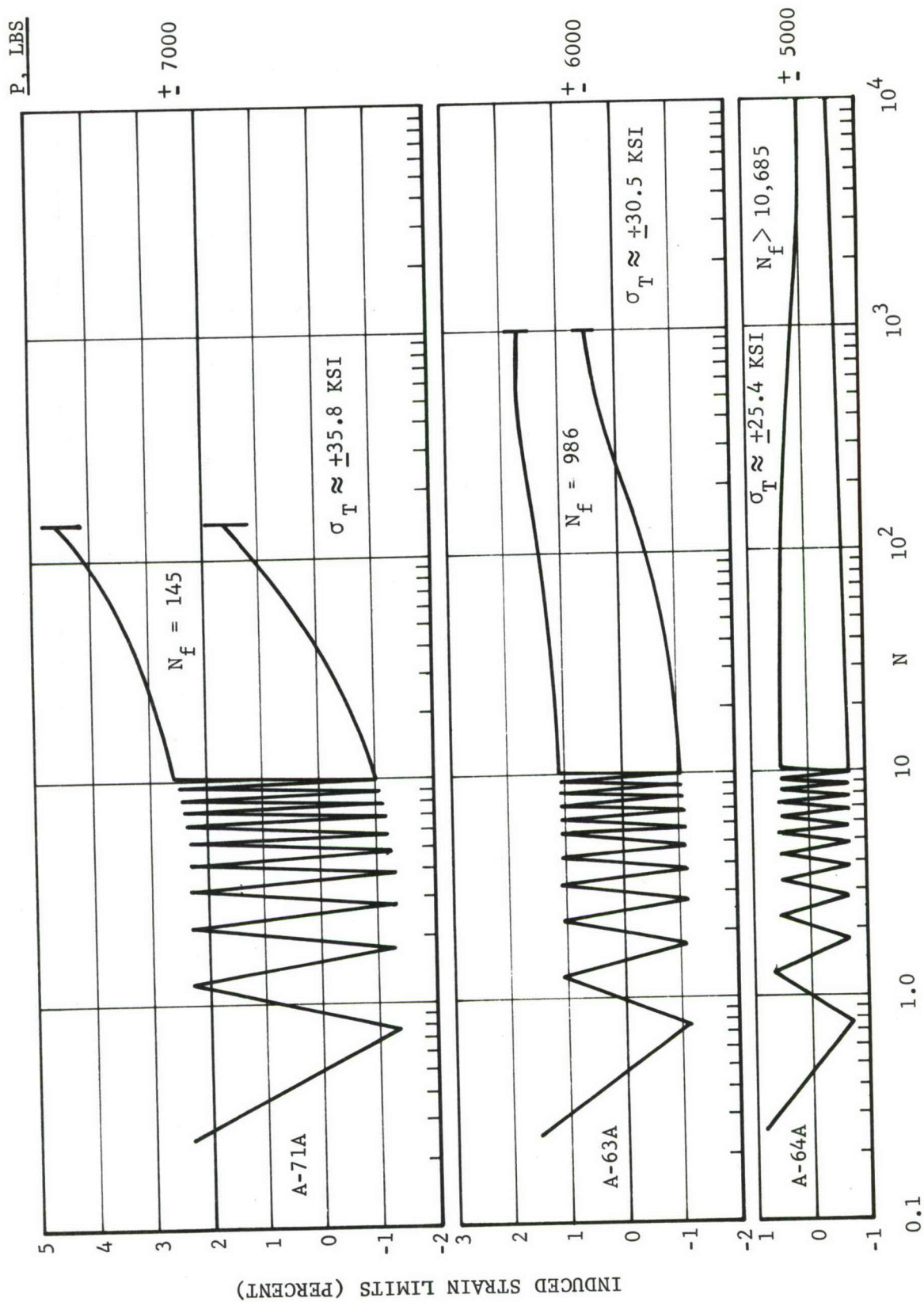


FIGURE 10. STRAIN LIMIT VARIATIONS FOR 2024-0 DURING CYCLES OF CONSTANT LOAD RANGE ($R_p = -1$)

5000 psi higher than that found in the virgin tensile tests; therefore, some degree of hardening appears to have been introduced by the reversed load cycles. The failure surface of the specimen showed a fatigue surface extending over about 1/10th of the cross section with the crack beginning at the surface and propagating inward.

Specimens A-60A and A-55A failed as a result of fatigue and cyclic creep. That is, a fatigue crack had evidently propagated during the time that the cross-section was contracting from creep, and when the effective area was sufficiently reduced the specimen failed. The resulting fracture surface exhibited the characteristic features of both tensile failure and fatigue.

As mentioned earlier the hard aluminum alloy (2024-T351) was less susceptible to creep. Nevertheless, some evidence of creep was generally present for those load ranges producing failure in less than 10^4 cycles. Strain histories typical of the hard aluminum alloy are shown in Figures 11 through 13. As indicated by Figures 11 and 12, those load ranges producing fatigue failures between 10^3 and 10^4 cycles did not induce significant creep. The hard aluminum alloy was found to show a very definite compression creep during cycles of reversed stress. The low compression yield strength and the Bauschinger effect appeared to be the contributing factors. Figure 11 shows the negative shift in strain when the range of reversed stress is of proper magnitude. It should be noted that each of the ranges of stress producing compression creep fall in that narrow range of stresses for which the static tensile strain is elastic and the static compression strain is inelastic. (See stress-strain curves in Figure 4.)

Tension creep was found to be prominent during the application of reversed load ranges having sufficient magnitude to produce failure in less than 100 cycles. A typical example is shown in Figure 13. The peak tensile load in this test was very near the static ultimate load that the specimen could support before the onset of necking. Therefore, the creep exhibited in Figure 13 is in large part due to the necking process. Figure 8B gives the hysteresis record from which the data in Figure 13 were derived.

All specimens shown in Figures 11 and 12 failed in fatigue without significant effects from cyclic creep. Specimen A-35, on the other hand, failed in a predominantly tensile mode of failure with only a slight indication of a fatigue region on the fracture surface.

4.2.3 OFHC COPPER RESULTS

During the initial cyclic-load tests on the hard and soft-copper, it was found that completely reversed loading ($R_p = -1$) produced creep into compression. Therefore, the expedient of using a load ratio of -0.8 was employed and the negative creep was prevented.

Cyclic load tests were performed under several load ranges at each of three load ratios, -0.8, 0.0 and 0.4. Many of the tests extended to 10^4 cycles, but no fatigue-like failures were experienced. Cyclic creep was the cause of failure in every instance except for a few specimens that displayed

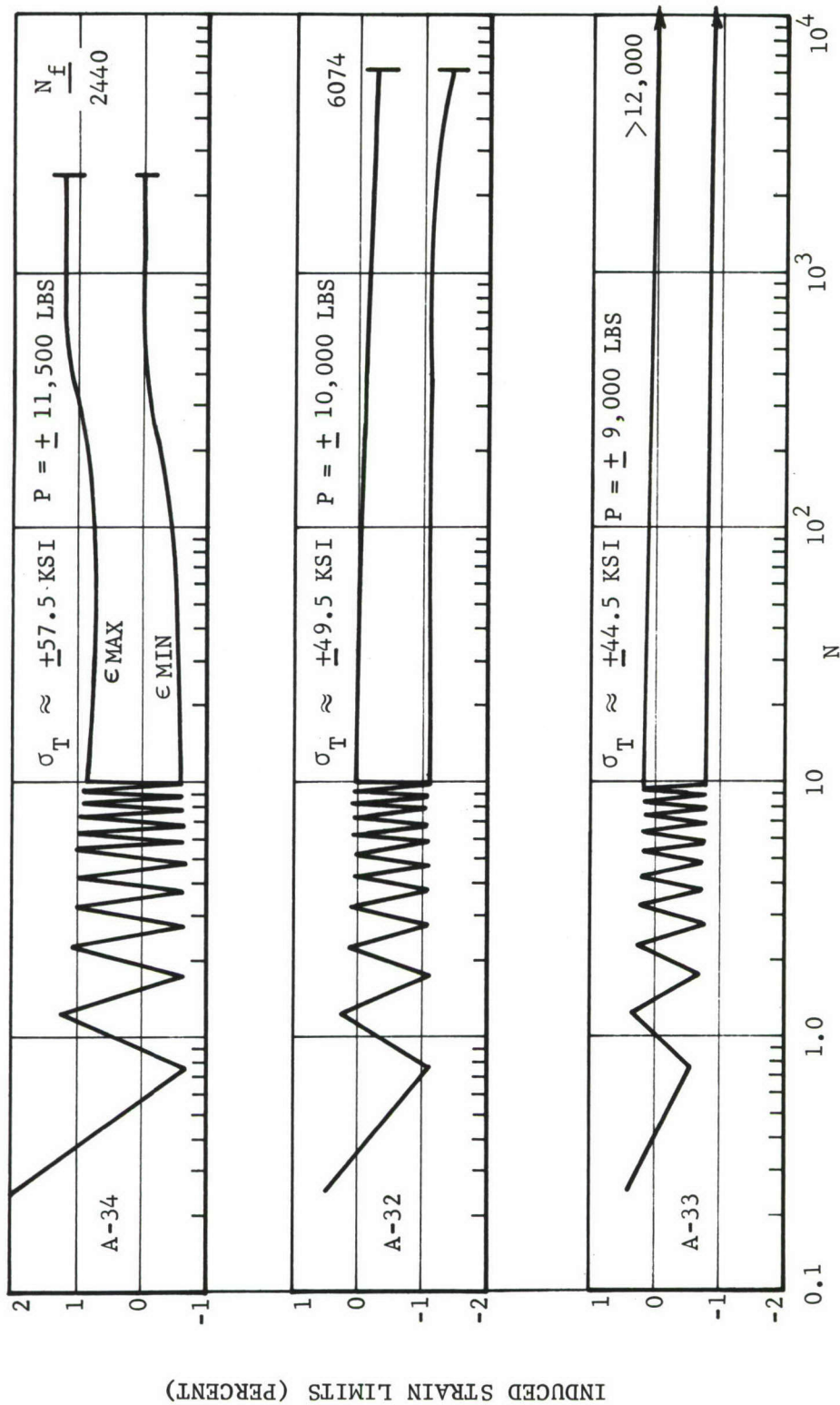


FIGURE 11. STRAIN LIMIT VARIATIONS FOR 2024-T351 DURING CYCLES OF CONSTANT LOAD RANGE ($R_p = -1$)

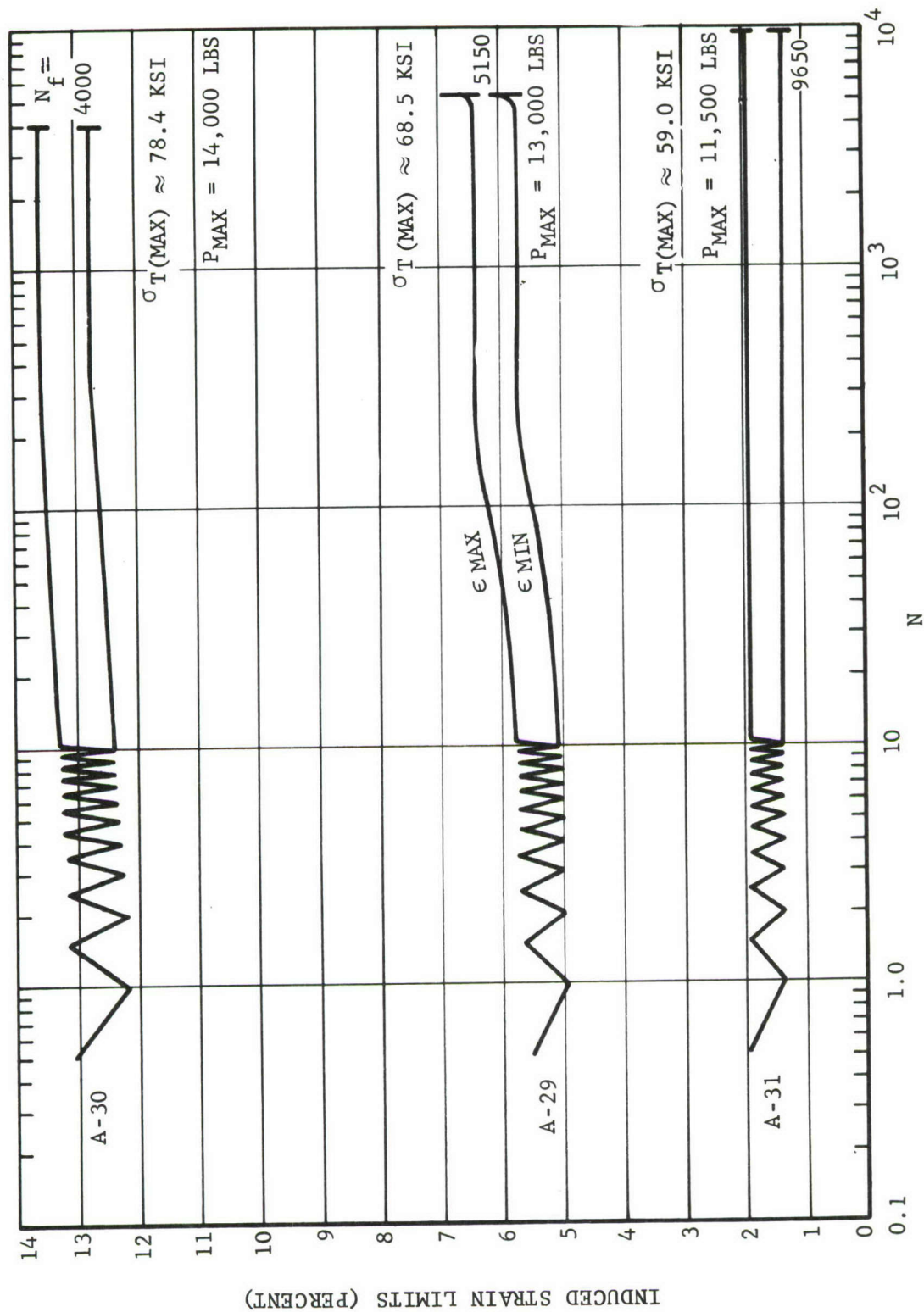


FIGURE 12. STRAIN LIMIT VARIATIONS FOR 2024-T351 DURING CYCLES OF CONSTANT LOAD RANGE ($R_p = 0$)

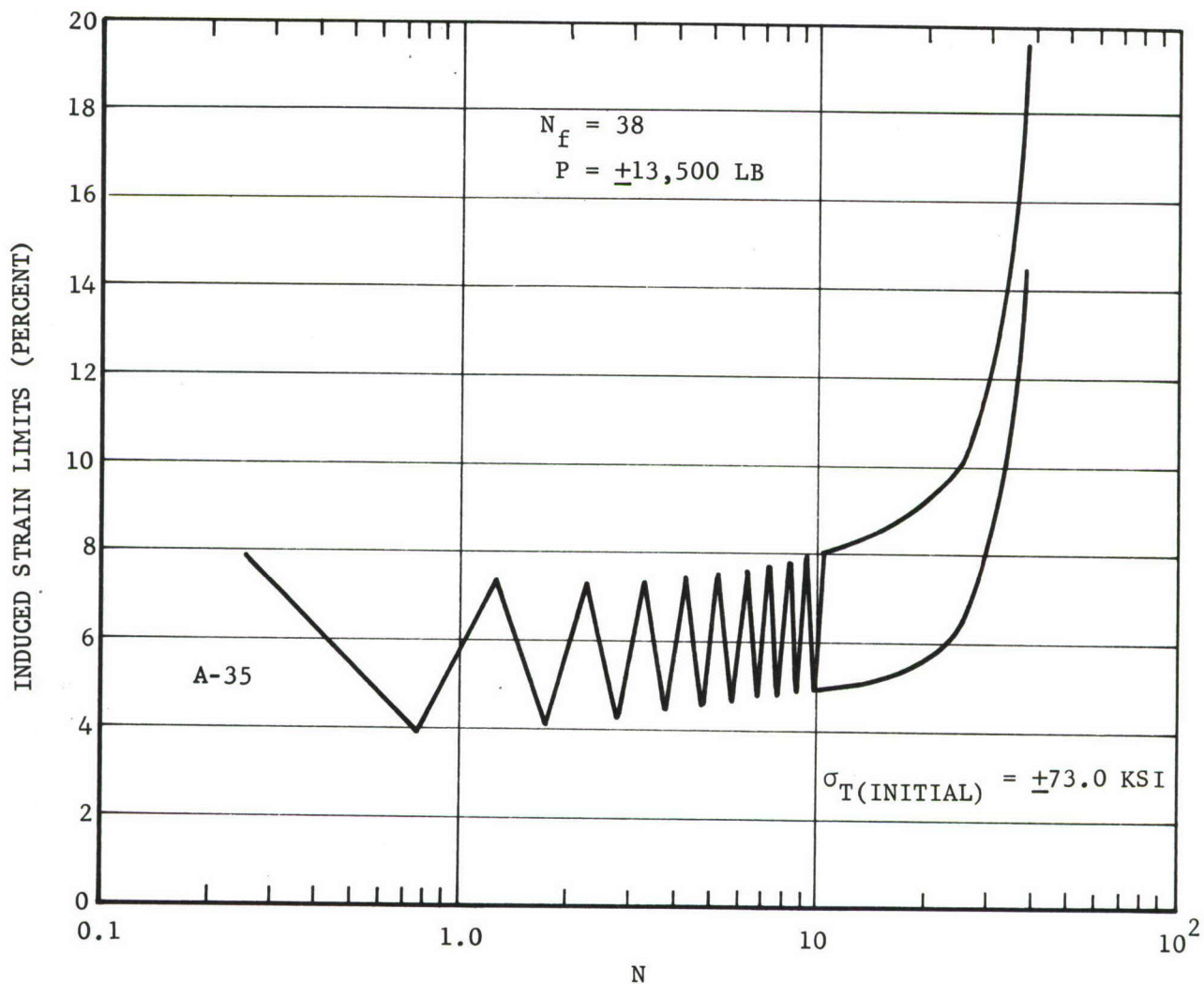


FIGURE 13. STRAIN LIMIT VARIATIONS FOR 2024-T351 DURING CYCLES OF CONSTANT LOAD RANGE ($R_P = -1$)

compression instability. Creep failure was considered to have occurred when the specimen could no longer accept the peak load of the cycle. At this point each specimen began to neck down, and failure was carried to completion by statically pulling the specimen to fracture in tension.

The cyclic creep experienced by hard copper is shown by the drum-recording reproduced in Figure 14. The hysteresis action is displayed from the first cycle to the last cycle which just preceded neck-down. Manual loading was required for the last few cycles since the sharply increased creep rate would have required continuous adjustment of the automatic load limits of the test machine. The point at which the mechanical extensometer switched from high to low magnification is clearly shown in the figure.

The creep strains induced in the hard copper by the cycles of constant load-range are shown in Figures 15 through 17. The maximum values of strain and the related alternating strains have been plotted against the corresponding cycles. It can be noted from the figures that the alternating strain remained constant during the period of slower creep; however, during the final stage of creep, the rapid rise of the peak strain was soon reflected in the alternating value. The last cycle of the creep process (at onset of necking) always occurred when the magnitude of the peak stress of the cycle reached the value corresponding to P_{max} on the true stress-true strain plot (Figure 7).

Similar strain variations that were induced in the soft copper by cyclic loads are shown in Figures 18 through 20. The constancy of the alternating strain during large variations in peak strain can again be noted. Regardless of the value of load ratio, R_p , the maximum and minimum strain of the cycle were both positive. The first load application was always in tension; and in the case of soft copper, this initial loading produced sufficient hardening to always insure that the minimum strain of the cycle would remain in tension. For cyclic lifetimes of less than 10^4 cycles, both the maximum and minimum strains inherited large tensile values which differed only by the amount of the alternating strain, $\Delta\epsilon$.

As shown in Figure 18, two specimens buckled during the near-reversed load cycles. These specimens were tested pin-ended, and as the specimens elongated and laterally contracted from the loading, a critical combination of geometry and effective modulus produced the instability. Buckling was only a problem, of course, when a large compressive load was present.

The soft copper specimens did not show the very sharp rise in creep exhibited by hard copper near the failure point. The more gradual creep of the soft copper can be directly associated with the different strain positions of the P_{max} region on the true stress-true strain plots. When the creep process carried the applied stresses into the region of P_{max} , the last cycle was imminent. This explains the constant level of peak strains at creep failure as shown in Figures 19 and 20. An induced peak strain of approximately 40 percent as measured by the extensometer always accompanied the attainment of the "critical" stress level at P_{max} on the true stress-true strain plot. As shown by the true stress-true strain plot in Figure 7, the true strain,

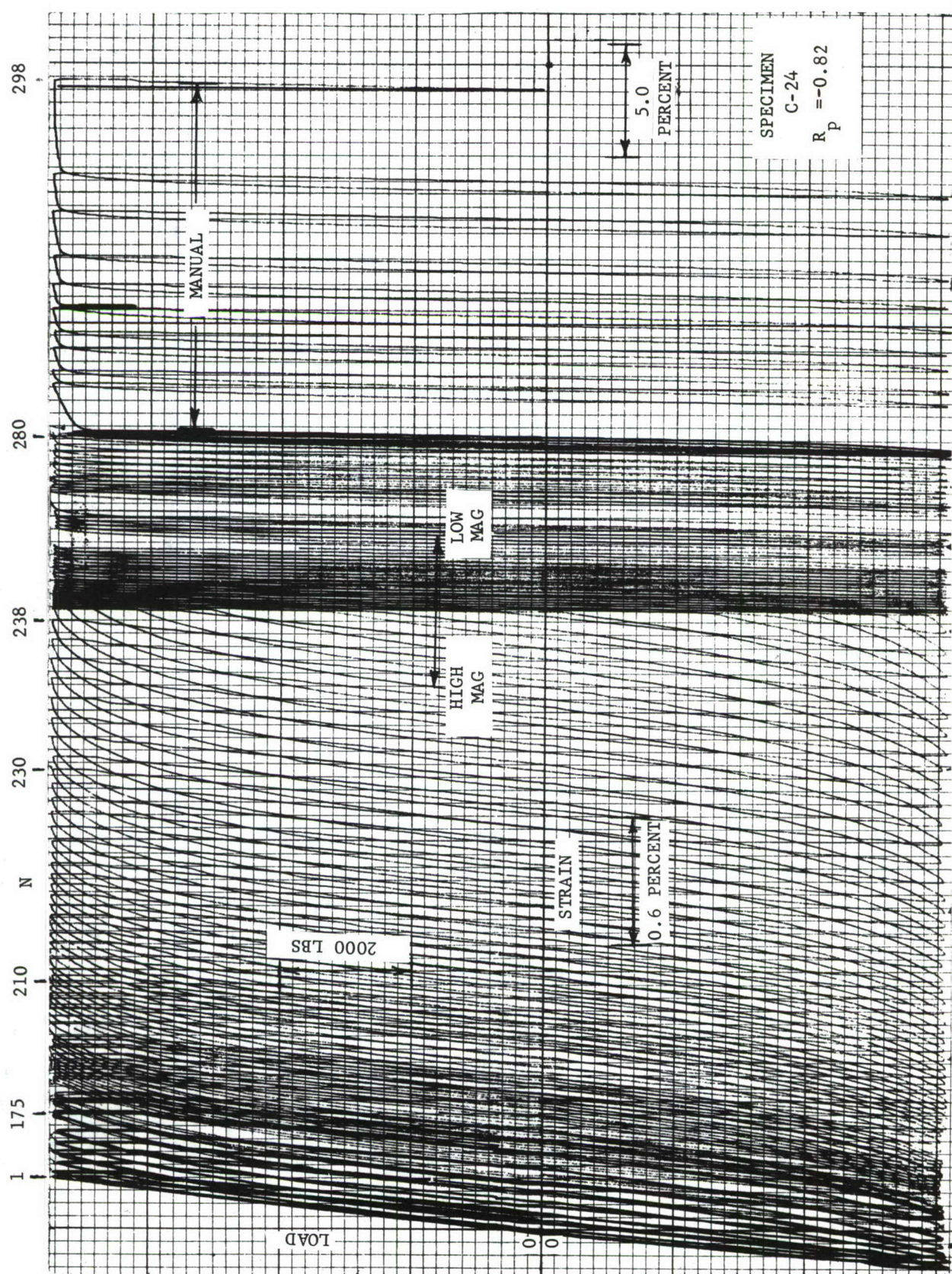


FIGURE 14. TYPICAL RECORDING DURING CYCLIC LOADING OF HARD COPPER

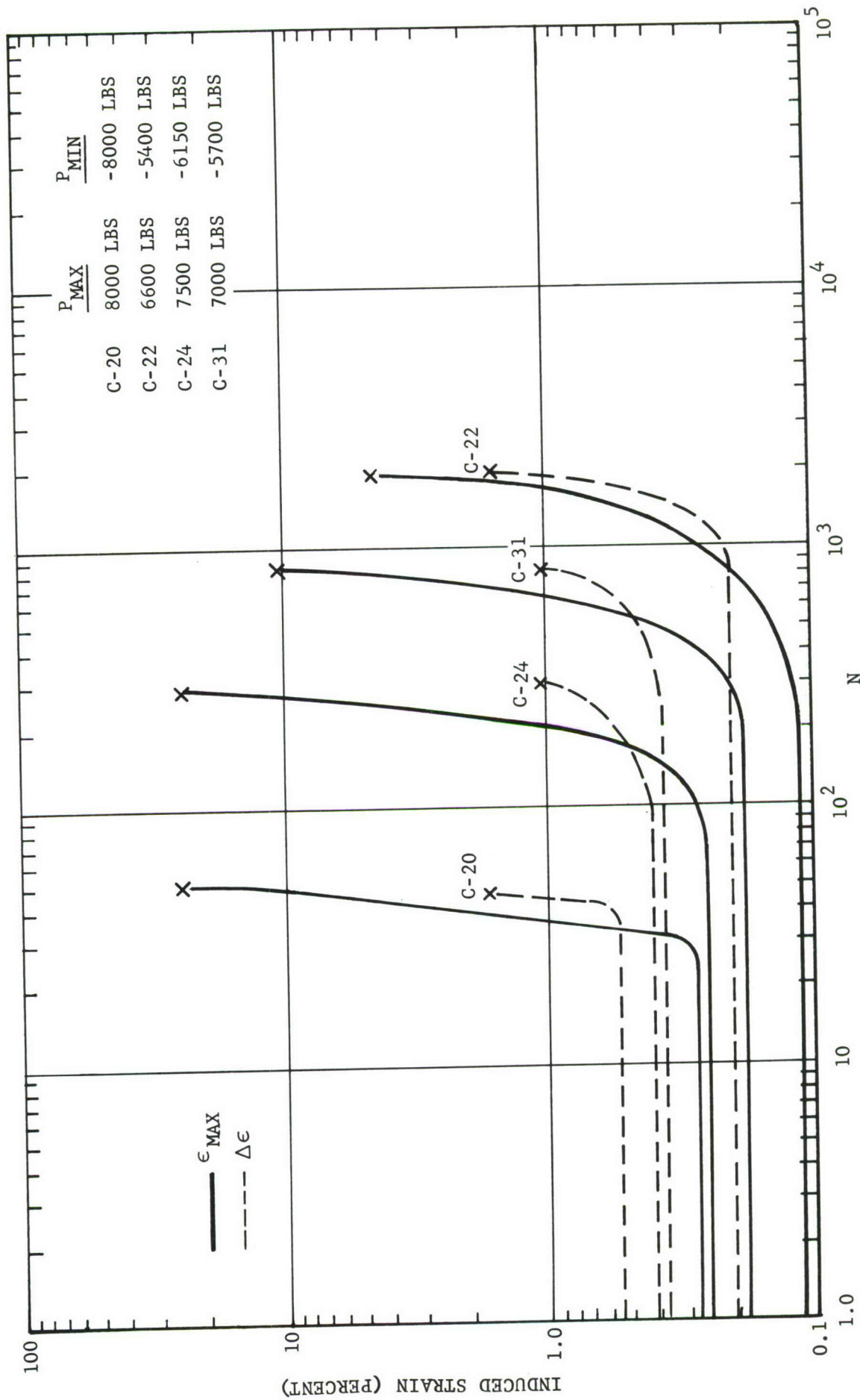


FIGURE 15. STRAIN VARIATIONS FOR HARD COPPER DURING CYCLES OF CONSTANT LOAD RANGE ($R_p = -1.0$ AND -0.82)

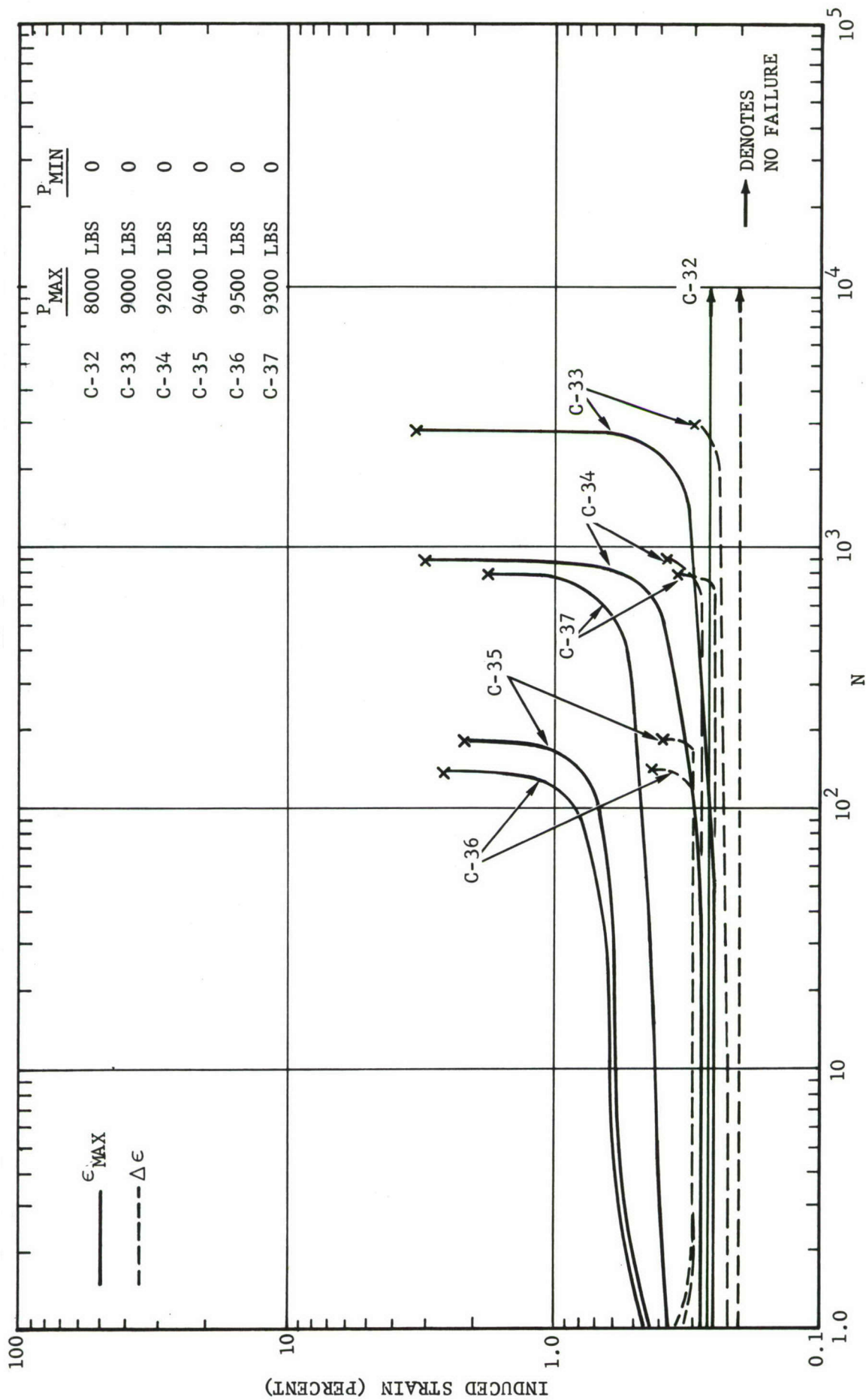


FIGURE 16. STRAIN VARIATIONS FOR HARD COPPER DURING CYCLES OF CONSTANT LOAD RANGE ($R_p = 0.0$)

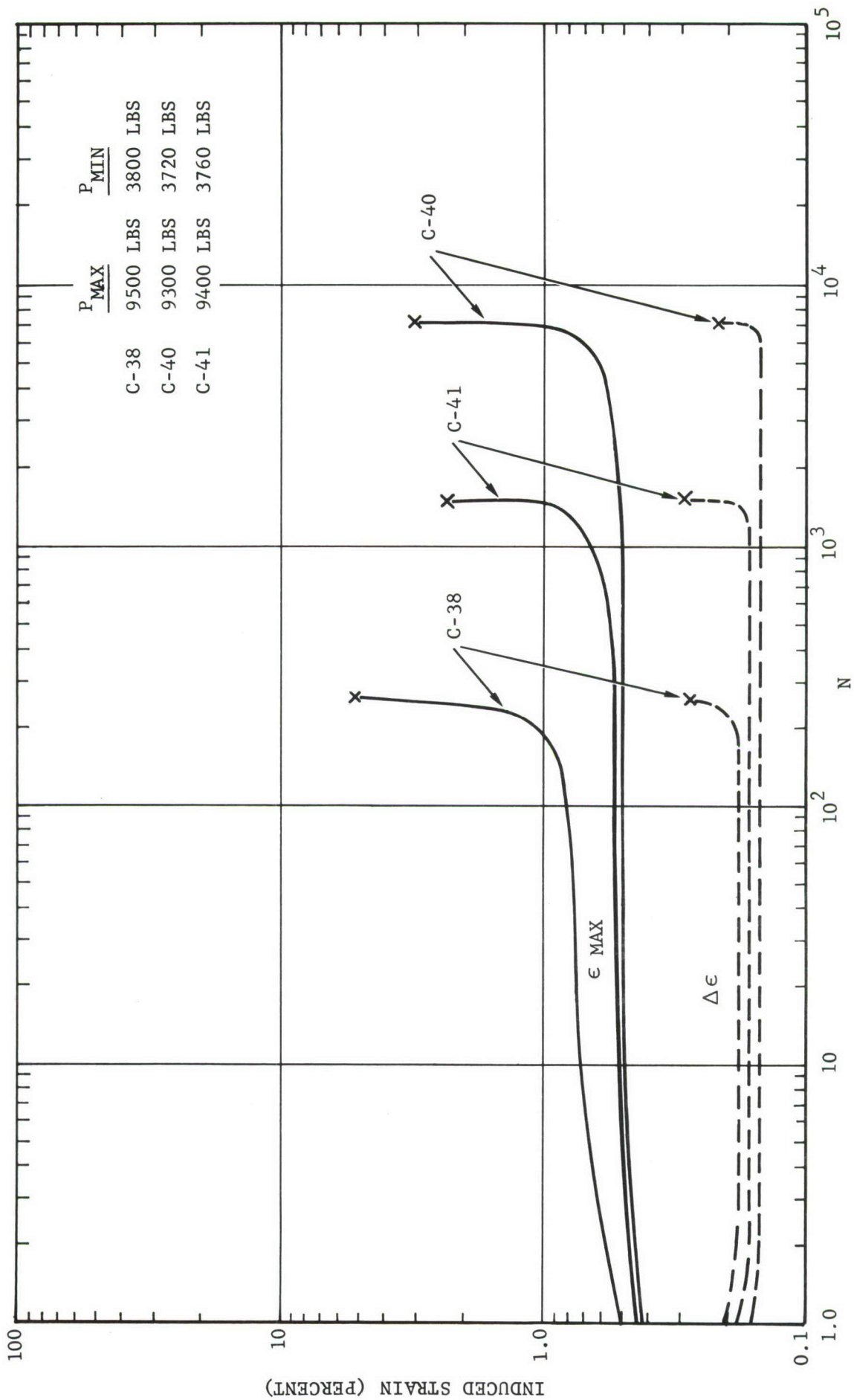


FIGURE 17. STRAIN VARIATIONS FOR HARD COPPER DURING CYCLES OF CONSTANT LOAD RANGE ($R_p = +0.4$)

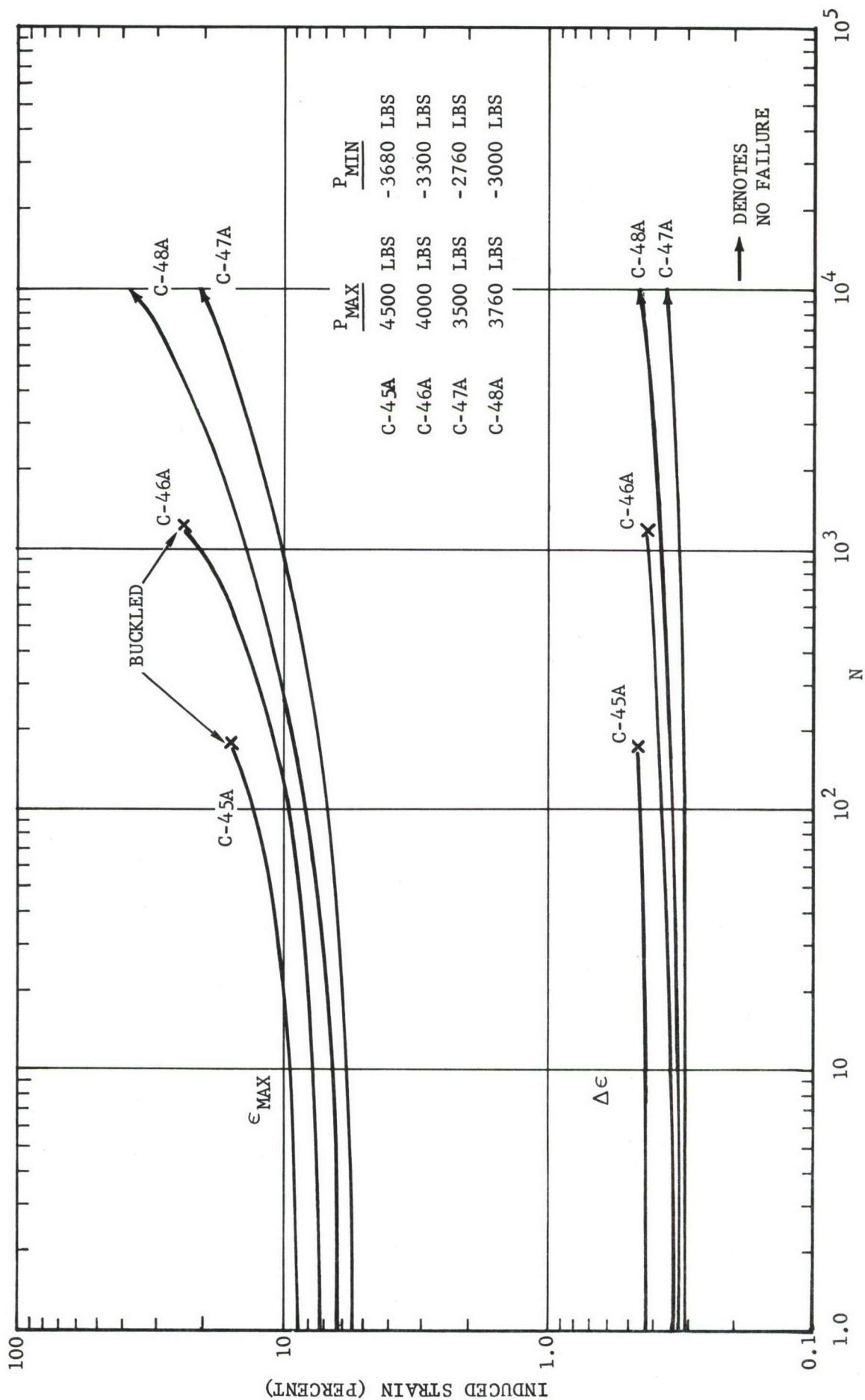


FIGURE 18. STRAIN VARIATIONS FOR SOFT COPPER DURING CYCLES OF CONSTANT LOAD RANGE ($R_p \approx -0.8$)

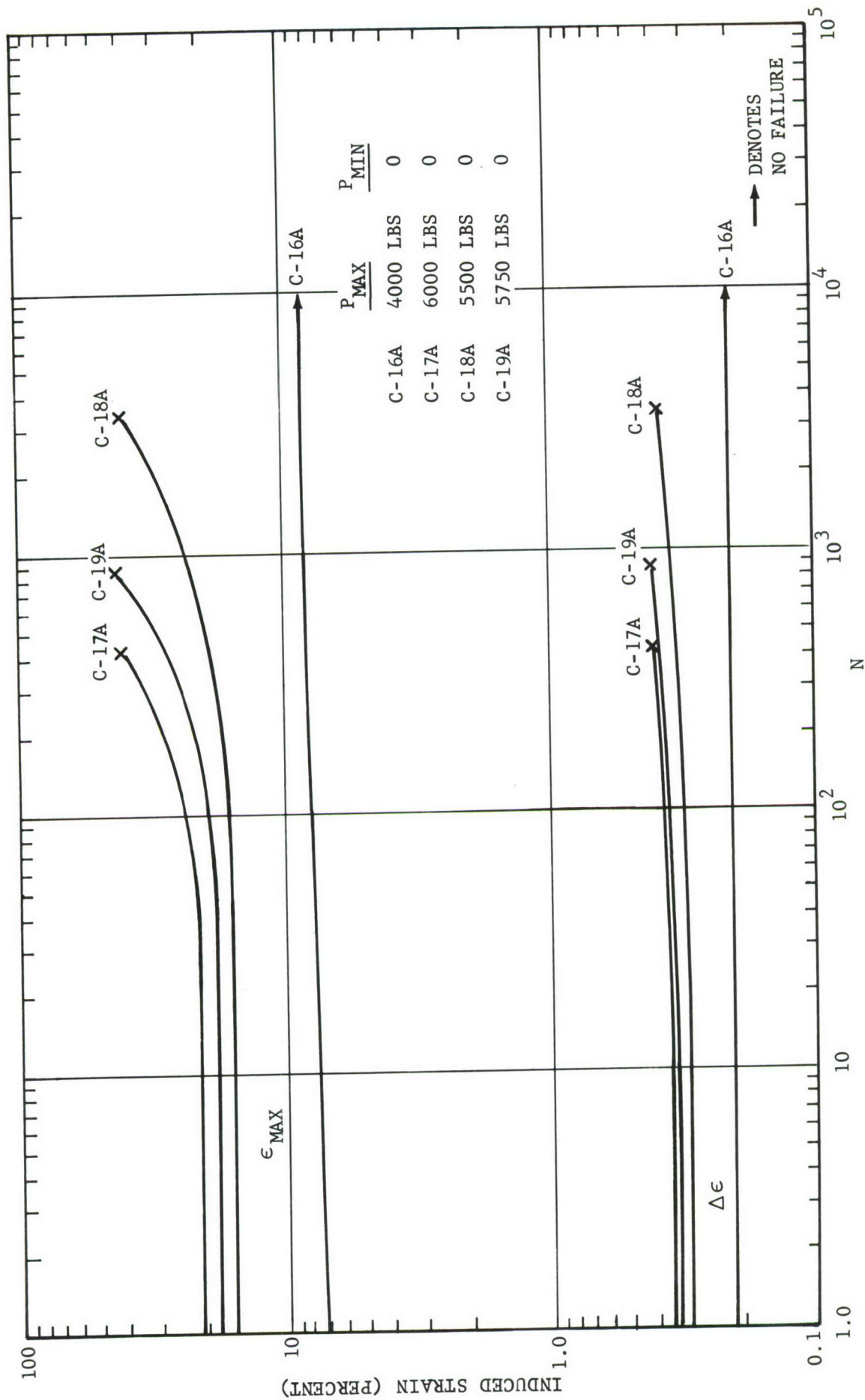


FIGURE 19. STRAIN VARIATIONS FOR SOFT COPPER DURING CYCLES OF CONSTANT LOAD RANGE ($R_p = 0.0$)

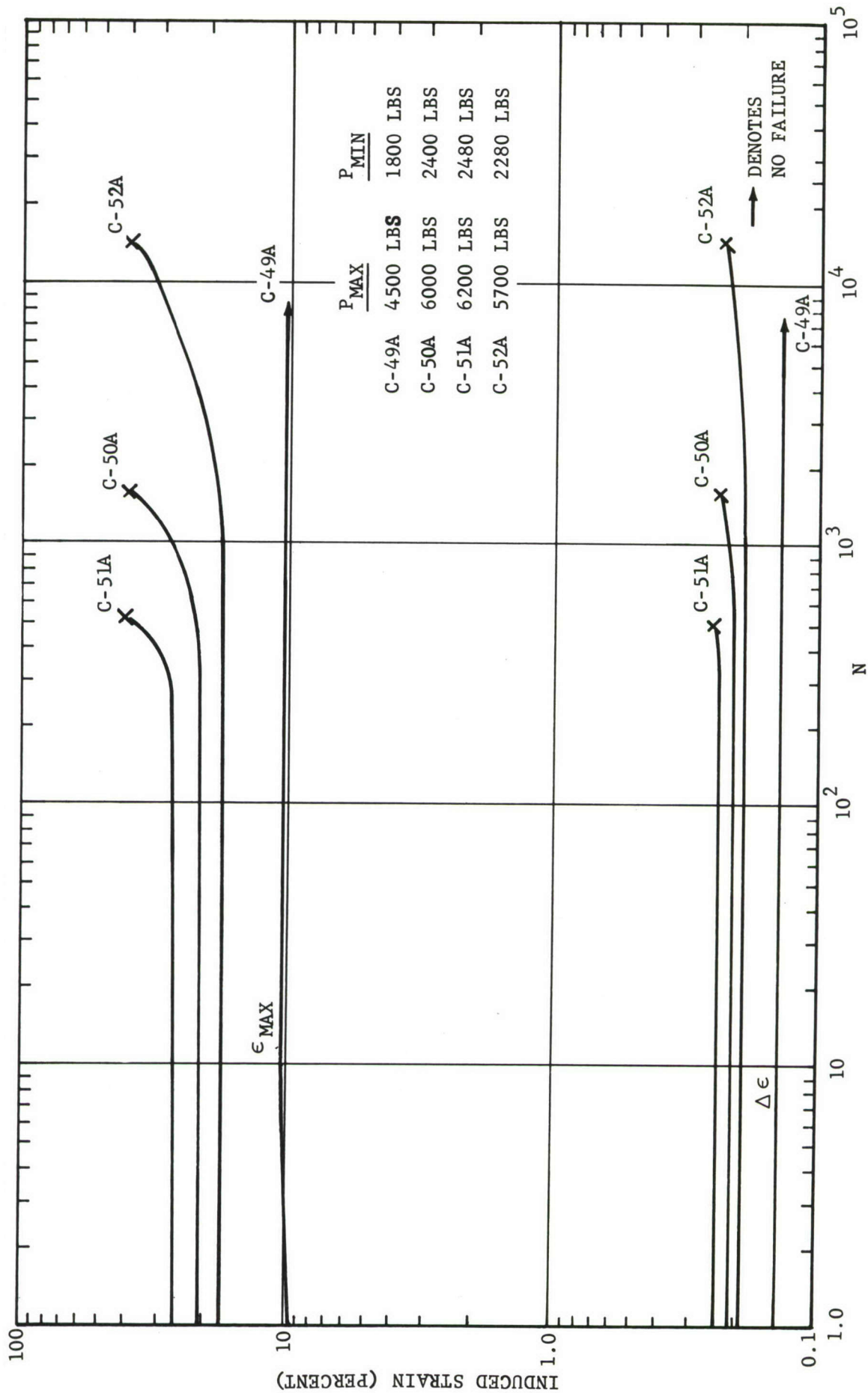


FIGURE 20. STRAIN VARIATIONS FOR SOFT COPPER DURING CYCLES OF CONSTANT LOAD RANGE ($R_p = 0.4$)

ϵ_{ln} , is also near 40 percent when the "critical" stress is reached for soft copper. This coincidence is related to the uniform nature of straining shown by soft copper. That is, up to cyclic creep strains near 50 percent, the extensometer readings reflected a constant volume deformation without a localized necking-down region affecting the uniformity of the strains.

4.2.4 TEMPERATURE-RISE TEST RESULTS

Although the cyclic creep exhibited by the aluminum alloy and OFHC copper specimens was suspected to be the result of gradually accumulating, irreversible, elongations related to second-order deformation processes (Reference 40), a short series of tests were performed on two soft copper and one hard copper specimen to determine if a significant temperature-rise existed in the specimens.

On the first soft copper specimen (C-54A), repeated loads between zero and 5750 pounds were applied at about 10 or 11 cycles per minute. The eventual cyclic life was 945 cycles. (The strain history of specimen C-19A shown in Figure 19 was almost exactly that of the present specimen.) Two thermocouples, mounted at the center and at one end of the gage length, showed no temperature rise up to 740 cycles. The thermocouples had been attached by bonding with an adhesive, and at the 740th cycle the thermocouples became unbonded due to the excessive surface strain.

Since some temperature rise in the specimen was expected (even though small) during the cyclic loading, the manner of mounting the thermocouple became suspect. Therefore, on the second soft copper specimen (C-53A) the thermocouples were attached mechanically as discussed in Section 3.3. Nevertheless, during cycles between zero and 5600 pounds at 11 cycles per minute, no temperature rise could be sensed. The cyclic life of 1818 cycles corresponded to the point at which the upper load limit could no longer be supported.

The same mechanical scheme for attaching the thermocouples was employed on the third specimen of hard copper (C-57). This specimen was cycled between zero and 9000 pounds at 10 cycles per minute. The cyclic life was found to be 1565 cycles. Again, no temperature rise could be measured.

The experimental set-up employed in the temperature-rise tests was by no means capable of precise studies of very small temperature rises. No attempt was made to insulate the ends of the specimens from the grips or to minimize the circulation of air about the test set-up. The instrumentation was capable of detecting $\pm 1/2$ degree F temperature changes about ambient; therefore, it was concluded that if a temperature rise existed during the cyclic tests it was less than about one degree and evidently contributed insignificantly to the cyclic creep.

4.3 TEST RESULTS DURING CYCLES OF CONSTANT STRAIN RANGE

4.3.1 GENERAL FEATURES

The controlled strain range test appears to be the better method for studying material behavior in the low-cycle fatigue range. When the strain limits are fixed, the effects of cyclic creep are eliminated, and the true features

of work-hardening and softening can be brought into focus. Whereas the cyclic load tests offered little or no control over either stress or strain, the constant strain-range test essentially controlled both. The strain limits, of course, were under direct control while the stress limits were held within stable magnitudes.

The soft- and hard-copper materials showed a very definite saturation hardening or softening, respectively, with the application of strain cycles. Similar saturation levels were exhibited by the two conditions of the 2024 aluminum alloy, although much less pronounced. In general, a stabilization at the peak stress level was accompanied by a stabilization at the minimum level of stress. During the hardening or softening process for each material, it was found that the range of stress adjusted very close to a complete reversal position, regardless of the strain ratio, R_ϵ . However, when fatigue failure occurred near 10^4 cycles, and beyond, it was found that the plastic component accompanying the smaller ranges of strain was insufficient to permit adjustment to stress-level symmetry. Such constraint in the attainment of a complete stress relaxation was most pronounced in the less ductile aluminum alloys.

Compression instability* was experienced in a number of specimens during the constant strain-range tests. As indicated above, the materials adjusted to completely reversed stress levels regardless of the strain ratio. Therefore, compressive stresses were invariably present and instability was potentially a problem. The larger the strain range, the larger the induced compressive stress and the greater the susceptibility to buckling. Buckling was found to be related not only to the peak compression stress level, σ_c , but also to the tangent modulus, E_{tan} , of the hysteresis loop measured at the point of peak compression. As in the case of unidirectionally loaded columns, once a critical value of the ratio, σ_c/E_{tan} , is reached, buckling ensues. In the cyclic load tests, however, these critical conditions can be developed through the changing shape and size of the compression-half of the hysteresis loop.

In the constant-strain tests on soft- and hard-copper, both the compressive stress and the tangent modulus changed considerably during the early cycles. As the soft-copper strain hardened, the peak compressive stress sharply increased by a factor of two to four while the tangent modulus remained reasonably constant. In the case of hard-copper, the peak compressive stress diminished during the softening process by about 30 percent while the tangent modulus decreased by a factor of two or three. Therefore, in each instance, the cycle-induced changes in stress and modulus led to ratios that approached the critical value. Even strain ranges of intermediate magnitude produced cycle-induced buckling during the early phases of the program when self-aligning, spherical seats were employed at the ends of the specimens. However, by applying loads under fixed-end conditions ($C \approx 4$) in later tests, large strain ranges could be incorporated without buckling.

*Compression instability denotes buckling or column failure.

In no instance did the aluminum alloys show cycle-dependent buckling. That is, if the aluminum specimens did not buckle on the first application of compressive load, the susceptibility to buckling had passed. Evidently, the absence of cycle-dependent buckling in the aluminum alloys is related to the combination of hardening and increased tangent modulus occurring during the cyclic straining.

4.3.2 ALUMINUM ALLOY RESULTS

Drum-recordings of hysteresis loops obtained for the 2024-0 and 2024-T351 aluminum alloy in a typical test are shown in Figure 21. These were obtained during fixed strain-ranges of nearly the same magnitude, however, it should be noted that the load scale for the traces differ by a factor of 2.5. As shown by the records, the maximum and minimum stress levels were cycle dependent with the greater changes being experienced at the minimum stress. The greater induced adjustment at the lower stress level was found to be typical of the aluminum alloys for all ranges of strain and strain ratios, except possibly the very large strain ranges which led to failure in less than 100 cycles.

The true stress limit variations for 2024-0 aluminum alloy are shown in Figures 22 through 24. Three values of strain ratio are covered by these figures. When the soft aluminum alloy is viewed only with respect to the maximum stress variation, it would appear that softening has taken place at $R\epsilon \leq 0$, and hardening at $R\epsilon \approx -1$. A complete view of both maximum and minimum stresses shows, however, that hardening has actually taken place under each set of conditions. That is, the range of stress has increased with cycles for a given strain range and the induced mean stress has shifted toward zero. The zig-zag lines and the dashed lines in the figures serve to emphasize the fact that all curves have been generated as a locus of peak stress points, and therefore the curves have little meaning below 10 cycles.

A similar set of curves showing the true stress variations for 2024-T351 aluminum alloy during cycles of constant strain range are shown in Figures 25 through 27. Again, as in the tests on the soft aluminum alloy, the greater stress variation is at the lower peak stress. Also, based upon the increasing range of induced stress for a fixed value of strain range, the hard aluminum alloy work hardened more significantly than the soft alloy.

Under the repetition of the smaller strain ranges which led to fatigue failure near 10^4 cycles, the induced peak stresses were unable to achieve a zero mean stress. These cycles were essentially elastic, with negligible plastic component; therefore, zero mean stress could only be reached at the expense of a diminishing maximum stress which never occurred.

4.3.3 OFHC COPPER RESULTS

The softening and hardening characteristics of hard- and soft-copper, respectively, are shown by the recorder traces in Figure 28. The records were obtained from specimens subjected to strain ratios having a value near

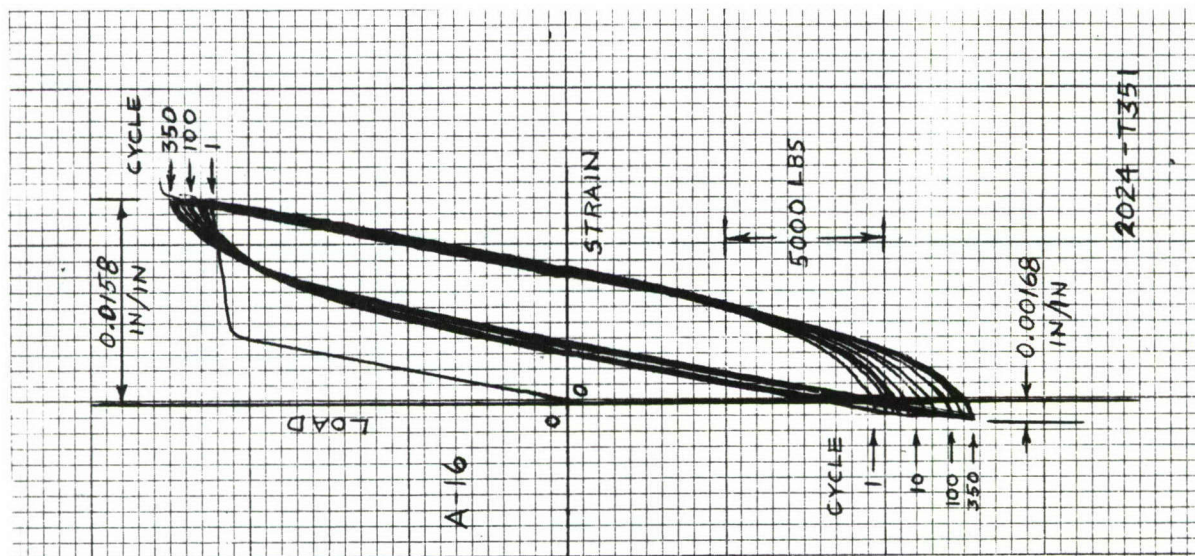
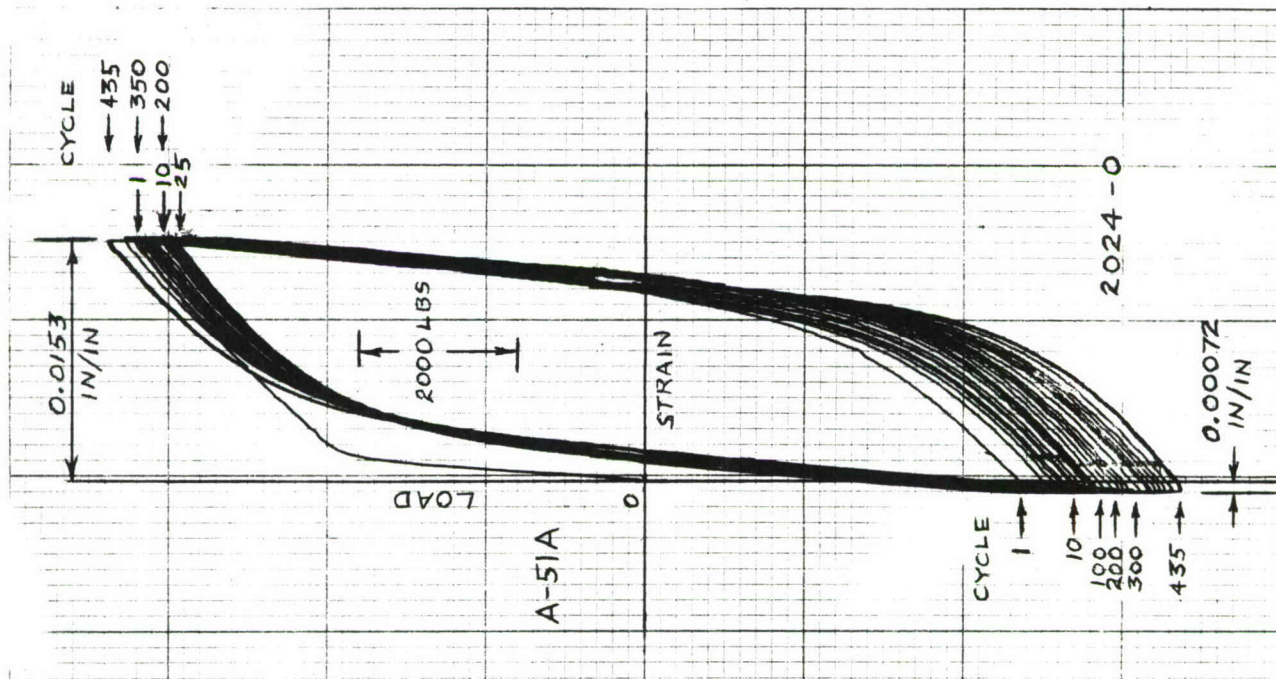


FIGURE 21. DRUM-RECORDINGS OF STRESS (LOAD) VARIATIONS DURING CYCLES OF CONSTANT STRAIN RANGE

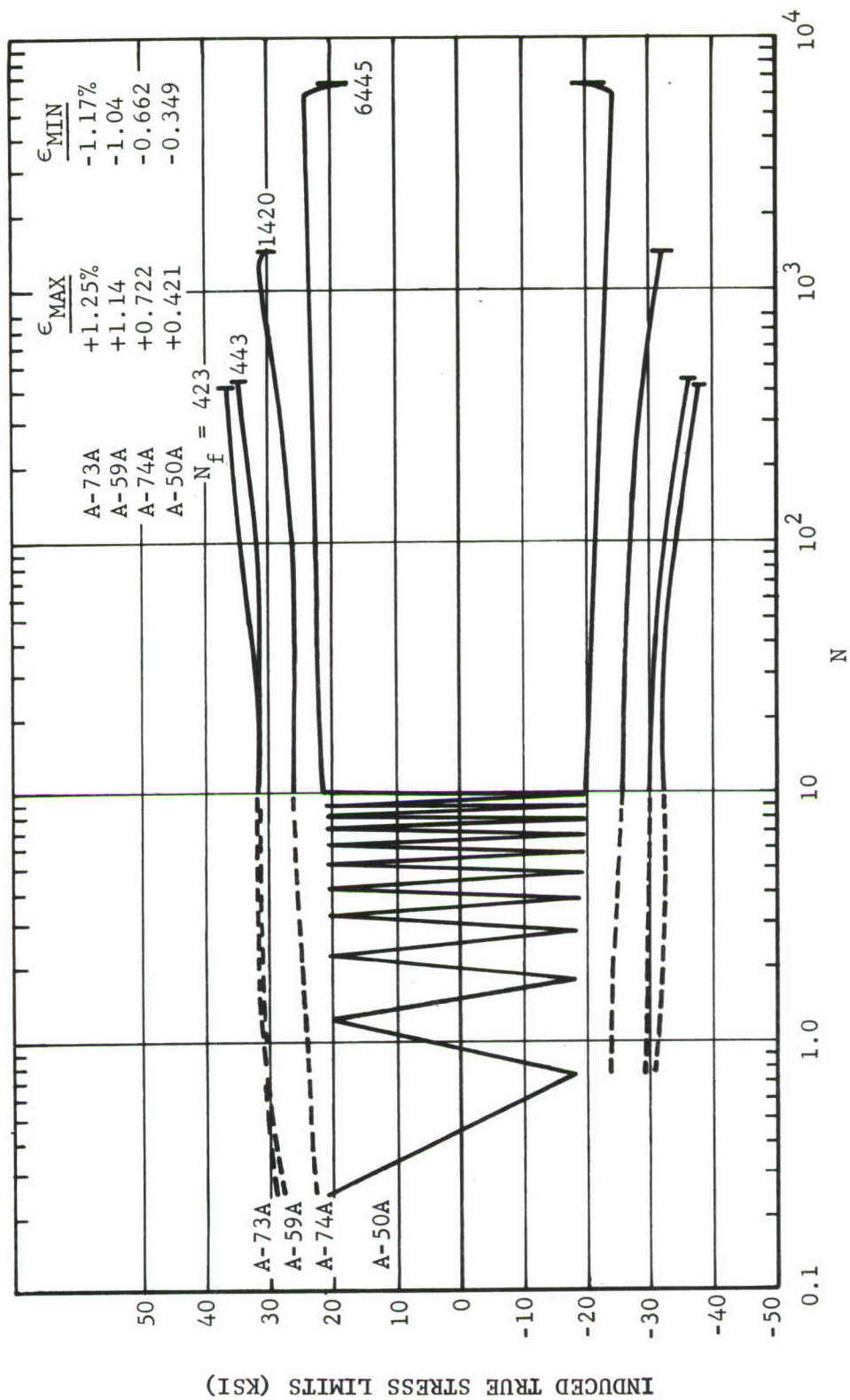


FIGURE 22. STRESS LIMIT VARIATIONS FOR 2024-0 DURING CYCLES OF CONSTANT STRAIN RANGE ($R_{\epsilon} \approx -1$)

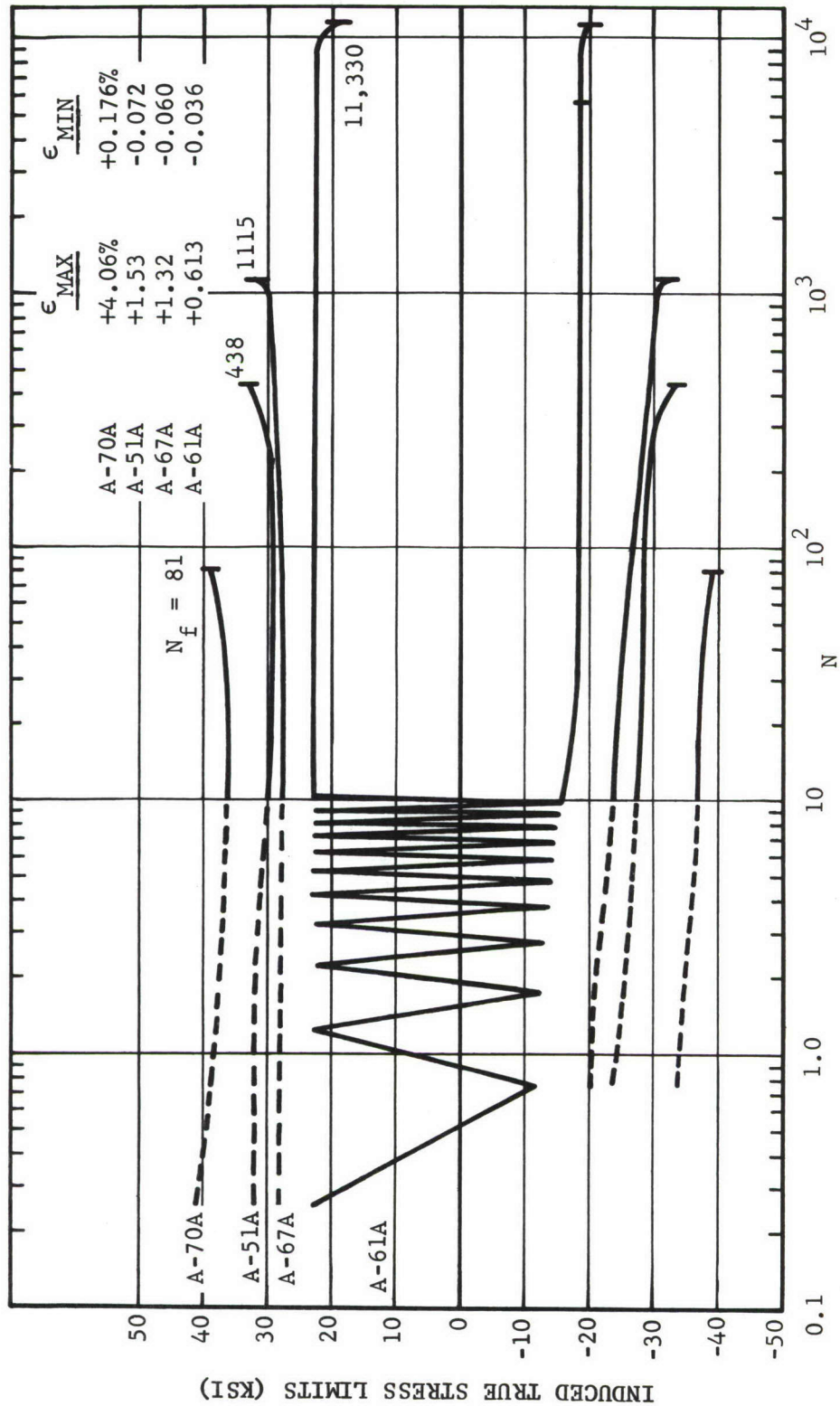


FIGURE 23. STRESS LIMIT VARIATIONS FOR 2024-0 DURING CYCLES OF CONSTANT STRAIN RANGE ($R_\epsilon \approx 0$)

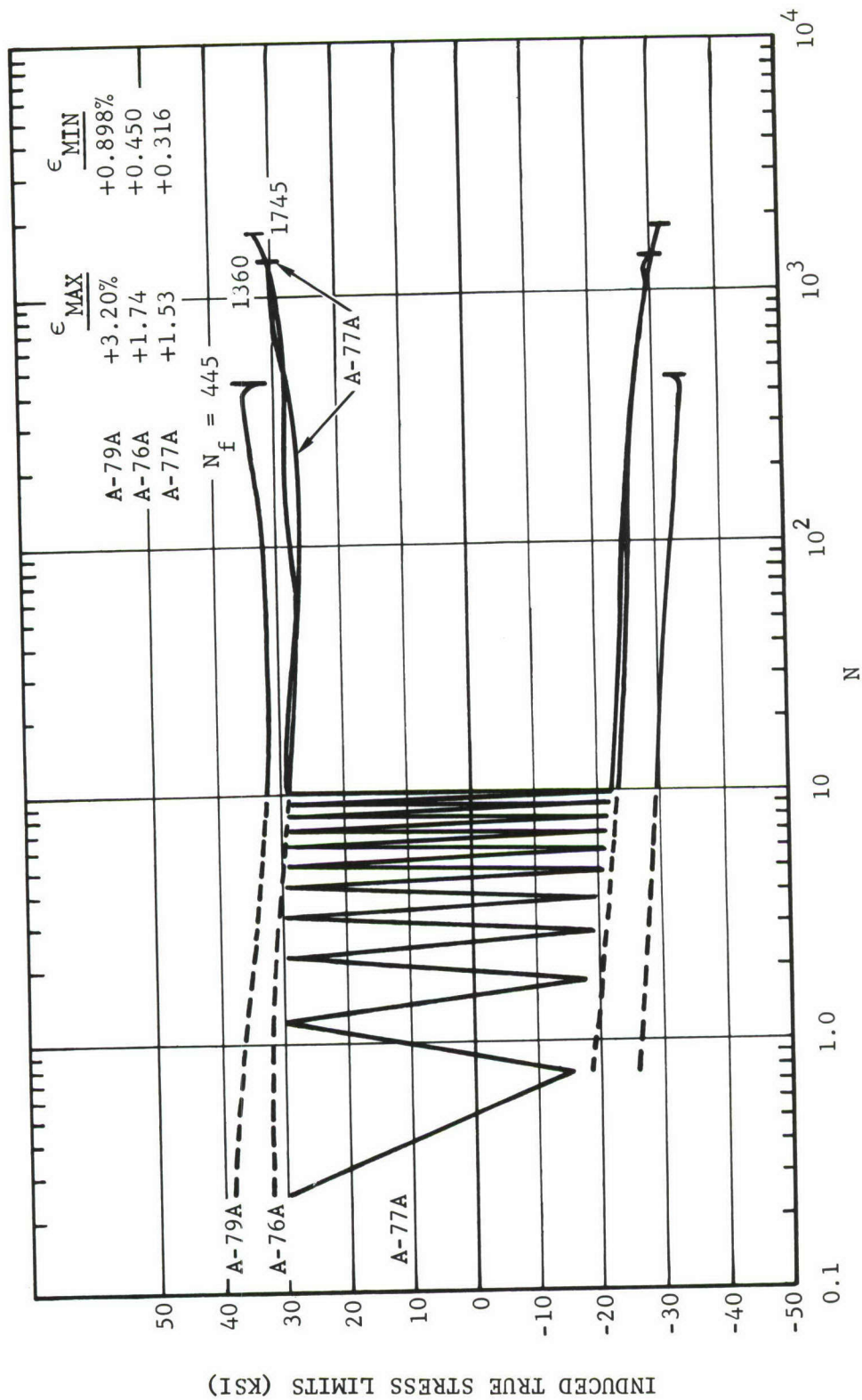


FIGURE 24. STRESS LIMIT VARIATIONS FOR 2024-0 DURING CYCLES OF CONSTANT STRAIN RANGE ($R_\epsilon > 0$)

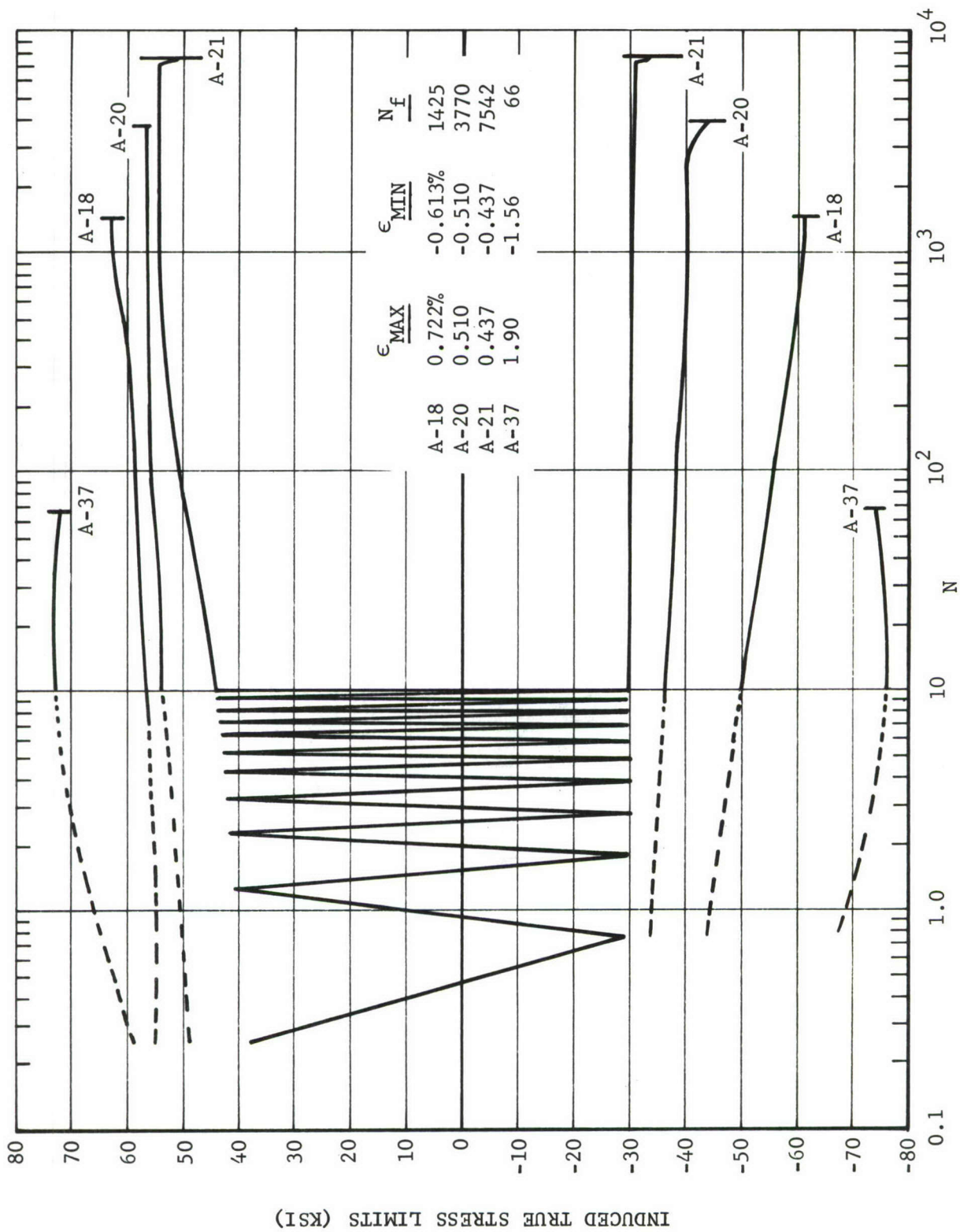


FIGURE 25. STRESS LIMIT VARIATIONS FOR 2024-T351 DURING CYCLES OF CONSTANT STRAIN RANGE ($R_\epsilon \approx -1$)

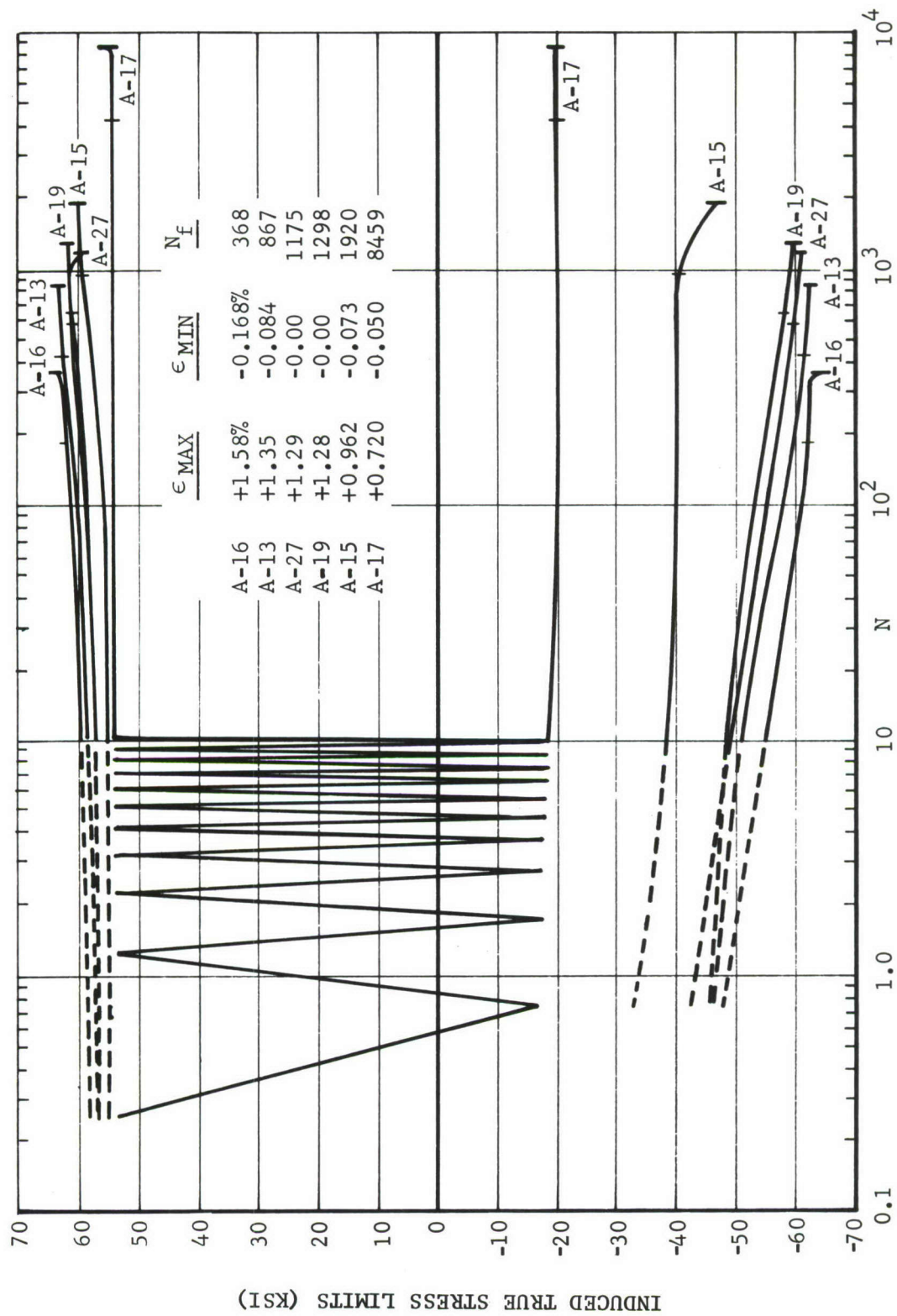


FIGURE 26. STRESS LIMIT VARIATIONS FOR 2024-T351 DURING CYCLES OF
CONSTANT STRAIN RANGE ($R_\epsilon \approx 0$)

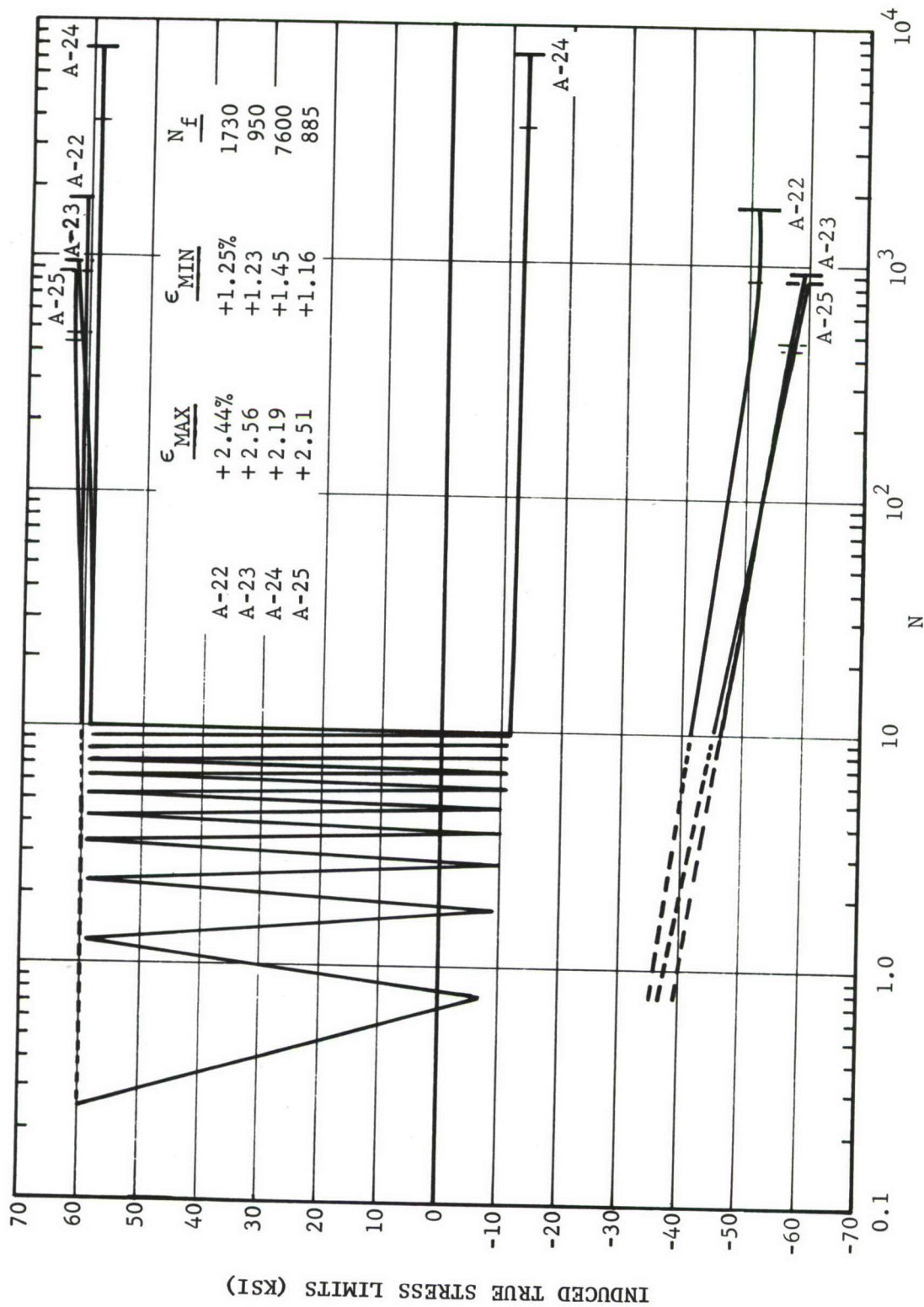


FIGURE 27. STRESS LIMIT VARIATIONS FOR 2024-T351 DURING CYCLES OF CONSTANT STRAIN RANGE ($R_\epsilon > 0$)

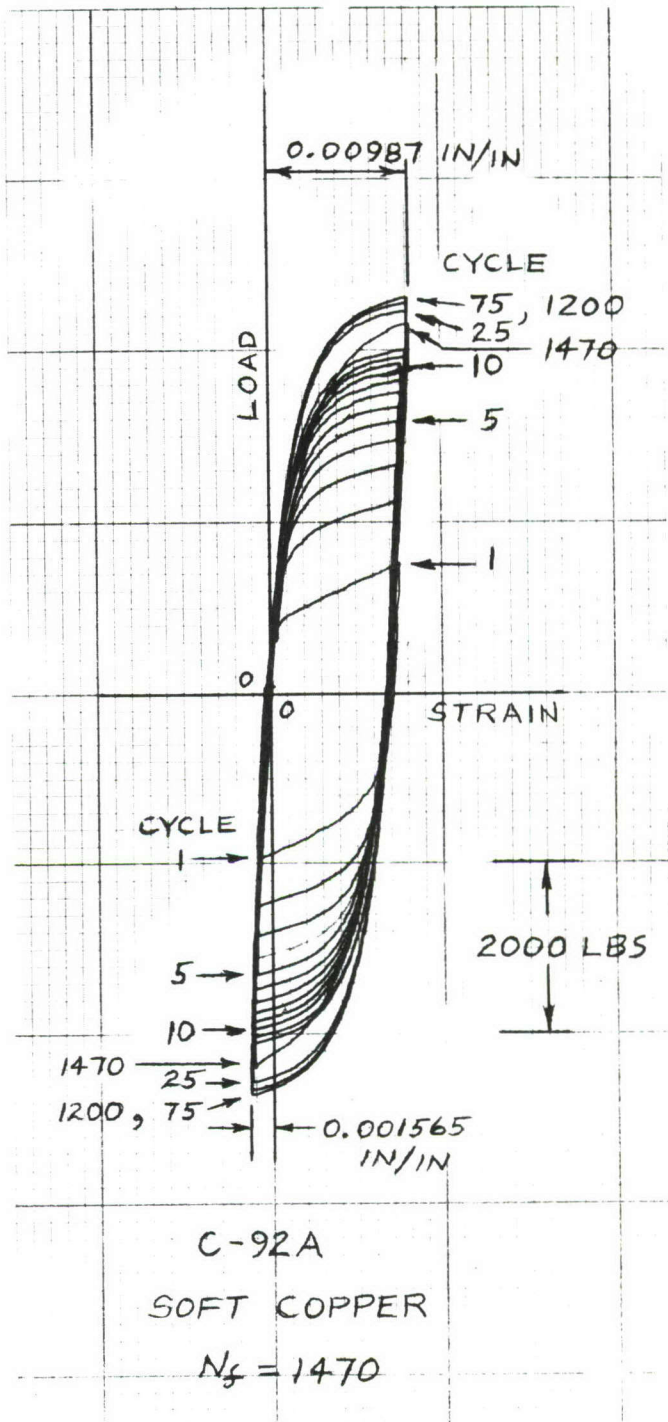
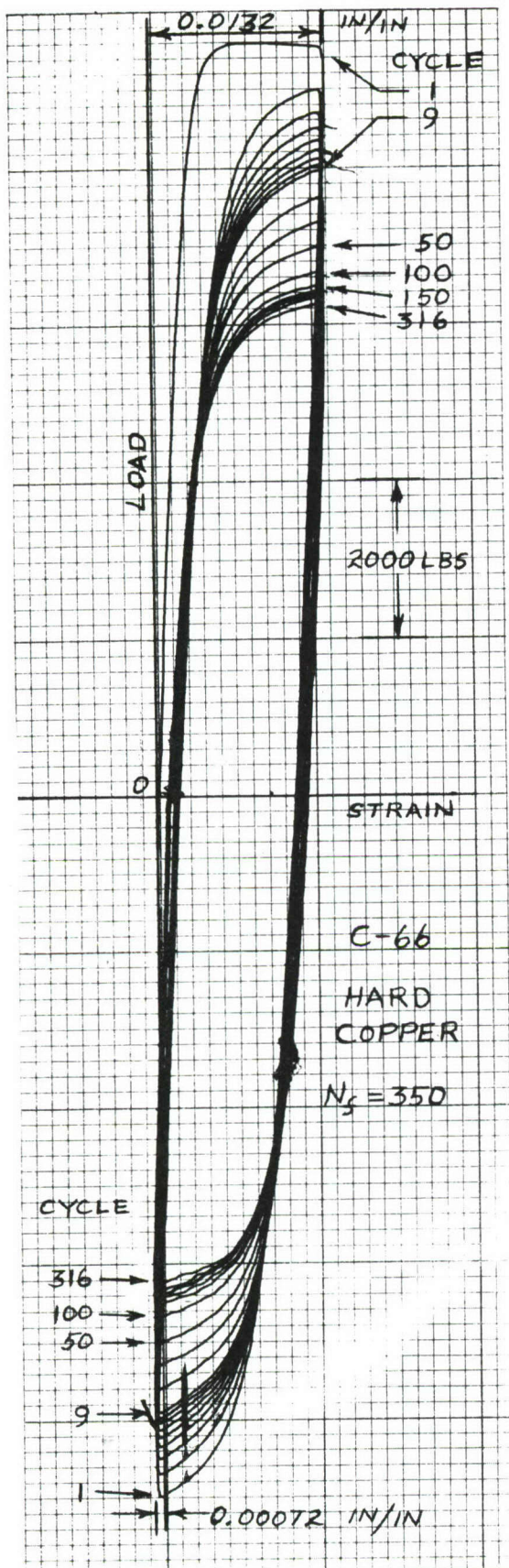


FIGURE 28. DRUM-RECORDINGS SHOWING STRESS (LOAD) VARIATIONS FOR HARD AND SOFT COPPER DURING CYCLES OF CONSTANT STRAIN RANGE

zero. Both the load and strain scales are identical; therefore, direct comparison can be made of the stabilized hysteresis condition eventually reached by the materials. Different fatigue life-times are expressed by the loops; however, it can be noted that the hard and soft conditions of copper approached closely the same magnitude and shape of the stabilized loop. The simultaneous variations in compression stress-level and tangent modulus, referenced earlier with respect to the buckling problem, can also be noted.

The true stress variations for the annealed condition of the OFHC copper are shown in Figures 29 through 31. A large spread in strain ratio is covered by the three figures which permits a number of general observations to be made. Regardless of strain ratio and strain range, it appears that saturation hardening cannot be reached before 100 cycles of cyclic straining. Saturation hardening was very definite for the initially soft copper, and these conditions generally prevailed beyond the half-life point. During the latter half of the fatigue life, it was commonplace to observe a slow rise in stress level followed by an abrupt stress change near the end of the test. A crack was generally visible at the time of the abrupt stress variation but not during the preceding slow rise. The presence of a crack, and the eccentricity it imparted to the axial load path during the tension half of the load cycle, produced a slight lateral deflection and localized yielding that in turn caused significant deviations from the previously stable condition. Therefore, once a crack appeared in the last few percent of the fatigue life, the recorded values of stress and strain have little meaning.

In attempts to achieve fatigue failure below 100 cycles severe buckling generally occurred and caused termination of the test even when the specimens were tested fixed-ended. Specimens C-80A and -85A buckled in this manner. In a number of instances, the buckling was very slight (lateral deflection less than 0.02-inch) and testing was continued to eventual fatigue failure. Specimen C-81A, -92A, -93A, and -99A fell into this category, however in the instance of C-92A and C-93A the buckling was extremely slight and these failures were recorded as pure fatigue failures.

The true stress variations associated with the hard-copper specimens during cycles of constant strain-range are shown in Figures 32 through 34. All specimens shown in these figures produced fatigue failures without the superimposed buckling problem. The softening during cyclic straining was very definite at all values of strain ratio and strain range, but it can be noted that stabilized stress levels were seldom reached in less than 300 cycles. This number of strain-softening cycles is approximately twice that required to strain-harden the soft copper. The asymptotic stress levels reached by the hard-copper correspond closely to those reached by soft-copper, and symmetry about zero stress was almost invariably attained well before the fatigue half-life.

The strong characteristic of materials to seek a hysteresis condition which has stress-level symmetry is forcibly shown by the copper materials. In particular, specimen C-67 of Figure 32A and the three specimens in

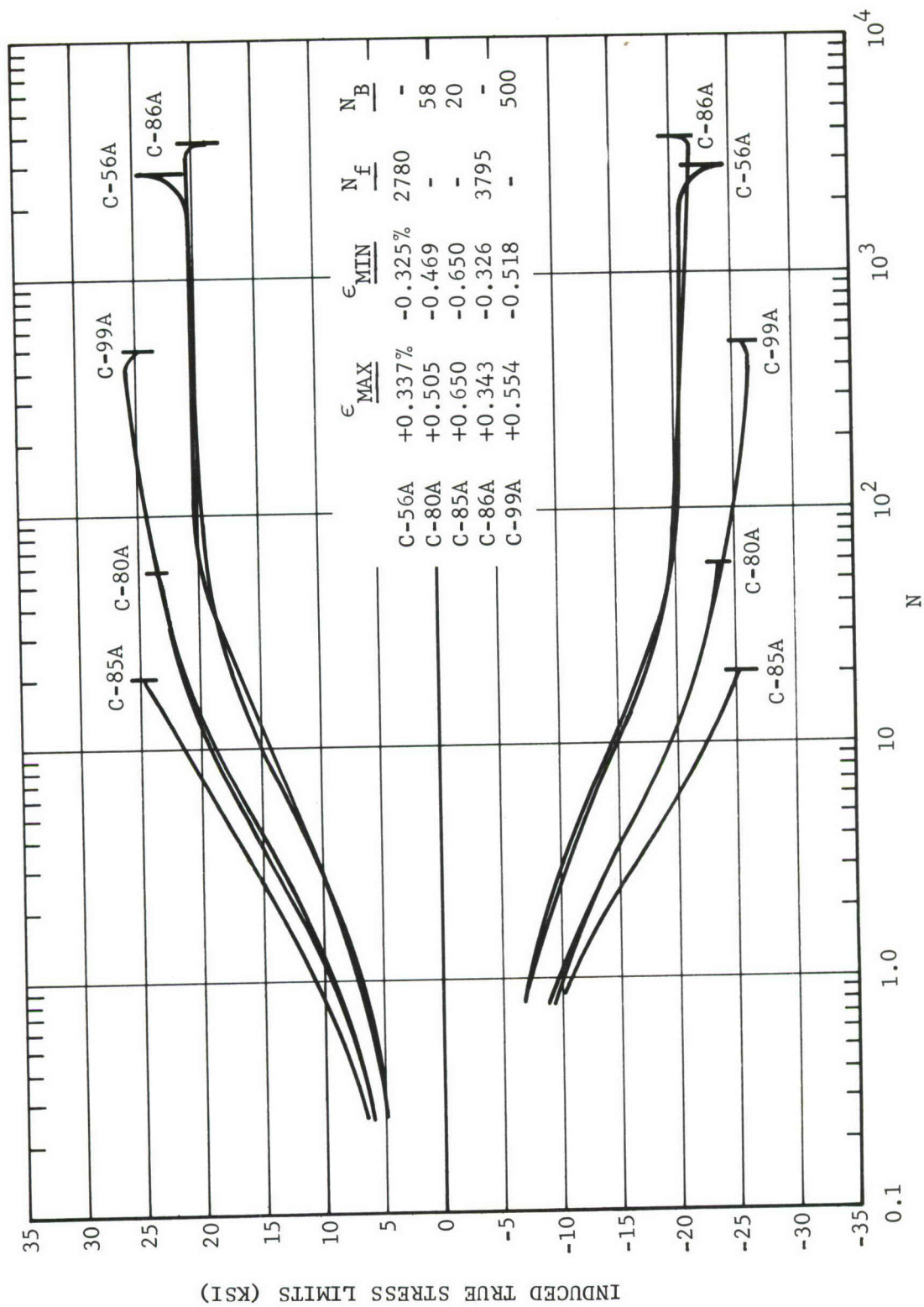


FIGURE 29. STRESS LIMIT VARIATIONS FOR ANNEALED COPPER DURING CYCLES OF
CONSTANT STRAIN RANGE ($R_\epsilon \approx -1$)

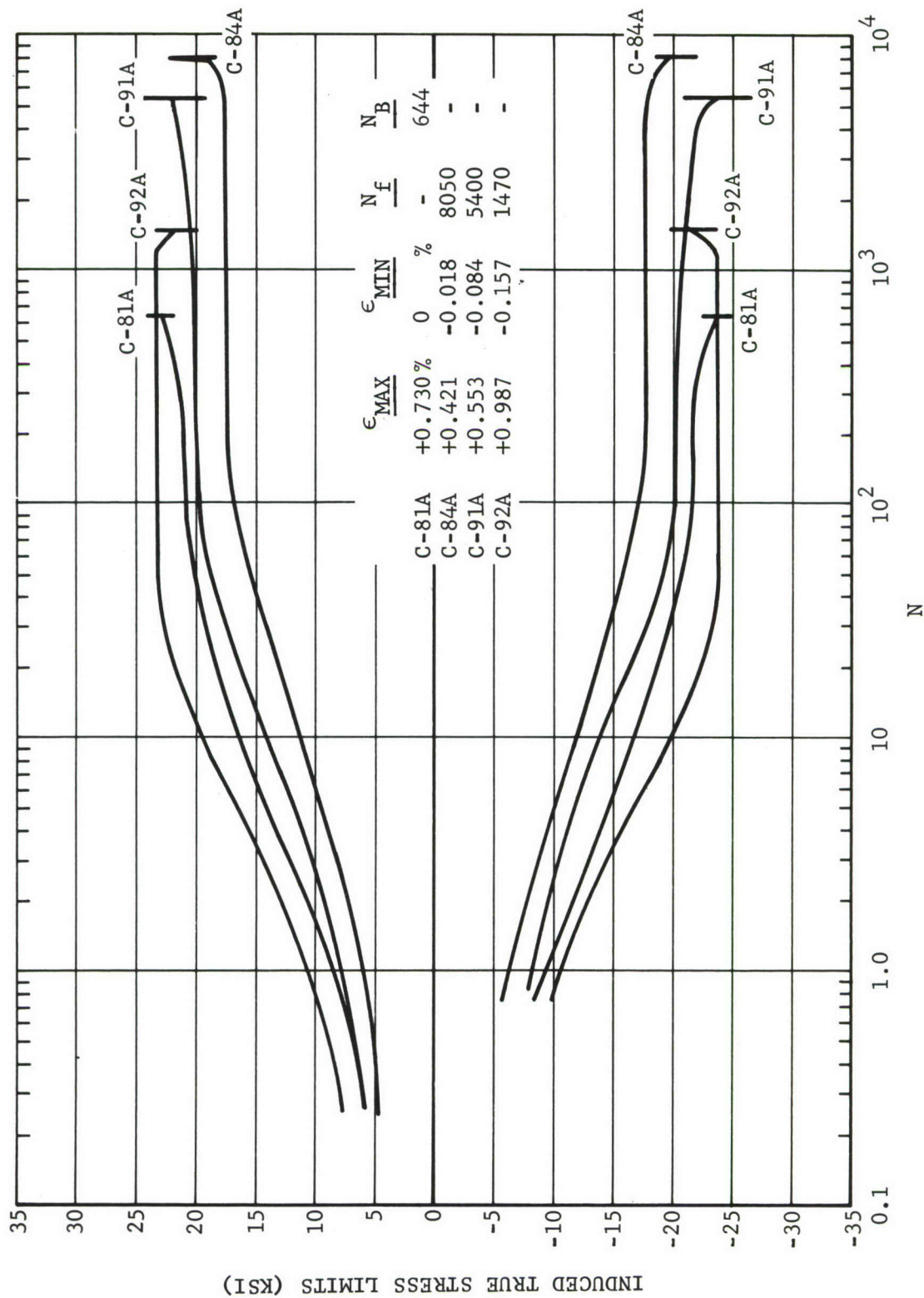


FIGURE 30. STRESS LIMIT VARIATIONS FOR ANNEALED COPPER DURING CYCLES OF
CONSTANT STRAIN RANGE ($R_\epsilon \approx 0$)

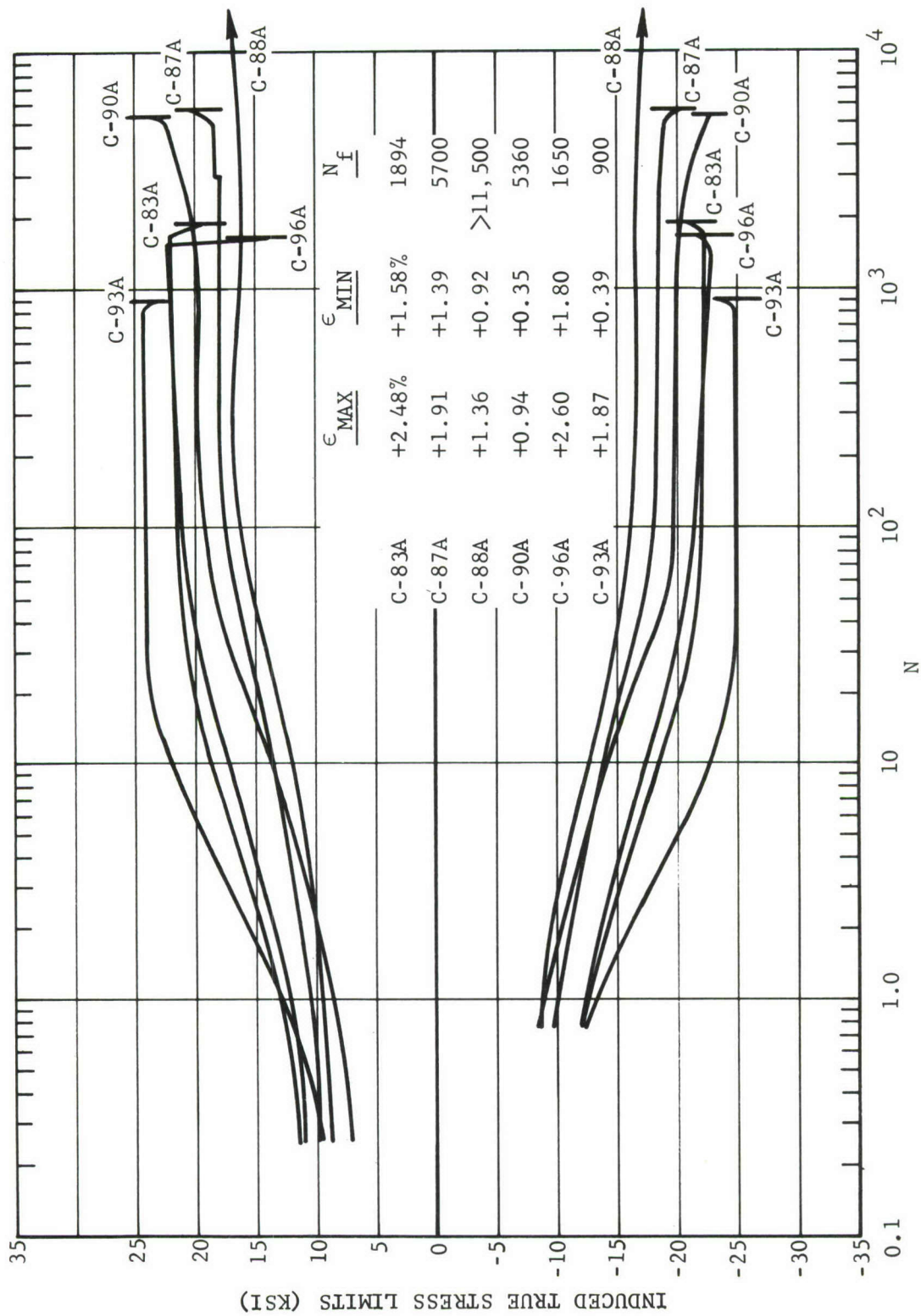


FIGURE 31. STRESS LIMIT VARIATIONS FOR ANNEALED COPPER DURING CYCLES OF CONSTANT STRAIN RANGE ($R_\epsilon > 0$)

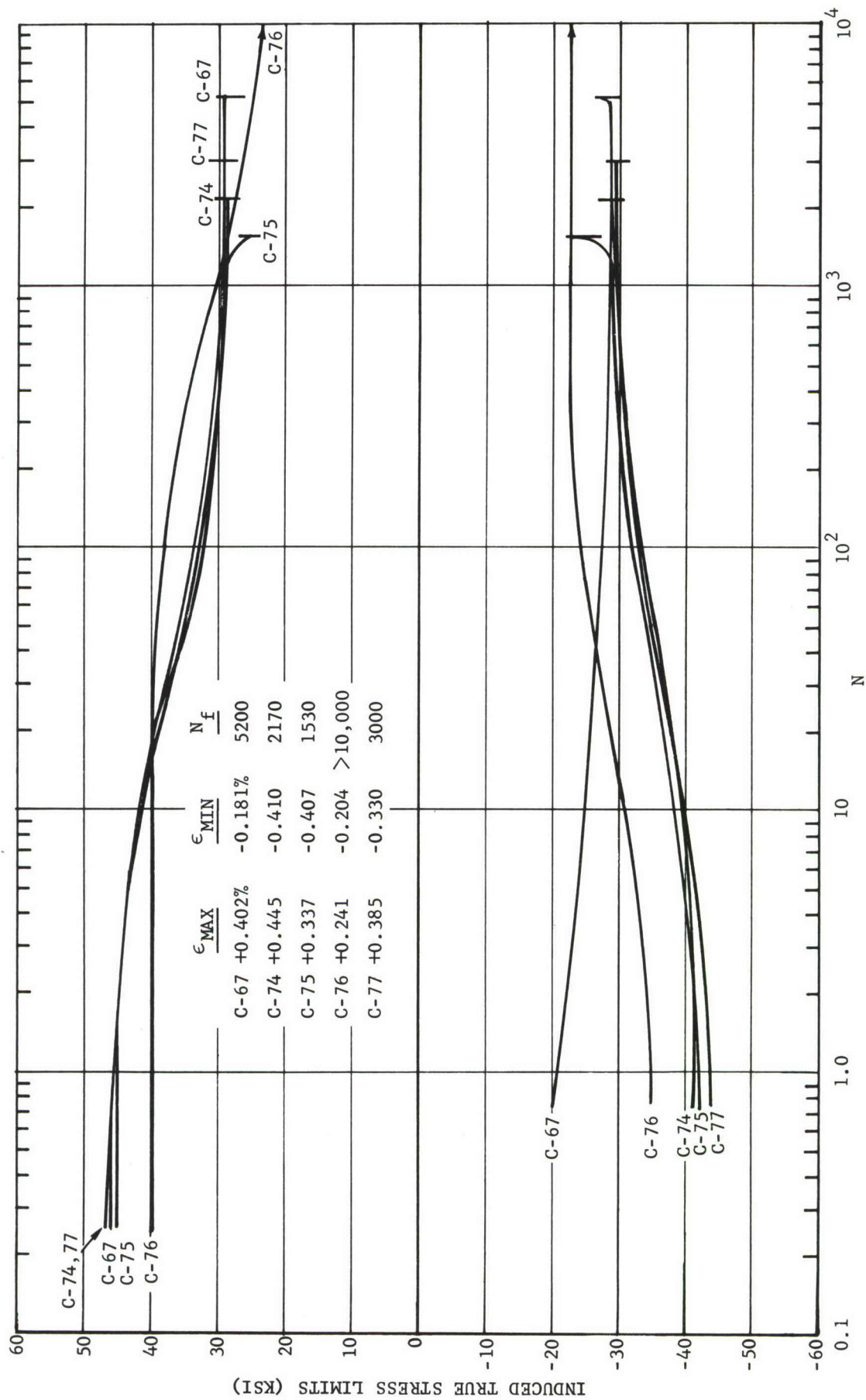


FIGURE 32A. STRESS LIMIT VARIATIONS FOR HARD COPPER DURING CYCLES OF
CONSTANT STRAIN RANGE ($-1 < R_\epsilon < 0$)

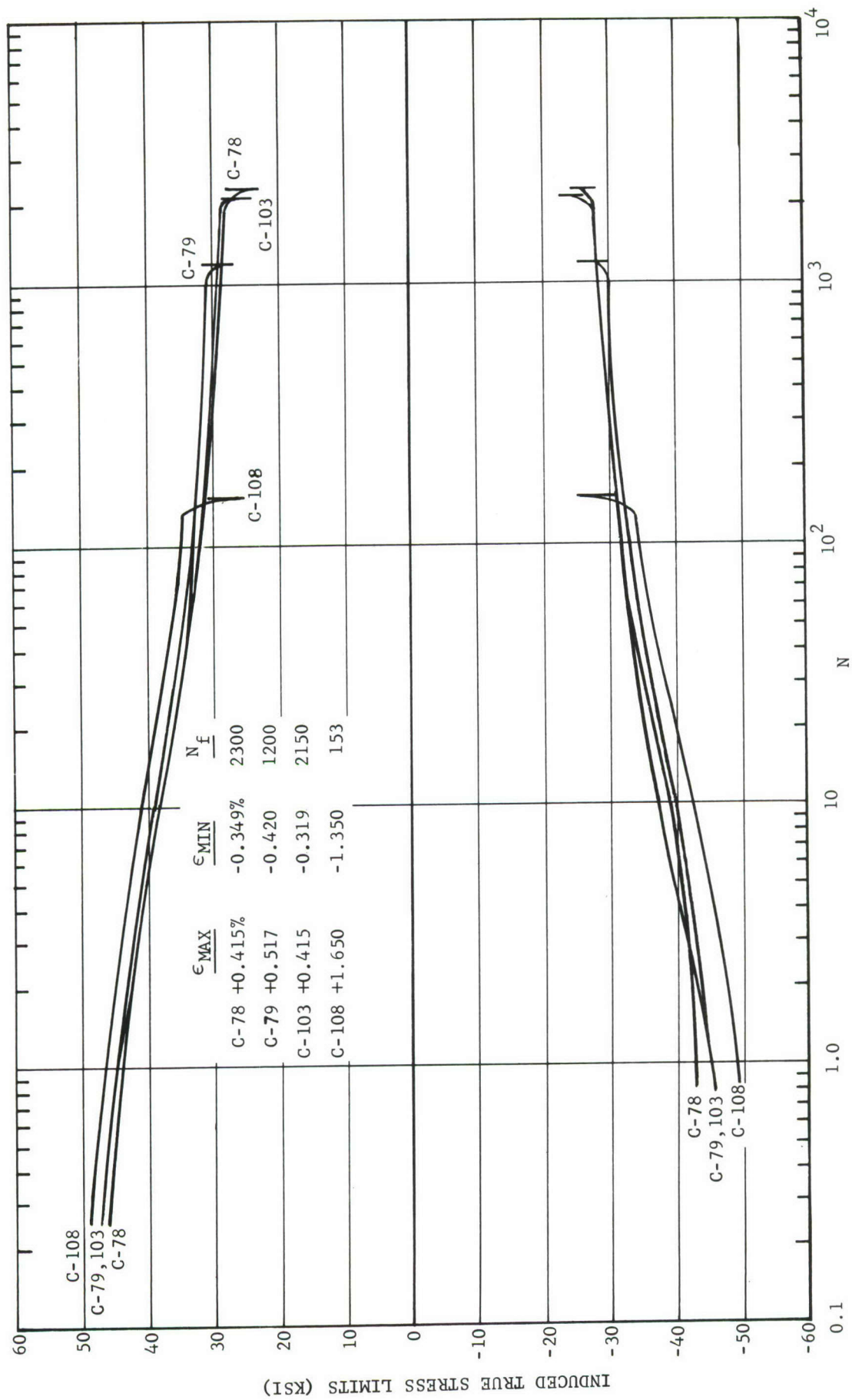


FIGURE 32B. STRESS LIMIT VARIATIONS FOR HARD COPPER DURING CYCLES OF
CONSTANT STRAIN RANGE ($-1 < R_\epsilon < 0$)

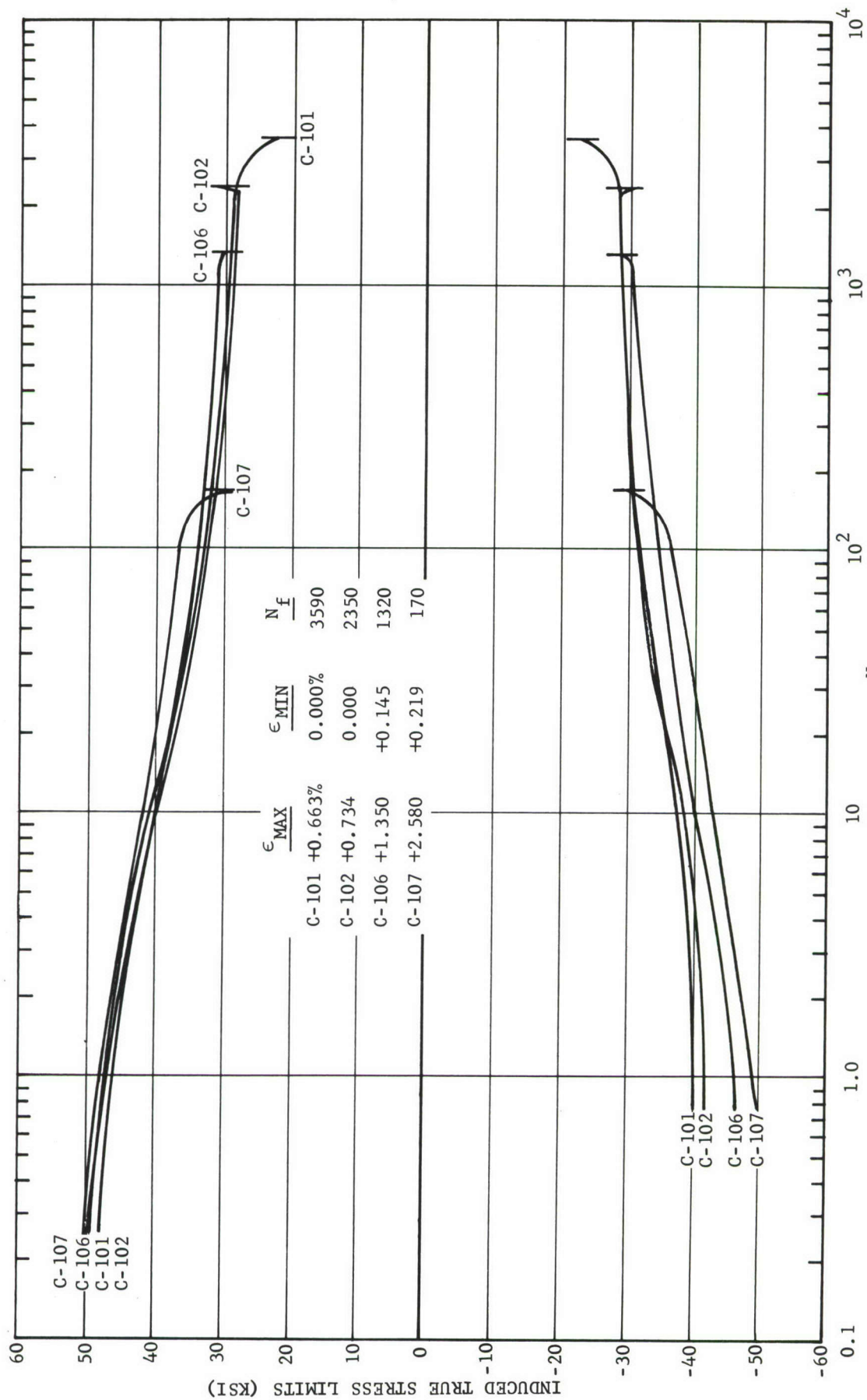


FIGURE 33. STRESS LIMIT VARIATIONS FOR HARD COPPER DURING CYCLES OF CONSTANT STRAIN RANGE ($R_\epsilon \approx 0$)

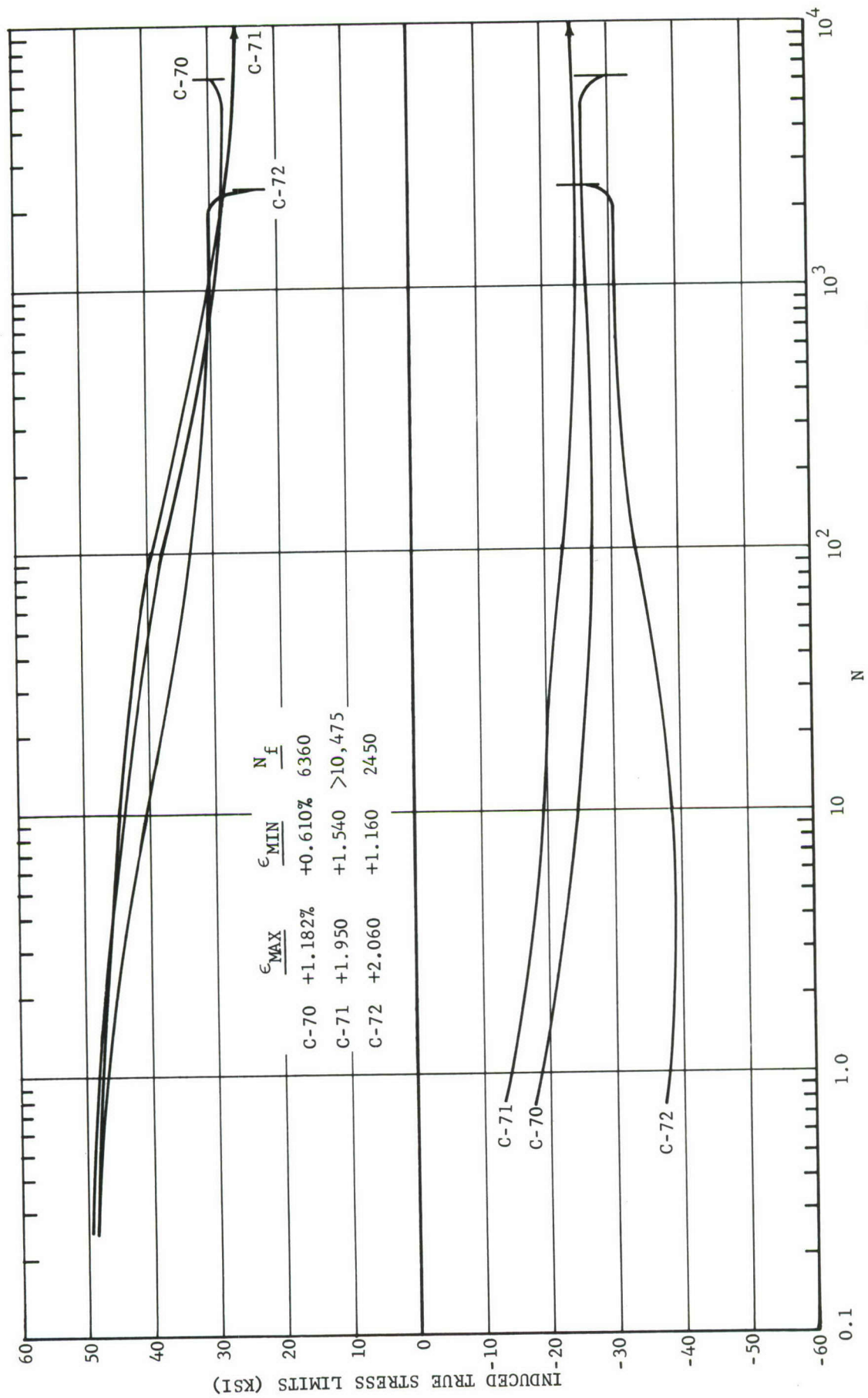


FIGURE 34. STRESS LIMIT VARIATIONS FOR HARD COPPER DURING CYCLES OF
CONSTANT STRAIN RANGE ($R_\epsilon \gg 0$)

Figure 34 reflect the affinity for symmetry. After the first cycle, the tests on these specimens produced hysteresis loops having highly unsymmetrical peak stresses. However, through an interrelated fluctuation of the induced peak stresses, symmetry was eventually achieved.

The abrupt changes shown by the stress-level traces near failure of the hard copper specimens carry the same explanation given earlier for soft copper. That is, the change is due to the effect of a sizeable crack on the response of the extensometer and its control over the strain-range.

SECTION V

CORRELATION OF PHENOMENOLOGICAL BEHAVIOR

Cyclic strain-hardening or -softening typical of the response displayed by the aluminum alloys and the pure copper materials in the previous section are common to a wide range of metals having varied crystalline structures (References 6, 7, 8 and 9). Furthermore, for most of these metals, the cycle-induced processes have been found to lead to saturation. The saturation is manifest on the macroscopic scale by the asymptotic stress-range reached during the early cycles of the constant strain-range test. The end result of the saturation process appears to be the revelation of a characteristic coupling that exists between stress- and strain-range during fatigue. That is, a stabilized stress-strain relationship is revealed that is unique to cyclic loadings with little resemblance to the stress-strain relations obtained from the tensile test.

The stabilized relationship determined from the cyclic loadings is actually a locus of stabilized stress-strain conditions which are determined by tests on a series of separate specimens. It should be noted, however, that experiments performed by Younger (Reference 10) and Tuler (Reference 11) have indicated that a single specimen subjected to a specific loading can give good definition to the locus curve. The role that the locus curve plays in fatigue analysis is not completely understood, but there are indications that the cyclic-state relationship is virtually independent of the type of load cycling, the range of loading, and mean values.

The locus curve can be determined from the stabilized stress- and strain-range data derived from a number of specimens (or possibly, a single specimen) without subjecting the specimens to failure by fatigue. Therefore, the locus curve, as it is now understood, cannot be used without failure data in the analysis or prediction of fatigue failure. If, however, the locus curve is derived from fatigue-failure data, as in the present program, then the necessary information is available to employ the locus curve in fatigue analyses. The details of this procedure are covered in the remaining paragraphs.

5.1 FUNDAMENTAL RELATIONSHIPS

The state of the art of estimating the fatigue life of materials from a minimum of experimental data has improved rapidly during the past several years. Manson (Reference 12) and Coffin (Reference 13) are credited with the present impetus when they proposed a power law relationship between fatigue life and plastic strain. [It should be noted, however, that earlier studies (References 26 and 27) introduced the power-law relationship in fatigue correlations.] Coffin applied this relationship to the analysis of data during thermal fatigue, and he showed that the relationship

$$N_f^k \Delta \epsilon_p = C_1 \quad (6)$$

accurately fit his strain cycling data. The exponent, k , was assigned the value of $\frac{1}{2}$ and the constant C_1 was assumed to be related to the fracture ductility. Later, Tavernelli and Coffin (Reference 14) showed more precisely for completely reversed strain cycles ($R_\epsilon = -1$) that

$$C_1 = -\frac{1}{2} \ln (A_f/A_o) \text{ [or } C_1 = \frac{1}{2} \ln (A_o/A_f)] \quad (7)$$

Although physical arguments based upon the rate of crack growth (References 15 and 16) have established the validity for the choice of $k = \frac{1}{2}$, Manson (References 17 and 18) has shown for a wide range of materials that k is not universally equal to $\frac{1}{2}$; therefore, he has suggested that a purely empirical value of $k = 0.6$ be used to give wider applicability. In Reference 18, Manson has made the additional suggestion that values having a high degree of empiricism be assigned to the constant, C_1 . That is, he has suggested that C_1 be assigned values as follows,

For Four-Point Correlation Method

$$C_1 \approx 0.97 [\ln (A_o/A_f)]^{0.75} \quad (8)$$

For Method of Universal Slopes

$$C_1 = [\ln (A_o/A_f)]^{0.6} \quad (9)$$

No physical significance can be attached to the above values. Over the usual range of values for fracture ductility, namely $\ln(A_o/A_f) = 0.2$ to 1.5 , Equations (8) and (9) give values for C_1 that differ by about 30 percent for materials of low ductility and closely similar values for the highly-ductile materials.

The above discussion has been focused on the use of Equation (6) in the prediction of fatigue failure. For those predictions that extend into the longer life range, say beyond 500 cycles, it is necessary to introduce into the life relationship a term which recognizes the significant effect of elastic strains. Tavernelli and Coffin (Reference 14) proposed that the elastic strain-range component be derived from a knowledge of the endurance limit. This value was, then, to be employed as a cycle-independent term having a fixed magnitude between $N_f = 1$ and 10^8 cycles. The resulting relationship would be conservative and could be useful as a design tool; however, attention during the present program has been restricted to those relationships that reflect the true phenomenological aspects of fatigue. That is, those relationships that treat the elastic term as a cycle-dependent term would be expected to best correlate with fatigue-failure data.

The elastic term proposed by Manson (Reference 19) has been selected as the more suitable term for the extension of the life equation. This term which reflects the stabilized stress-range for $R_\epsilon = -1$ can be expressed as follows:

$$\Delta\epsilon_e = \Delta\sigma/E = (C_2/E)N_f^m \quad (10)$$

Thus, the total strain-range, $\Delta\epsilon$, can be found from the sum of the plastic and elastic strain components given by Equations (6) and (10), respectively. The total strain-range equation for $R_\epsilon = -1$ becomes

$$\Delta\epsilon = \Delta\epsilon_e + \Delta\epsilon_p = (C_2/E)N_f^m + C_1N_f^n \quad (11)$$

where $n = -k$.

Equation (11) which relates the total strain-range and the number of cycles to failure is composed of two power-law terms which are linear expressions of $\log(\Delta\epsilon_e \text{ or } \Delta\epsilon_p)$ and $\log N_f$. The slope of the elastic and plastic lines (on log-log plot) are m and n and the intercepts at $N_f = 1$ are C_2/E and C_1 , respectively.

The value originally assigned to C_2 , (Reference 19) was $2\sigma_f$, twice the true fracture stress. Later, however, in the interest of finding a value that would better correlate with data from a wide range of materials, Manson (Reference 18) proposed that C_2 to be taken equal to $2.12 \sigma_f$ or $3.5 \sigma_{ult}$.

In Equations (6), (10), and (11) the use of engineering strain and nominal stress has been implied by References 14 and 19, however, the constants C_1 and C_2 were proposed to be expressed in terms of true strain and true stress, respectively. Thus, for fatigue lifetimes less than a hundred cycles, for which total strain-ranges exceed two or three percent, the proper expressions for stresses and strains are rather ill defined. Furthermore, within this same region of fatigue failure ($N_f < 100$) stable hysteresis is seldom fully achieved which leads to failure data in this region that has not met the specified requirements for stabilized stress and strain conditions prior to failure. Nevertheless, the power-law relationships, Equations (6) and (10) and their sum, Equation (11), have been assumed to traverse this extremely short life region to give the semi-empirical intercepts at $N_f = 1$ as indicated above. For most metals, fatigue lifetimes greater than 100 cycles are the result of repeated applications of total strain-ranges below two or three percent. Over this region nominal stresses and engineering strains adequately express the stress-strain relationship.

The correlations of the data obtained from the four materials in the present program indicate that the constants C_1 and C_2 that best correlate with the data are as follows,

$$C_1 = (\epsilon_f - C_2/E) \approx \epsilon_f \quad (12)$$

$$C_2 = 2(F)_f \approx 2\sigma_f \quad (13)$$

The strain ϵ_f is the conventional engineering strain at failure in the standard tensile test as measured by an extensometer. The assignment of $2\sigma_f$ to the value of C_2 corresponds to the original selection by Manson (Reference 19).

Furthermore, as will be shown later in Sections 5.2.1 and 5.2.2 for the four materials tested in this program, the power-law relationship which describes

the plastic line, Equation (6), was found to closely correlate with the plotted value of fracture ductility, D_f , when the line is extended back to $1/4$ cycle. Thus, the intercept at $N_f = 1/4$, as hypothesized by Coffin and employed in Reference 14, is essentially confirmed. It must be noted, however, that the attainment of the confirmation is based upon the fact that conventional engineering strain was used as a measure of cyclic strain.

Were true strains or natural strains employed in the measurement of the controlled cyclic strains, then the numerical value of the total strains would be larger than that given by conventional engineering strain measurements; and, it would be found necessary to plot $2D_f$ at $1/4$ cycle (or D_f at 1 cycle) to achieve correlation between the tensile test and fatigue. Sachs and Liu (Reference 20) have provided a basis for the above statement in their studies of failure below two cycles. A brief description of their findings is presented in the following paragraph.

Liu and Sachs have shown for $R_\epsilon = -1$ that the life-equation is largely discontinuous in the range, $1/4 \leq N_f \leq 2$, and failures can only exist between $N - 1/4$ and $N + 1/4$. For the larger values of cycles the discontinuities become negligible, but at very low cycles, the failure data may be misleading. The expedient of taking D_f or ϵ_f (depending on the manner of defining strains) from a tensile test and assigning this value to $\Delta\epsilon$ in the life equation for $N_f = 1/4$ is incorrect. The error in such procedures was displayed by the authors by straining a specimen to a point just short of tensile failure and measuring the true strain. They then removed the tensile load and applied a compressive load to give a completely reversed true strain. Next, they removed the compressive load. After this procedure the specimen was at zero load, had been subjected to a range of strain near $2D_f$, was at the $3/4$ point of the cycle, and yet had not failed. Shortly after applying the second tension, however, failure did occur. Their studies of a 2024-T aluminum alloy specimen showed failure at $N_f = 1$ when it was subjected to completely reversed strains near $\pm D_f/2$ giving a total strain range of approximately D_f . A number of additional specimens were tested to lower values of reversed strain leading to failures at $N_f > 1$. The trend of the data extrapolated to $N_f = 1/4$ showed that the corresponding $\Delta\epsilon$ should be $2D_f$. This selection also leads to $\Delta\epsilon \approx D_f$ at $N_f = 1$. Were conventional engineering strains ($\Delta\ell/\ell_0$) employed for the strain measurements, then essentially the same observations would have been made with ϵ_f replacing D_f as the fracture parameter.

The above observations lead to $C_1 \approx D_f$ in the correlation of fatigue data when longitudinal strains are assigned true strain values, or $C_1 \approx \epsilon_f$ when longitudinal strains are expressed in terms of conventional engineering strain. The latter value for C_1 confirms the findings of the present study.

The physical basis for equating C_2 to $2(F)_f$ or $2\sigma_f$ lies in the observation that for $R_\epsilon = -1$ the hysteresis loop giving failure in one cycle has stress peaks that are near symmetrical. Thus, a stress range of $2\sigma_f$ is active for the one cycle. When the correction for flow stress on the specimen surface (Equation 4) is warranted, the value of σ_f should be replaced by $(F)_f$.

5.2 FATIGUE LIFE CORRELATIONS

The stabilized stress-strain data and the fatigue data presented in the previous sections have been organized in this section to show the strain-range vs. fatigue-life correlations for the four materials. For the aluminum alloys both constant stress-range (constant load-range) and constant strain-range correlations have been made. However, due to the high degree of cyclic creep induced in the copper materials during the cyclic loading, only the constant strain-range data have been used in their correlations. For each of the materials, several values of stress- or strain-ratio have been included.

Failure has been defined as complete fracture of the specimens, and the asymptotic stress levels were considered to have been established at one-half the eventual fatigue life. Both of these assumptions are consistent with previous studies of this nature (References 9, 18, and 21).

The cyclic stresses and the strain components of the stabilized hysteresis loops employed in the correlations are defined in Figure 35. Five typical stabilized hysteresis loops are shown in the figure with the definitions being made with respect to loop #3. It should be understood that although these loops may have been obtained from tests employing completely reversed strains, it has been expedient in the figure to shift the loops to a common origin at peak compression so as to give a comparison of the stress- and strain-ranges.

5.2.1 ALUMINUM ALLOY CORRELATIONS

The correlations found for the soft aluminum alloy, 2024-0, are shown in Figures 36 and 37. The data points include results found under both constant strain-range and constant load-range testing. The black data-points depict the results of the constant load-range testing. Each of the specimens represented by these points showed cyclic creep to varying degrees during the test. It is not yet clear why these data showed the same correlation as that obtained from constant strain-range testing in which creep was absent. However, during the cyclic creep it was noted that the hysteresis loop did reach stability in strain-range even though the loop slowly crept along the strain axis. That is, regardless of superimposed creep, the width of the loop became constant and essentially persisted to failure. The graph shown earlier for Specimen A-55A in Figure 9 emphasizes the constancy of the strain-range, $\Delta\epsilon$. The creep in these specimens, of course, produced a slow reduction in the cross-section which, under constant load-range cycles, induced slowly rising true-stress limits. The levels of stress that were used in the determination of $\Delta\sigma_T$ were those measured at approximately the half-life point in the fatigue life.

For those specimens showing the greater creep (Specimens A-55A, -62A, and -65A in Figure 9) it was found at the half-life point that the true-stress limits had increased approximately 20 percent beyond those of the first cycle. Also, in each instance, it was found that the half-life point was

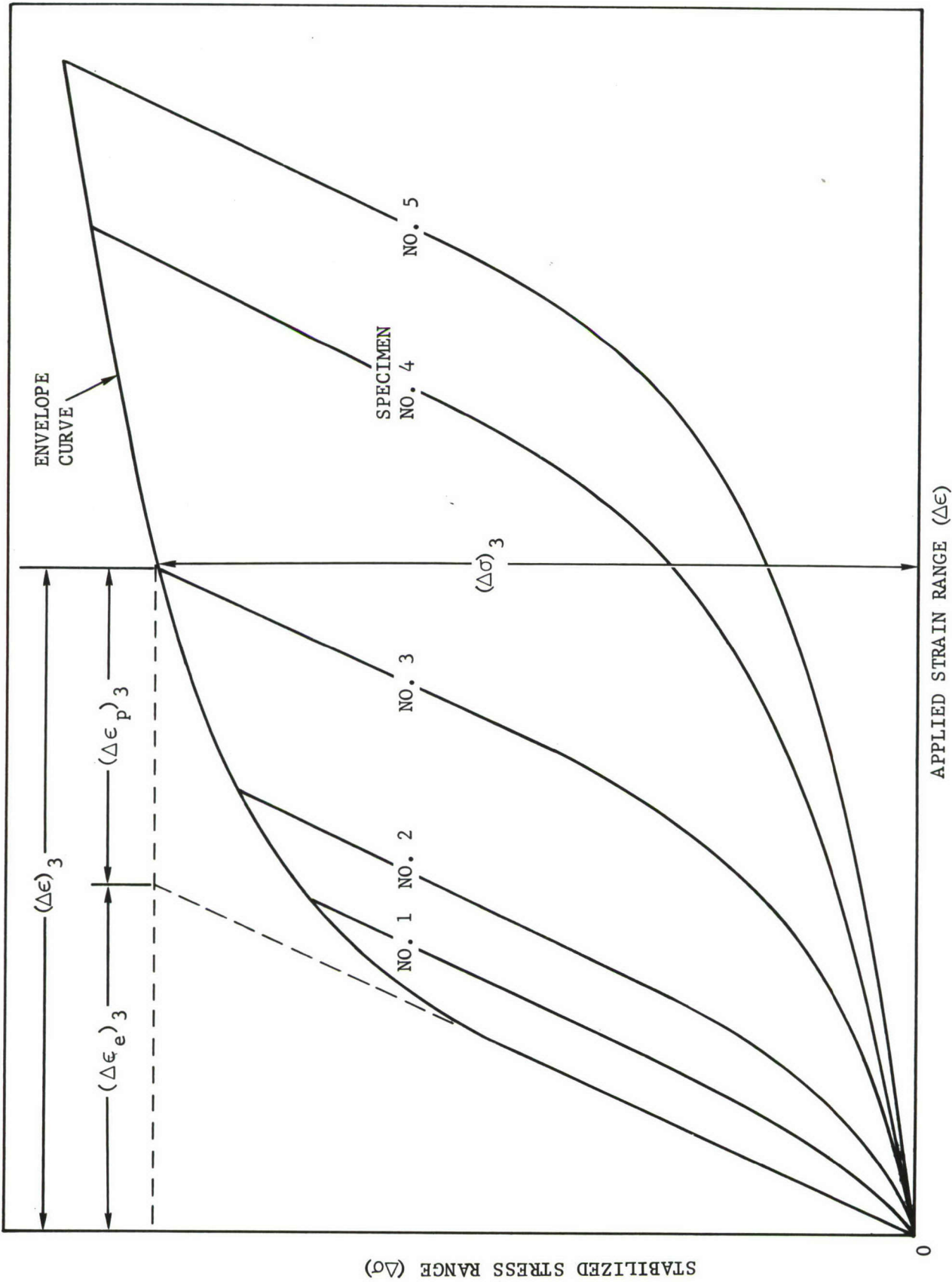


FIGURE 35. DEFINITION OF CYCLIC STRESS AND STRAIN COMPONENTS FOR STABLE HYSTERESIS CONDITIONS

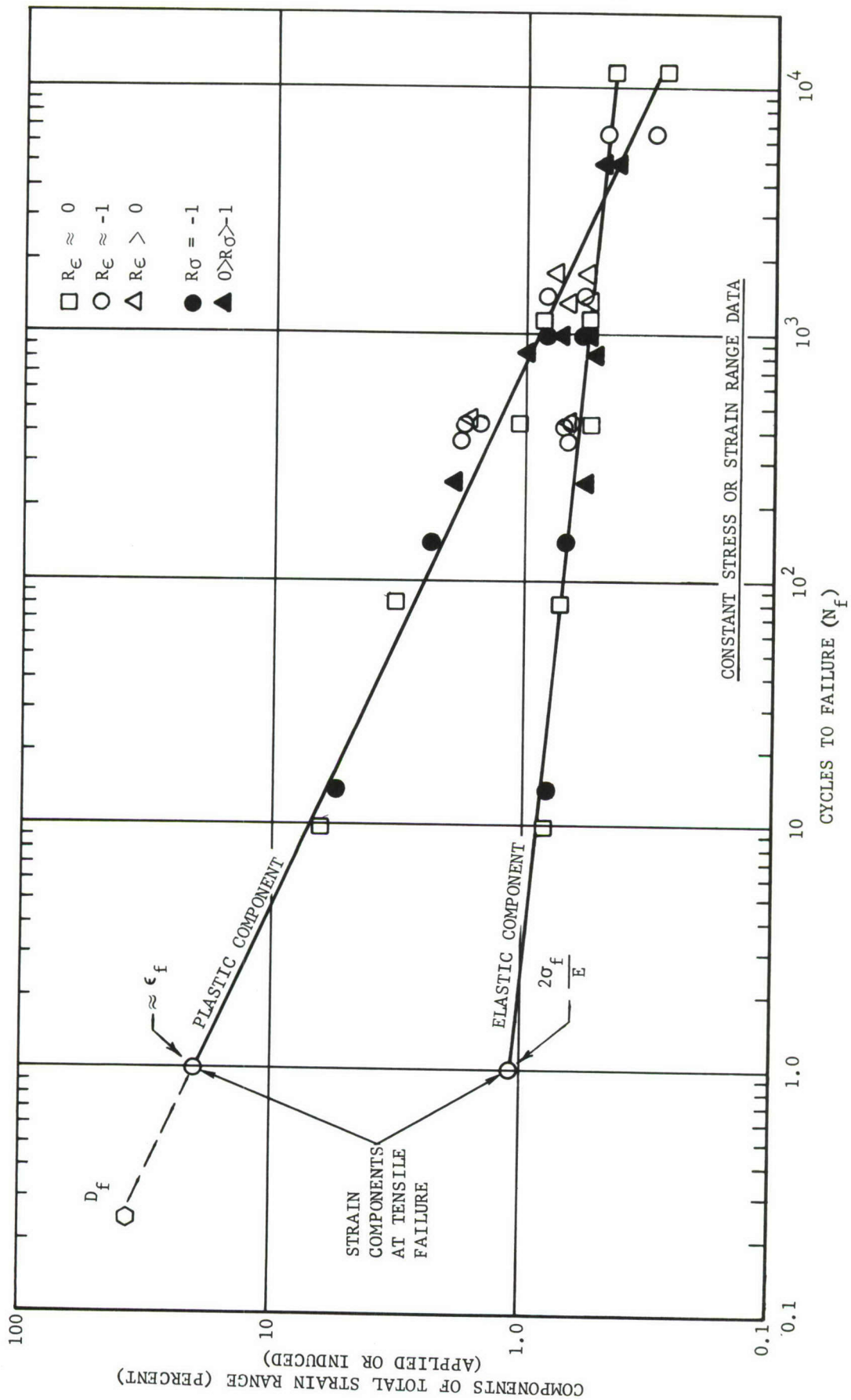


FIGURE 36. RELATIONSHIP BETWEEN STRAIN RANGE COMPONENTS AND FATIGUE LIFE (2024-T3 ALUMINUM ALLOY)

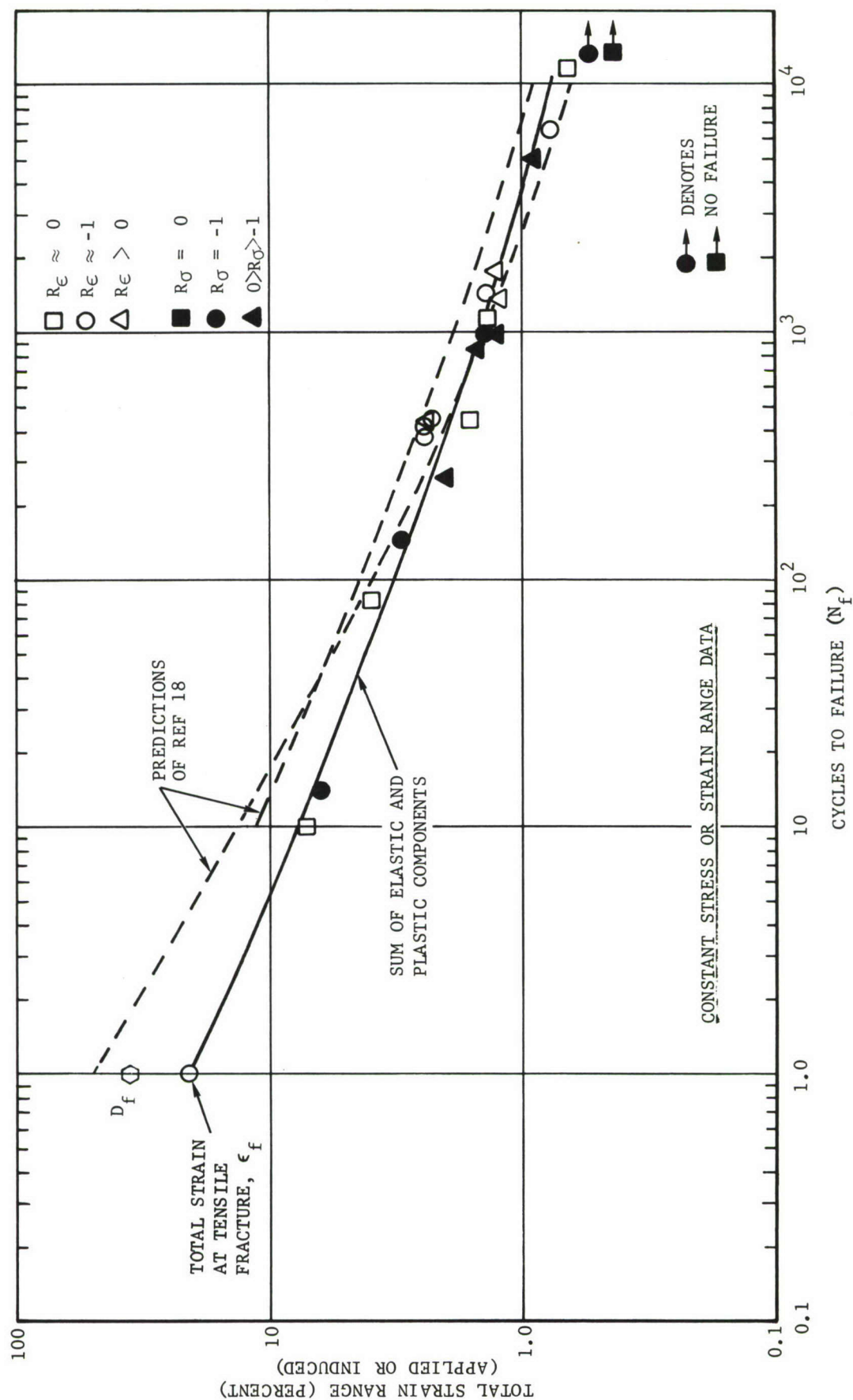


FIGURE 37. RELATIONSHIP BETWEEN TOTAL STRAIN RANGE AND FATIGUE LIFE
(2024-0 ALUMINUM ALLOY)

reached when the peak strain limit attained a conventional engineering strain of approximately 16% (true or natural strain $\approx 17\%$). These values of strain were observed to coincide with the region of strains giving P_{\max} on the true-stress strain plot in Figure 6. Nevertheless, these observations were limited to only a few tests and the only explanation for the good correlations shown by the cyclic-creep specimens that will be ventured at this time is that the $\Delta\epsilon$ of these specimens remained essentially constant during the cyclic creep.

The open-points in Figures 36 and 37 depict data obtained under constant strain-range testing. Straight lines have been faired through the data points and the singular relationships for the elastic and plastic components appear to be unaffected by either the stress- or strain-ratios. The lack of a strain-ratio effect has been reported previously (Reference 22) from studies of total strains rather than strain components. Below, say 50 cycles, the independence of strain ratio in the correlation would not be expected to hold. The reason for expecting a strain-ratio effect at very short life-times is based on the fact that failure will generally occur from tensile-mode cracking before stress adjustments are complete and stable hysteresis is attained. (See Section 7.1.)

The power-law relationships represented by the straight lines in Figure 36 are as follows:

2024-0 Aluminum Alloy

$$\Delta\epsilon_e = 0.0105 N_f^{-0.097} \quad (14)$$

$$\Delta\epsilon_p = 0.200 N_f^{-0.455} \quad (15)$$

The relationship between the total strain range and the fatigue life shown by the solid line in Figure 37 was obtained by adding the corresponding components given in Figure 36. The resulting sum, of course, does not produce a straight line since the sum of two power-law relationships is not, in itself, a power-law relationship. However, attempts have been made (References 21, 22 and 23) to pass a straight line through the total strain range points to give a simple power-law relationship between $\Delta\epsilon$ and N_f . These simplifying procedures, of course, lead to difficulties in assigning physical meaning to the intercept at $N_f = 1$. The slightly curved summation line (solid line) passes through the total strain, $\Delta\epsilon = \epsilon_f$ at $N_f = 1$, as justified earlier from the observations of Liu and Sachs (Reference 20).

In Figures 36 and 37 the plotted value of fracture ductility, D_f , has been shown. In Figure 36 fracture ductility has been plotted at $N_f = 1/4$ and the extension of the plastic line confirms the hypothesis of Coffin (Reference 14) when employed, as here, with conventional engineering strain data. In Figure 37, on the other hand, the fracture ductility is plotted at $N_f = 1$. This is the proper cyclic-life position for D_f when correlations are attempted to be made with longitudinal strains derived from diametral strain measurements (Reference 20).

The two dashed lines shown in Figure 37 are the predicted relationships using the methods of Reference (18). These methods are the Four-Point Correlation Method and the Method of Universal Slopes. The two methods result in the predictions that are shown to terminate at $N_f = 10$ and 1, respectively. These total strain predictions appear to be high, however, it must be noted from Reference (18) that the longitudinal strains associated with the dashed-line predictions are based upon diametral strain measurements. Thus, the strains should be higher since constant-volume deformation has been assumed in the conversion of strains from diametral to longitudinal (See Appendix). The plotted value of D_f at $N_f = 1$ in Figure 37 should be viewed with respect to the dash-line predictions and not the solid line depicting conventional engineering strain measurements.

Similar correlations were found for the data collected from the 2024-T351 specimens. These are presented in Figures 38 and 39. As found for soft aluminum the straight lines satisfy both constant strain-range and load-range data obtained at several ratios.

Cyclic creep in the hard aluminum alloy was not significant during constant load-range testing for those ranges of load that led to fatigue-life beyond a hundred cycles. Therefore, beyond $N_f = 100$, the constant load-ranges were accompanied by stress ranges that were essentially constant. The specimen that led to the data point at $N_f = 38$ (black circle) showed considerable creep (See discussion in Section 4.2.2); however, at the 19th cycle (half-life) the creep was just beginning to accelerate and, therefore, had little effect on the recorded values of $\Delta\sigma_T$ and $\Delta\epsilon$. Again, as found for the cyclic creep data on soft aluminum, the final failure was predominately a tensile mode but the value of N_f still coincided with the power-law relationship.

The relationships presented by the straight lines in Figure 38 are described as follows,

2024-T351 Aluminum Alloy

$$\Delta\epsilon_e = 0.0191 N_f^{-0.091} \quad (16)$$

$$\Delta\epsilon_p = 0.271 N_f^{-0.700} \quad (17)$$

The relationship for total strain range versus fatigue-life for the hard aluminum alloy is shown by the solid curve in Figure 39. Superimposed on the figure are the two predictions of Reference (18) as well as additional fatigue data taken from Reference (22). The data points from the latter reference were obtained from specimens of the same material but having an "hour-glass" test section. Direct measurements of longitudinal strains, rather than diametral strains, were made to give conventional engineering values similar to those recorded in the present program. An SR-4 type test machine was also used; therefore, test results of the present program and those of Reference (22) can be assumed to have been obtained under similar conditions. D'Amato and DeBoer restricted their data reduction,

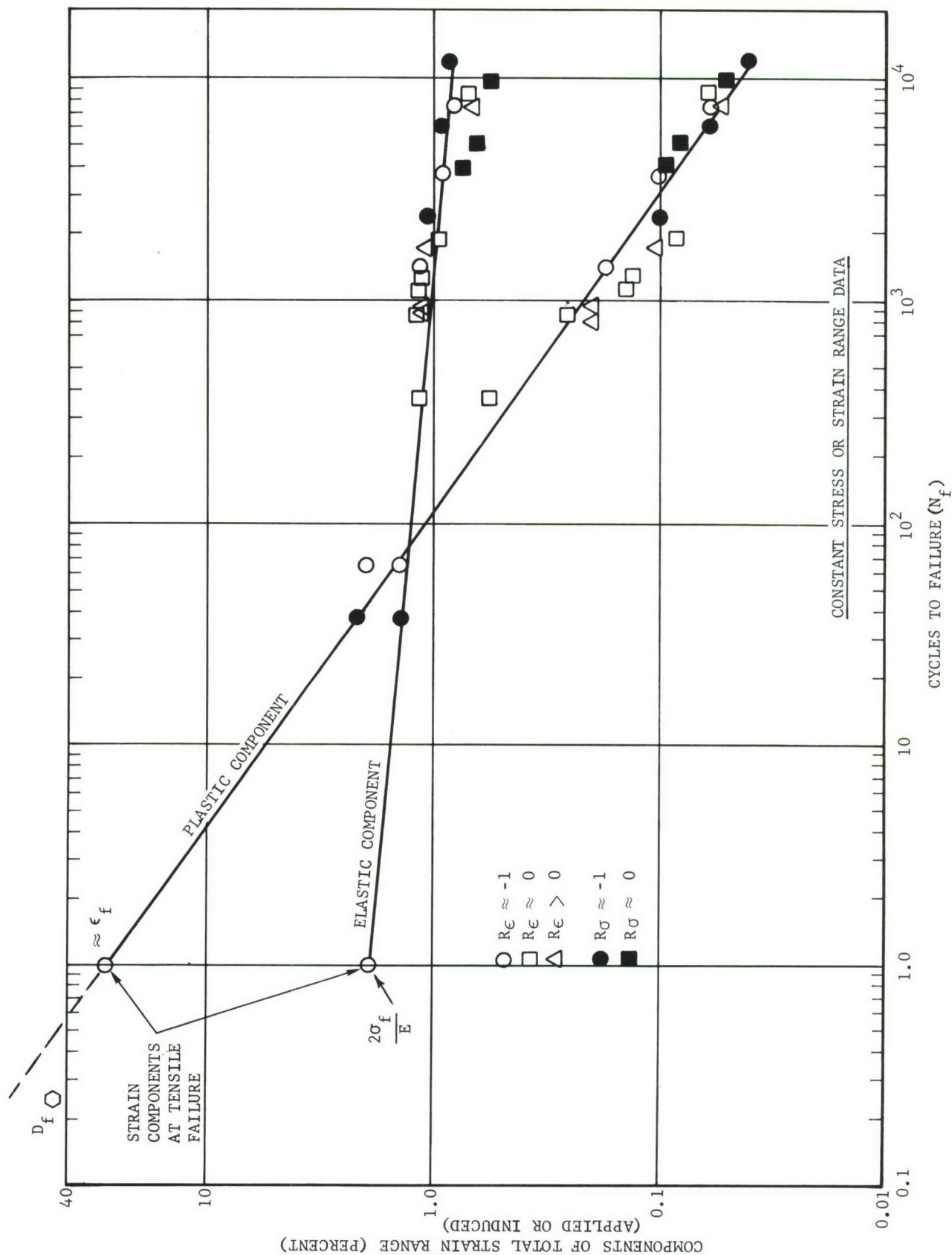


FIGURE 38. RELATIONSHIP BETWEEN STRAIN RANGE COMPONENTS AND FATIGUE LIFE
(2024-T351 ALUMINUM ALLOY)

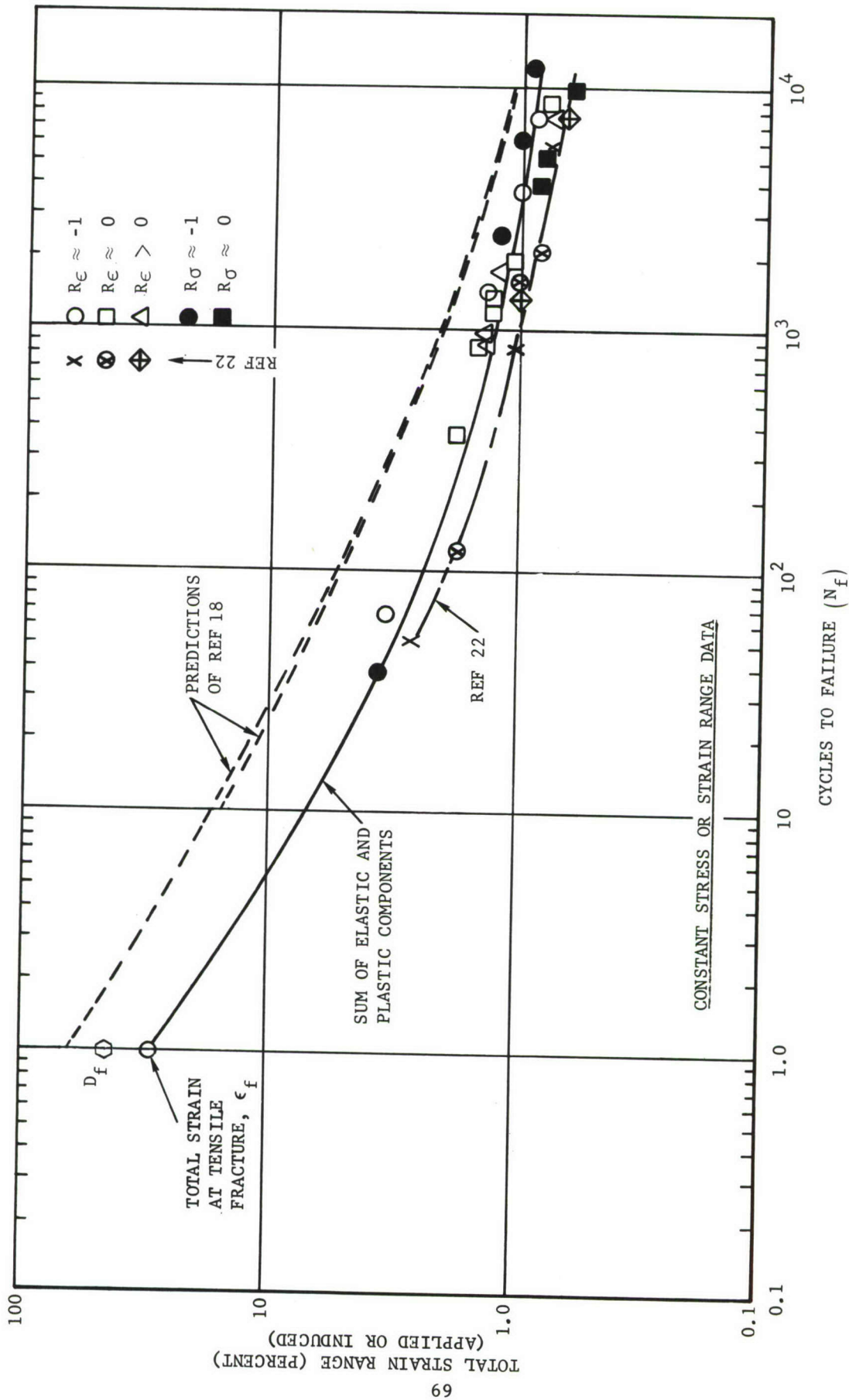


FIGURE 39. RELATIONSHIP BETWEEN TOTAL STRAIN RANGE AND FATIGUE LIFE (2024-T351 ALUMINUM ALLOY)

however, to total strain-ranges, therefore, no comparison can be made with the strain components. Nevertheless, the two sets of total-strain data are in close agreement.

In Figure 38 the fracture ductility has, again, been plotted at $N_f = 1/4$ to show the close agreement with Coffin's observations. In Figure 39 the plot of fracture ductility has been moved to $N_f = 1$, the proper position for comparison with the two dashed-line predictions of Reference (18). As discussed previously, the seemingly higher total strains are the result of the method of deriving longitudinal strains from diametral strain measurements.

5.2.2 OFHC COPPER CORRELATIONS

The correlations found for the constant strain-range fatigue data of annealed OFHC copper are shown in Figures 40 and 41. No constant load-range data have been included in these figures. The open and closed (black) data points depict the data obtained in the present program. The small x-marks denote data taken from Reference (21). The solid lines which have been faired through the data of the present program, and the dash-dot lines faired through the data of Reference (21), meet the ϵ_f -intercept requirement at $N_f = 1$. Again, note that data for several values of strain ratio are shown.

Three lines are presented for the elastic component in Figure 40. The selection of the appropriate line depends upon the importance to be assigned the use of the "correction factors" given by Bridgeman (Reference 5). The stress corrections do not appear warranted in the region of low-life fatigue ($N_f < 10^4$) since such refinements have an insignificant effect on total strains. That is, in low-life fatigue the plastic component generally overshadows the elastic component. In the event the elastic line is to be extrapolated into the long-life (low-stress) fatigue region, the correction may be warranted since it affects the slope of the elastic line. If a correction on stress is warranted, then it is not clear whether true stress (average) should be replaced by the flow stress or the stress on the axis. Although fracture in the tensile test actually occurs at the axis of the neck during neck-down, fatigue failures are generally ascribed to surface stresses (or flow stresses). The problem of selecting the proper stress correction factor for fatigue application is not yet resolved; however, for the elastic-component data shown in Figure 40 and similar data to be presented later for hard copper, the flow stress line offers the better correlation with the fatigue data.

The power-law relationships for annealed OFHC copper represented by the solid line for the plastic component and the flow-stress line for the elastic component are as follows,

Annealed OFHC Copper

$$\Delta\epsilon_e = 0.0082 N_f^{-0.150} \quad (18)$$

$$\Delta\epsilon_p = 0.820 N_f^{-0.634} \quad (19)$$

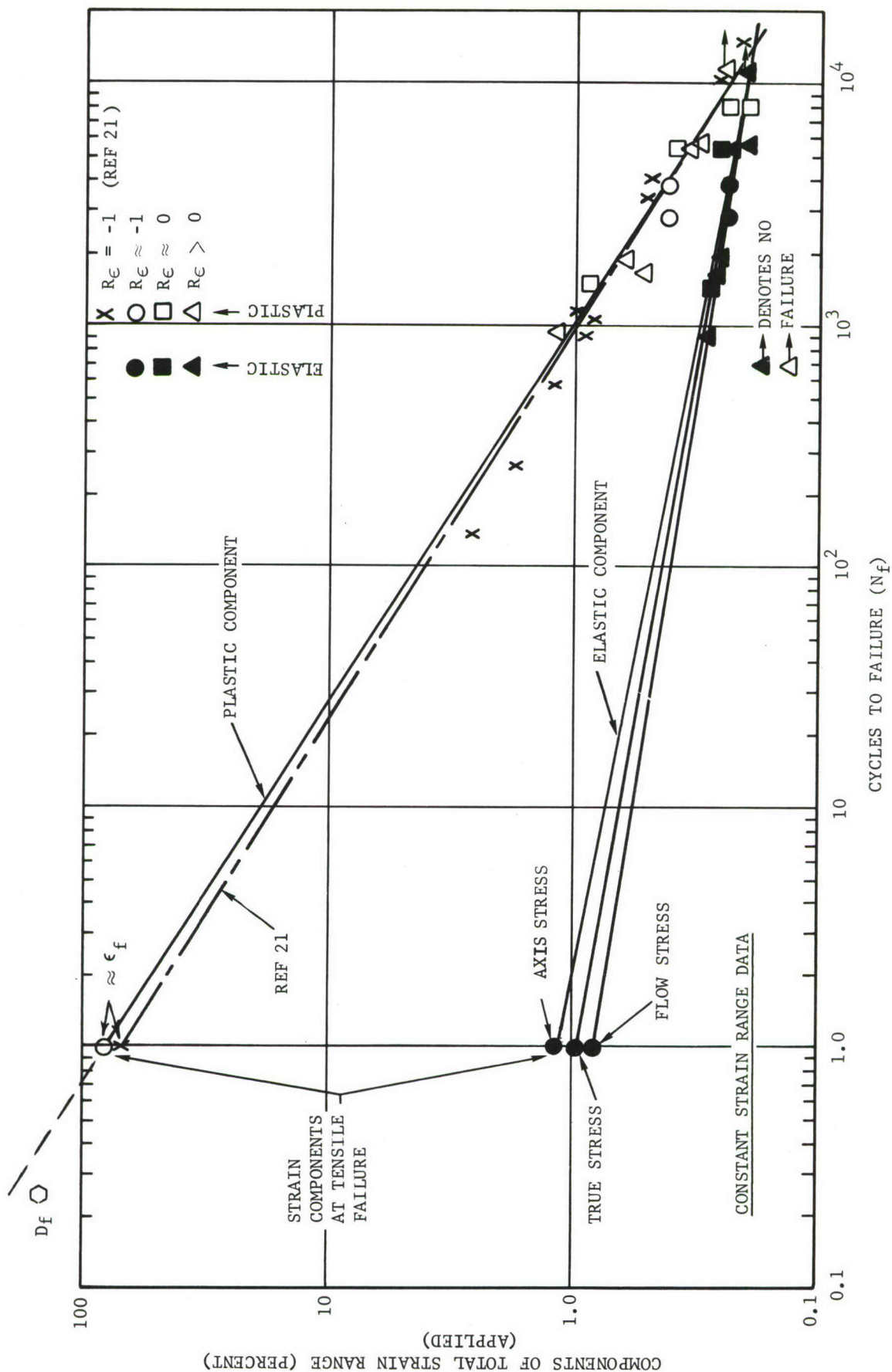


FIGURE 40. RELATIONSHIP BETWEEN STRAIN RANGE COMPONENTS AND FATIGUE LIFE (ANNEALED OFHC COPPER)

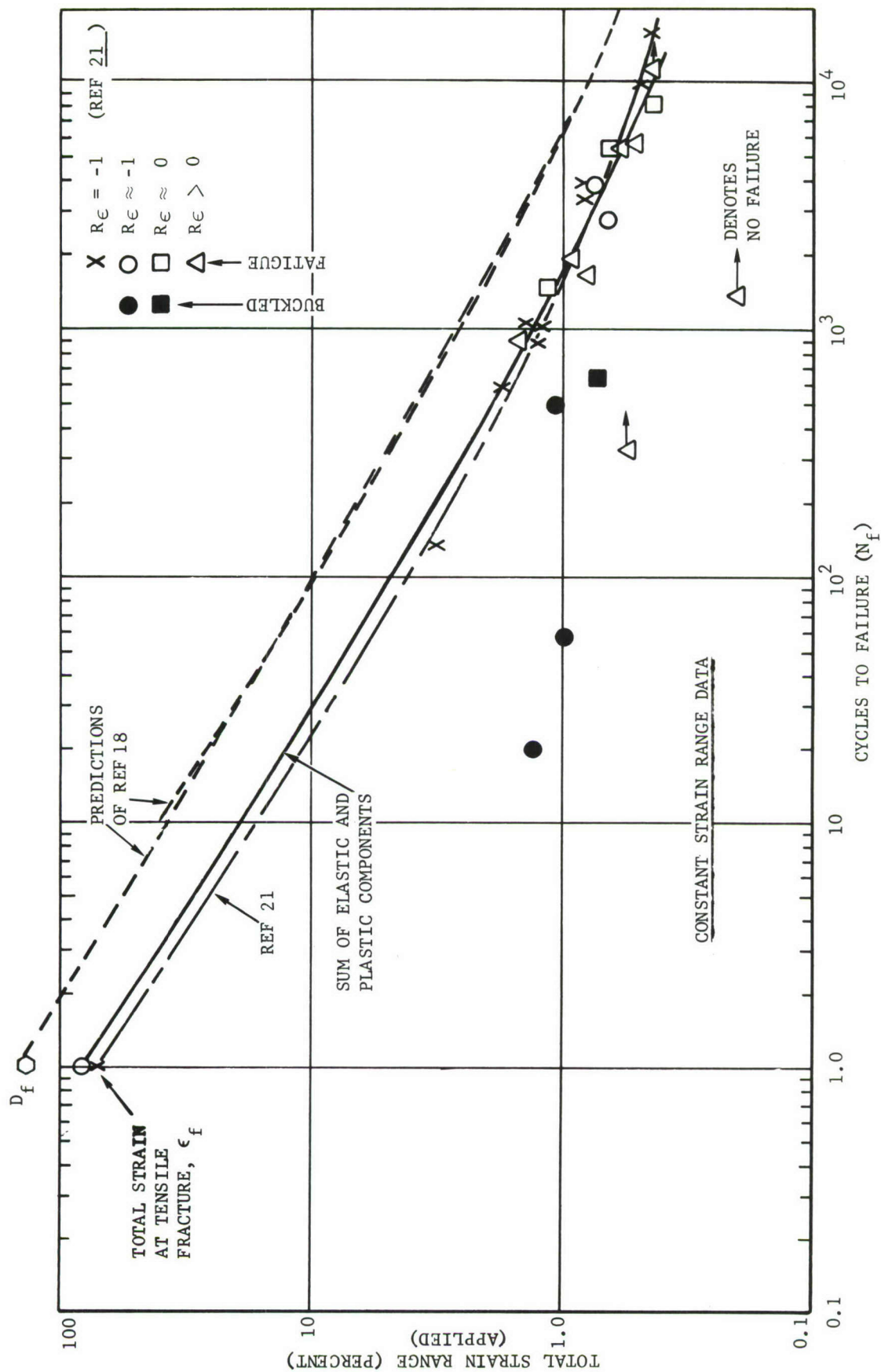


FIGURE 41. RELATIONSHIP BETWEEN TOTAL STRAIN RANGE AND FATIGUE LIFE (ANNEALED OFHC COPPER)

The fracture ductility values for the annealed copper have been plotted at $N_f = 1/4$ and 1, respectively, in Figures 40 and 41. The reason for plotting D_f at these two positions was explained in Section 5.2.1. The dashed lines in Figure 41 give the predictions of Reference (18). Note the agreement with D_f when plotted at one cycle.

The black data-points in Figure 41 denote premature failures by pure buckling or a combination of buckling and fatigue. The failures of these fixed ended specimens were discussed earlier in Section 4.3.3.

The results for hard OFHC copper are given in Figures 42 and 43. All data were obtained under conditions of constant strain-range testing. The solid lines give the relationships determined from the data of the present program. The data points using x-marks were taken from Reference (21). A dash-dot line has been faired through the latter data. Both sets of data show very close correspondence for the relationships representing the plastic component and the total strain-range.

In Figure 42 the plastic-component relationship is represented by three lines. Again, as for annealed copper, the appropriate relationship depends on the selection of Bridgman's correction-factor. The data shown, however, tend to confirm that the flow-stress gives the proper stress level for computing $\Delta\epsilon_e$ at $N_f = 1$ (Equation 10).

The power-law equations representing the hard OFHC copper are presented below. The equations are based upon the solid line for the plastic component and the flow-stress line for the elastic component.

Hard OFHC Copper

$$\Delta\epsilon_e = 0.0082 N_f^{-0.112} \quad (20)$$

$$\Delta\epsilon_p = 0.375 N_f^{-0.575} \quad (21)$$

The relationship between the total strain-range and fatigue life is given in Figure 43. It can be noted that no significant difference exists between the data of the present program and that of Reference (21). The solid line and the dash-dot line are faired through the respective data, and each line passes through the value of ϵ_f at $N_f = 1$ as found from the accompanying tensile test.

The predictions of Reference (18) are given in Figure 43 by the two dashed lines; and, again, the close agreement with D_f when plotted at one cycle should be noted. When D_f is plotted at $1/4$ cycle, as in Figure 42, close correspondence is shown with the plastic line defined by conventional engineering strains.

The black data-points in Figure 43 show the number of cycles at which several specimens failed through buckling. These specimens were tested under pin-ended conditions during the initial series of constant strain-range tests, whereas all other data in the figure were obtained under fixed-end conditions.

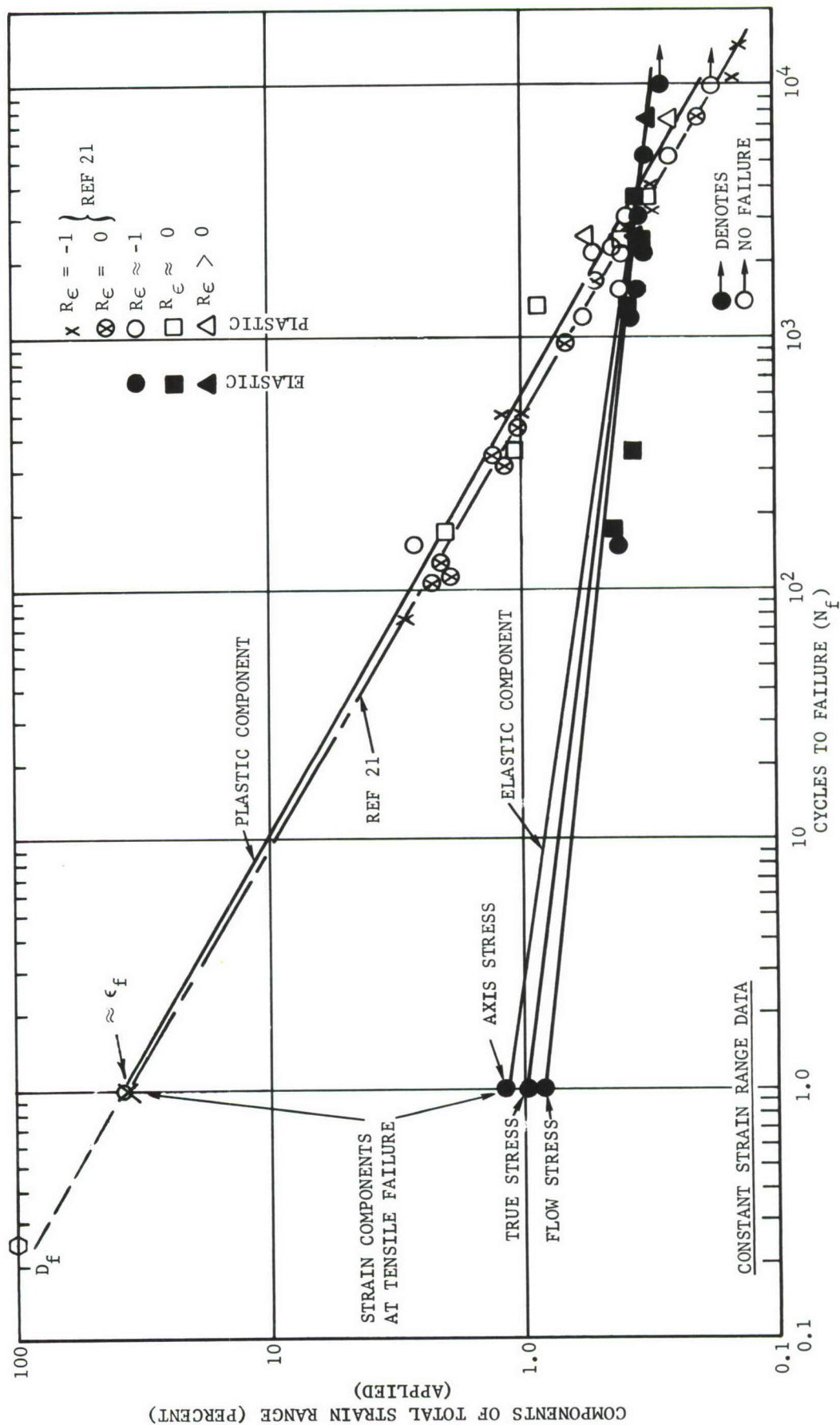


FIGURE 42. RELATIONSHIP BETWEEN STRAIN RANGE COMPONENTS AND FATIGUE LIFE (HARD OFHC COPPER)

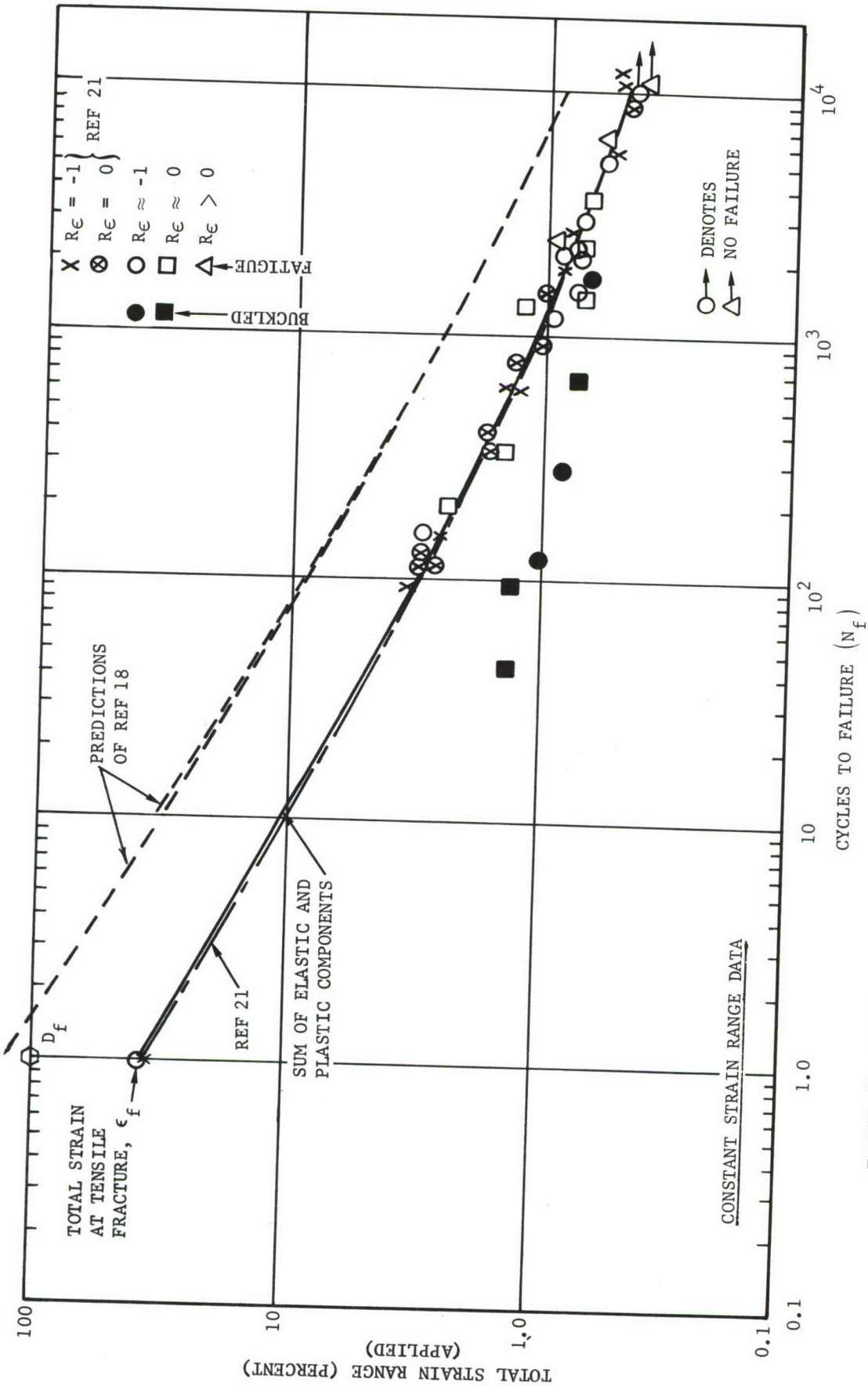


FIGURE 43. RELATIONSHIP BETWEEN TOTAL STRAIN RANGE AND FATIGUE LIFE (HARD OFHC COPPER)

5.2.3 POWER LAW EXPONENTS, m AND n

The exponents of the power law relationships which were found to equate $\Delta\epsilon_e$ and $\Delta\epsilon_p$ with fatigue life, N_f , can be summarized for the four materials as follows,

<u>Material</u>	<u>m</u>	<u>n</u>
2024-0 Aluminum Alloy	-0.097	-0.455
2024-T351 Aluminum Alloy	-0.091	-0.700
Annealed OFHC Copper	-0.150	-0.634
Hard OFHC Copper	<u>-0.112</u>	<u>-0.575</u>
Average Values	-0.113	-0.591

Fatigue tests on a wide range of materials have indicated (References 18 and 19) that good approximations for m and n are -0.12 and -0.6, respectively. These values are confirmed by the average values, indicated above, for this program. However, if 2024-0 aluminum alloy is considered indicative, the approximations may introduce errors as high as 30 percent in the value of power-law exponents for specific materials.

5.2.4 CYCLIC STRESS-STRAIN ENVELOPE CURVE

Once the power-law relationships relating fatigue life and the elastic and plastic components of strain range have been established for a given material, the equation for the cyclic stress-strain envelope curve can be derived. The cyclic stress-strain envelope curve gives the relationship between the stress range and strain range after steady-state hysteresis conditions have been reached. The relationship should not be confused with the locus curve (Reference 1) or the cyclic stress-strain curve (Reference 7). These latter curves relate stress and strain amplitudes rather than ranges, and for $R_\sigma = R_\epsilon = -1$ they are usually synonymously defined as "the curve which passes through the tips of several stable hysteresis loops oriented symmetrically about the origin." The envelope curve, on the other hand, is the envelope of the outer traces of the same stable loops which have been expediently shifted to a common point at their peak compression to enable graphical definition of the envelope.

The data gathered in this program for several values of strain ratio, R_ϵ , indicate that the definition of the above curves need not be restricted to the use of stable loops for which $R_\epsilon = -1$. That is, the data indicate that it is only necessary that each loop used in the curve definition be one that has relaxed to zero mean stress regardless of the value of R_ϵ . When this condition is met, the loop can be shifted to the origin or to a common reference point at peak compression so as to graphically define the cyclic curves. If a hysteresis loop is unable to exhibit relaxation to zero mean stress during constant strain-range cycles, then the loop cannot be used as indicated above

in the definition of the cyclic curves. Such loops show a constrained relationship between stress and strain range due to insufficient plastic component in the controlled strain-range cycle.

A graphical representation of an envelope curve as obtained from the shifting of five typical stabilized loops to a common point at peak compression is shown in Figure 35. At this point in the discussion it is also of interest to note that an envelope curve of the type shown in Figure 35 has also been directly demonstrated by a test series on a single specimen of SAE 4340 steel (Reference 24) subjected to controlled strain cycles. In these single-specimen tests the minimum strain was held constant and the maximum strain was varied by equal increments on successive cycles. The same envelope curve was found to be generated from cycles having either decreasing or increasing maximum strains. Furthermore, a similar controlled strain test on single crystals of aluminum and copper (Reference 25) has exhibited identical results. In each of the above tests on polycrystalline and single crystal materials, the strain history was found to leave no lasting effects which would alter the shape of the envelope curve significantly.

In developing the stress-strain envelope curve from the power-law relationship which relate the strain-range components and fatigue, it is convenient to combine Equations (10) and (11) through the elimination of fatigue life, N_f . This procedure gives the desired equation for the envelope curve as follows,

$$\Delta\epsilon = C_1 \left[\frac{\Delta\sigma}{C_2} \right]^{n/m} + \frac{\Delta\sigma}{E} \quad (22)$$

The reciprocal of the fractional exponent of the "plastic term," namely, m/n , is the strain-hardening exponent for the cyclic stress-strain relationship.

The envelope curve described by Equation (22) can be considered as the equation for the outer trace of the many individual stabilized loops which define the envelope. The largest of these loops would be that producing failure in one-cycle for which $\Delta\epsilon = \epsilon_f$ and $\Delta\sigma = 2\sigma_f$. It also follows that the strain-hardening exponent for each of the stable loops is the same as the cyclic strain-hardening exponent, m/n , determined for the envelope. These observations have lead to important correlations (Reference 11) between the plastic component of the envelope and plastic strain energy. That is, the plastic strain energy per cycle, ΔW , for any stress or plastic strain-range can be simply related to the product $(\Delta\sigma)(\Delta\epsilon_p)^{(n-m)/(n+m)}$, or in terms of the cyclic strain-hardening exponent,

$$\Delta W = (\Delta\sigma)(\Delta\epsilon_p)^{(1-m/n)/(1+m/n)} \quad (23)$$

The specific envelope equations for the four materials studied in the program are given below.

2024-0 Aluminum Alloy

$$\Delta\epsilon = 0.200 \left[\frac{\Delta\sigma}{1.1(10^5)} \right]^{4.69} + \frac{\Delta\sigma}{10.5(10^6)} \quad (24)$$

2024-T351 Aluminum Alloy

$$\Delta\epsilon = 0.271 \left[\frac{\Delta\sigma}{2.0(10^5)} \right]^{7.70} + \frac{\Delta\sigma}{10.5(10^6)} \quad (25)$$

Annealed OFHC Copper

$$\Delta\epsilon = 0.820 \left[\frac{\Delta\sigma}{1.4(10^5)} \right]^{4.22} + \frac{\Delta\sigma}{17.0(10^6)} \quad (26)$$

Hard OFHC Copper

$$\Delta\epsilon = 0.375 \left[\frac{\Delta\sigma}{1.4(10^5)} \right]^{5.13} + \frac{\Delta\sigma}{17.0(10^6)} \quad (27)$$

SECTION VI

CYCLIC STATE RELATIONSHIPS

6.1 MICROSCOPIC AND MACROSCOPIC VIEWPOINTS AND A HYPOTHESIS

The introductory remarks of the preceding section emphasized that the cyclic stress-strain envelope curve may be found experimentally without carrying test specimens to failure in fatigue. That is, for most materials the envelope curve is established by stable hysteresis loops that have reached stability well before half the fatigue life is expended. Also, it was indicated that the envelope curve may be developed from a single specimen. The single specimen, in this instance, would be subjected to a specific series of controlled strain cycles which would not cause failure and which would display negligible strain-history effects. It would appear, therefore, that the cyclic state is reached before damage is significant, thus providing an excellent baseline relationship for application to both failure and damage analyses.

Bauschinger (see Reference 28) and Bairstow, Reference (29) were the first investigators to recognize the cycle-dependent phenomenological behavior of metals. However, the full significance of their observations was not realized until 1950 when the author published a correlation, Reference (10), between the cyclic state and the Goodman Diagram. In this initial correlation study, it was found that the outer trace of a hysteresis loop correlated closely with the modified Goodman Diagram and thus, the loop appeared to offer a tool for establishing the mean-stress effect. In 1958, after additional evidence of the cyclic state began to unfold, a hypothesis was formulated and advanced, Reference (1), as follows:

"During the cyclic stressing of ductile polycrystalline metals a locus of stress levels versus saturated unidirectional deformations exists. The points forming the locus are single-valued functions of the maximum stress. The cyclic life for a given range of stress is uniquely determined by the corresponding range of stabilized deformation as measured from the locus."

and a corollary to the hypothesis was given as,

"Any ductile polycrystalline metal will exhibit equal cyclic life for equal ranges of stabilized deformation as measured from the locus."

In the development of the hypothesis, the unidirectional yielding, or the hardness variations, taking place at any stress (or strain) level in passing from the static state to the stabilized cyclic state was considered to have negligible effect on fatigue life. However, once the cyclic state

was attained, the basic processes of fatigue damage were considered to have commenced. The cyclic state, therefore, was envisioned as a baseline from which fatigue damage could be assessed.

The cyclic state, as envisioned in Reference (1), was considered to be attained at the microscopic level and it did not appear that the cyclic state could be accurately revealed at the macroscopic level of measurement for all materials. Therefore, in the hypothesis the macroscopic terms of "yielding" and "strain softening, or hardening" were replaced by the microscopic term, "unidirectional deformations (slip)" in describing the processes leading to cyclic stabilization. It is now evident, however, that when the proper balance exists between elastic and plastic strains in a given test, the gross effects of microscopic processes can be revealed at the macroscopic level. That is, an effective "analog" of the fatigue mechanism is available by which the uninhibited straining characteristics of a metal can be observed and measured. The cyclic strain conditions that produce the "analog" are those that exist near the transition life* of the material.

As shown in Figure 44, three regions can be identified along the fatigue-life axis for most metals during cyclic straining. At the low-life end of the axis a region, $1 \leq N_f \leq 10^2$, exists within which the material is in a "highly unstable" condition. Here, failure occurs before mean-stress relaxation or stable hysteresis is complete, thus the material exhibits a definite mean-stress (or mean-strain) effect (References 22 and 23). At the other end of the fatigue axis a region, $10^4 \leq N_f < \infty$, exists within which the plastic-strain component of the cycle is much too small to enable relaxation of mean stress, thus a mean-stress effect again exists. In addition, the hysteresis loops in this region have all but vanished and accurate macroscopic measurements of the plastic-strain component cannot be made.

Between these extremes of the fatigue range an ideal situation exists for detecting the adjustments that lead to a cyclic state at the microscopic level. In the region, $10^2 \leq N_f \leq 10^4$, stable hysteresis has time to occur, sufficient plastic flow is available for relaxation of mean stress, and the large strain components enable accurate measurement. Thus, secondary adjustments within the material and inaccurate measurements will not prohibit precise detection of the true cyclic state through this "analog" region.

Once the cyclic state has been accurately determined within the "analog" region of fatigue life, the relationship can be extended to the static test at $N_f = 1$ and to indefinite life at, say, $N_f = 10^7$ or 10^8 by means of the power-law relationship. This is the procedure discussed and

*Transition-life denotes the value of N_f at which the cyclic elastic strain, $\Delta\epsilon_e$, is equal to the cyclic plastic strain, $\Delta\epsilon_p$.

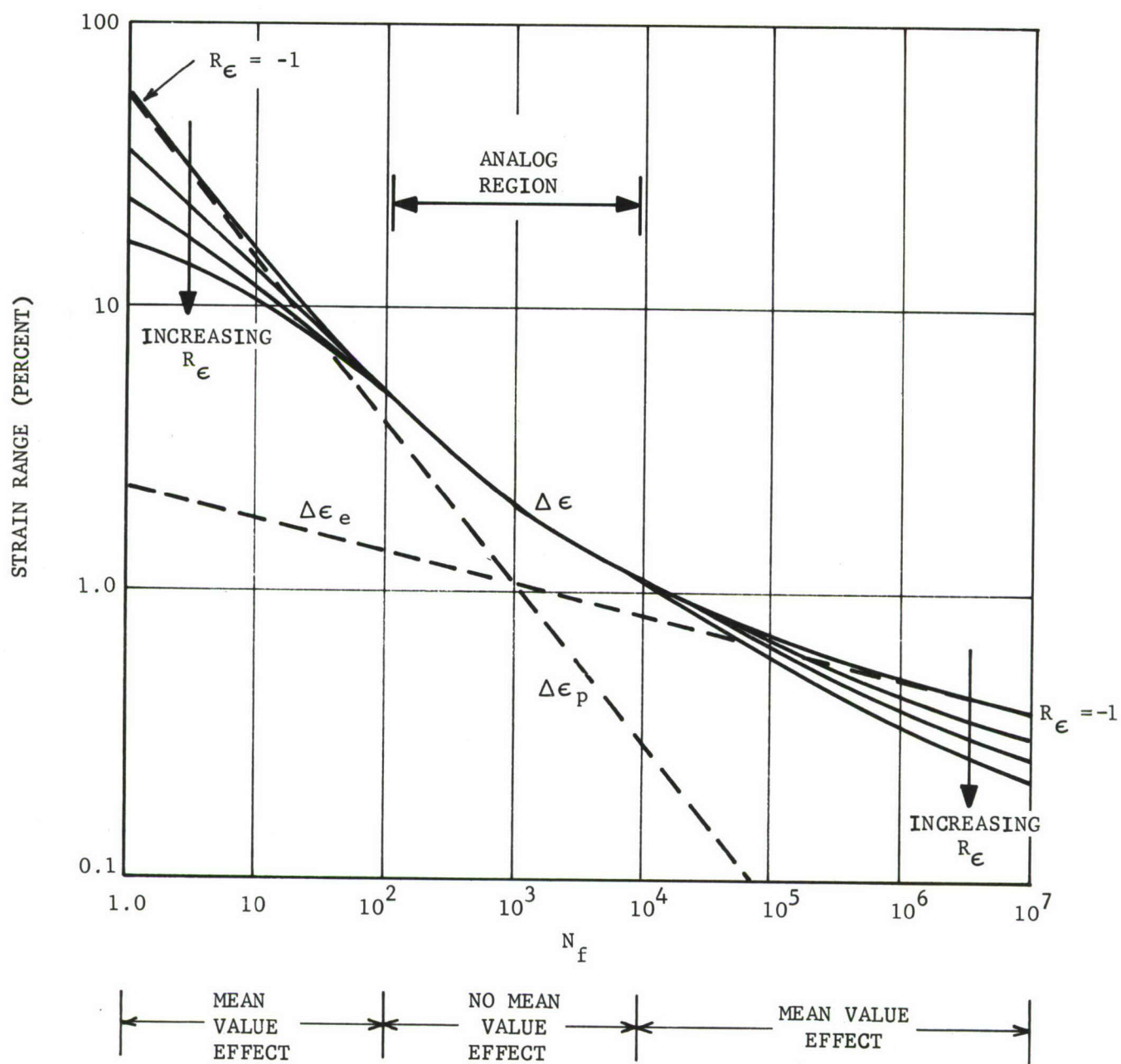


FIGURE 44. MACRO-MICRO FATIGUE ANALOG

employed in the previous section. The power-law relationship offers a fundamental mathematical tool for correlating the response parameters of materials undergoing both static and cyclic loadings. (References 11, 15, and 16). These include monotonic true stress-true strain, rate of crack growth, hysteresis energy dissipation, critical crack-length, etc.; therefore, its application to the correlation of strain-range components with fatigue life is more than fortuitous.

Since in the "analog" region of fatigue life the mean values of stress have relaxed to zero, all extrapolations to shorter and longer values of N_f must be made with $R_\sigma = R_\epsilon = -1$ so as to hold mean values at zero. (See Figure 44.) The end result of such extrapolations will be the two power-law relationships, Equations (6) and (10), extending across the full fatigue range with $R = -1$. These relationships, in turn, can be combined as in Equation (22) to give the basic relationship for the cyclic stress-strain envelope curve which appears to be valid on both the microscopic and macroscopic levels.

6.2 HYSTERESIS COMPONENTS AND THE ENVELOPE CURVE

The power-law relationships for each material tested in this program are shown on the composite plot in Figure 45. In this figure the relationships have been extended into the long-life region where the fatigue process is clouded at the macroscopic level by the predominant elastic component. In lieu of using Equation (22) for plotting the cyclic stress-strain envelope curve, values of the strain components at convenient intervals of N_f can be read directly from Figure 45 and replotted as $\Delta\sigma$ versus $\Delta\epsilon$ where

$$\Delta\sigma = E\Delta\epsilon_e \quad (10a)$$

$$\text{and } \Delta\epsilon = \Delta\epsilon_e + \Delta\epsilon_p \quad (11a)$$

The cyclic stress-strain envelope curves for the four materials are presented in Figure 46. The upper envelope curve for 2024-T351 aluminum alloy corresponds to that used earlier in Figure 35 for the definition of hysteresis components. Also shown in Figure 46 are two dashed curves which represent envelopes determined through incremental step tests (Reference 11) on single specimens of hard and annealed OFHC copper.

It should be noted that the coordinates, $\Delta\sigma$ and $\Delta\epsilon$, define the envelope curve whereas the coordinates, 2σ and 2ϵ must be reserved for the locus curve or cyclic stress-strain curve. The latter relationships will be discussed in the following paragraphs.

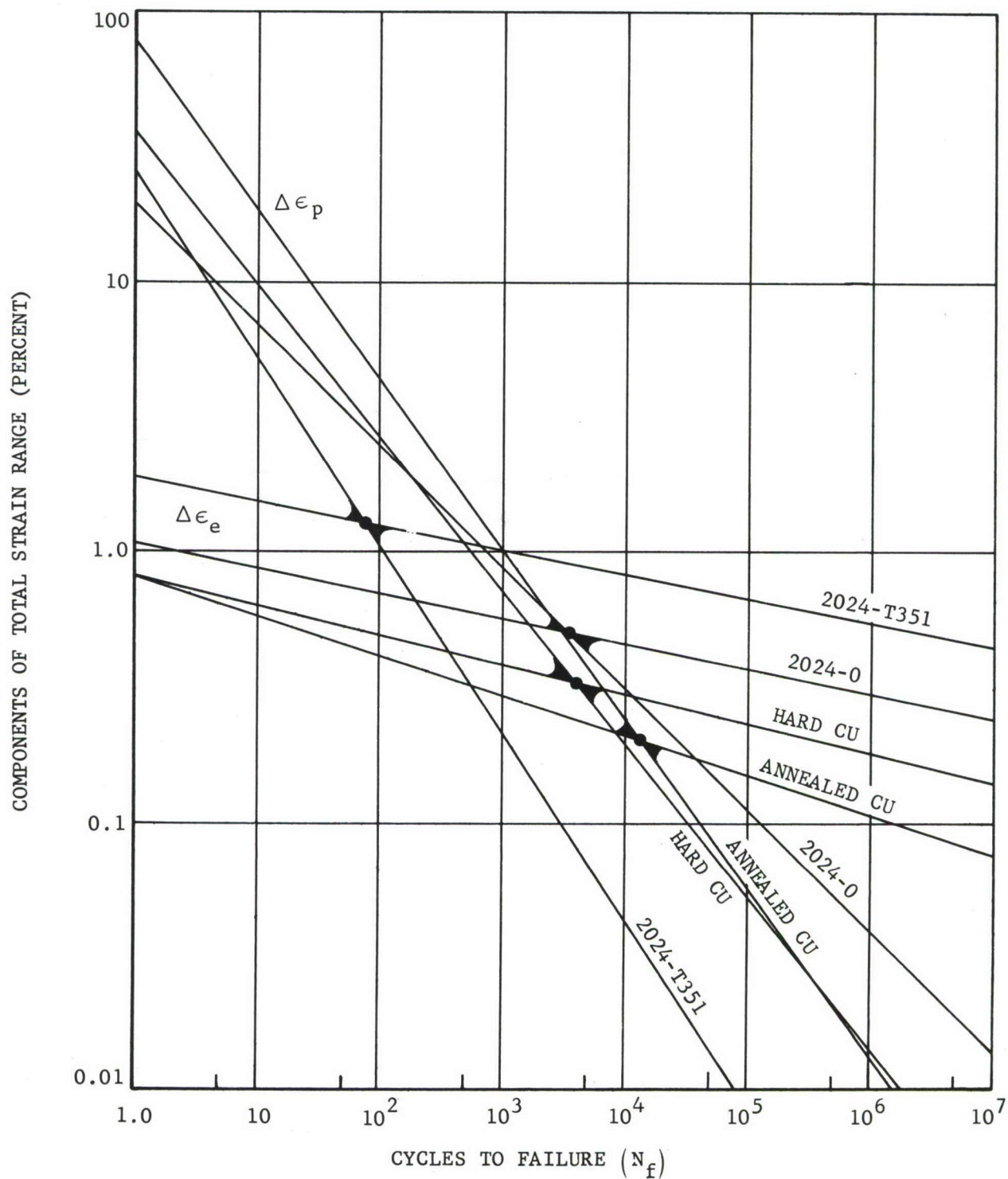


FIGURE 45. POWER-LAW RELATIONSHIPS BETWEEN STRAIN COMPONENTS OF THE CYCLIC STATE AND FATIGUE LIFE

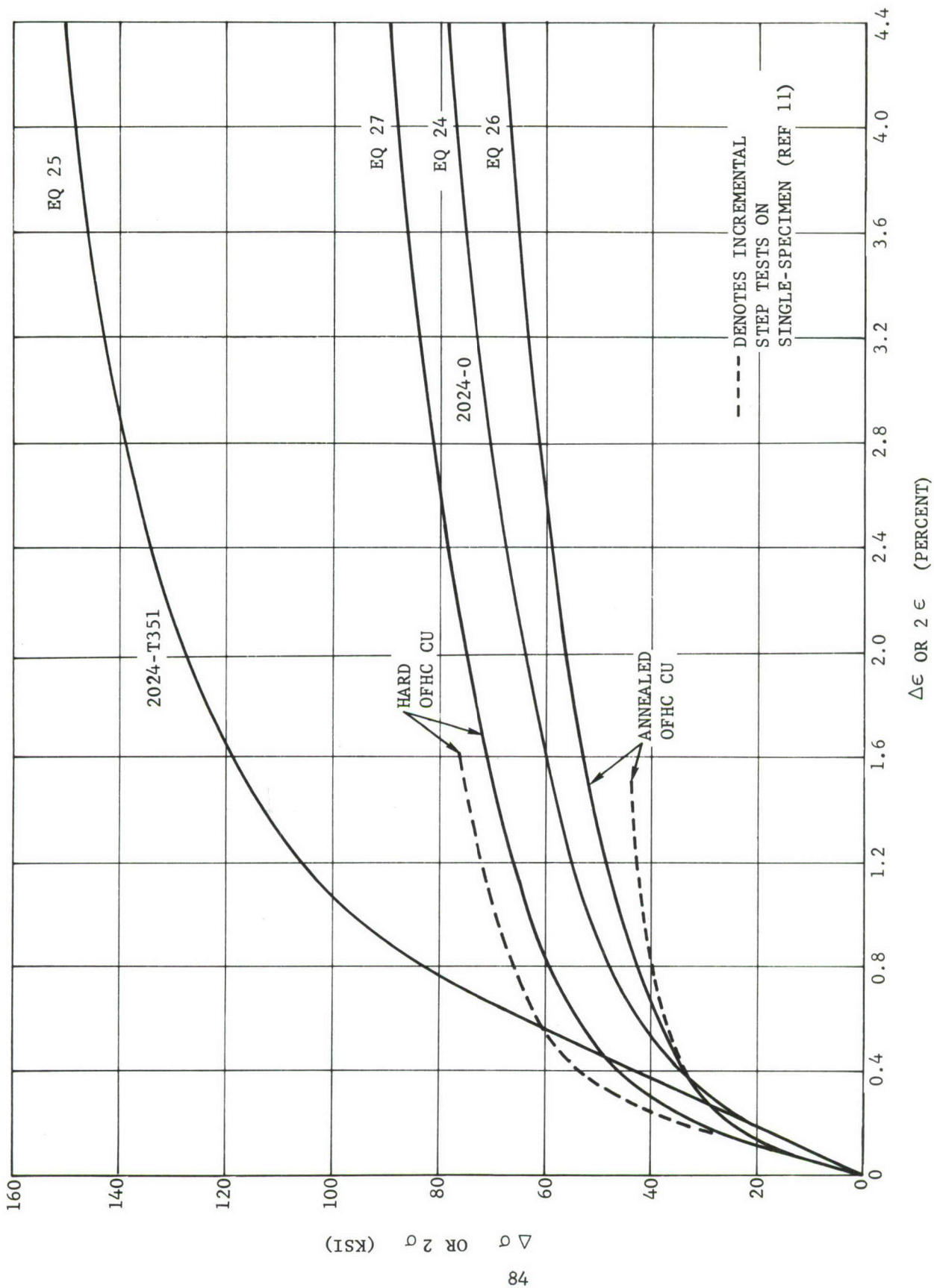


FIGURE 46. CYCLIC STRESS-STRAIN ENVELOPE AND LOCUS CURVES

6.3 CYCLIC STRESS-STRAIN CURVE OR LOCUS CURVE

6.3.1 VERIFICATION OF HYPOTHESIS

The early studies by Bauschinger and Bairstow prompted the present author (References 1 and 10) to hypothesize the existence of a cyclic state in materials which could be expressed by a cyclic stress-strain relationship and used in fatigue analysis. The proposition was made that the cyclic curve could be determined from either the outer-trace of a hysteresis loop having "limited size" (Reference 10) or the locus joining the stabilized maximum peaks reached at each level of cyclic loading (Reference 1). The statement of the hypothesis and its "limiting strain" corollary were given earlier (Section 6.1). In each of the above references a broad spectrum of knowledge drawn from many relevant investigations was used to give credence to the existence of the cyclic state and its application. The reader is encouraged to refer to Reference (1) where an extensive literature review has been presented.

At the time that the universal characteristics of the cyclic state were proposed, experimental data from which cyclic stress-strain curves could be accurately derived were nonexistent. Therefore, a direct test of the hypothesis was not possible. Nevertheless, the "limiting strain" corollary to the hypothesis provided the means by which a reverse application of the hypothesis could be employed to determine if a complete set* of S-N data were consistent with the existence of a singular stress-strain relationship. The singular σ - ϵ relationship in this case, of course, would be the proposed cyclic stress-strain curve. This reversed procedure, as explained in Reference 1, was applied to S-N data for eight alloys, including aluminum, magnesium, and steel. The long-life fatigue data for all of these materials were, indeed, found to be consistent with the proposed cyclic stress-strain curve and the strain-range dependence of fatigue.

Direct means are now available for verifying both the hypothesis which proposes the existence of a cyclic stress-strain relationship and the corollary which proposes its application. That is, the cyclic stress-strain curve as derived from the power-law relationships can now be shown to closely duplicate the singular stress-strain curve developed from the reverse application of the hypothesis.

A typical comparison is shown in Figure 47 of the cyclic stress-strain curve which has been developed in the two distinctly different manners. The dashed curve has been developed by the reverse procedure in which long-life data are used and the solid curve was derived from Equation (25) which is based on short- and intermediate-life data. The agreement for the 2024-T351 aluminum alloy must be considered exceptionally good in that the

*A complete set of S-N data or σ - N_f data consists of fatigue failure data obtained at several values of mean stress or stress ratio, R_σ .

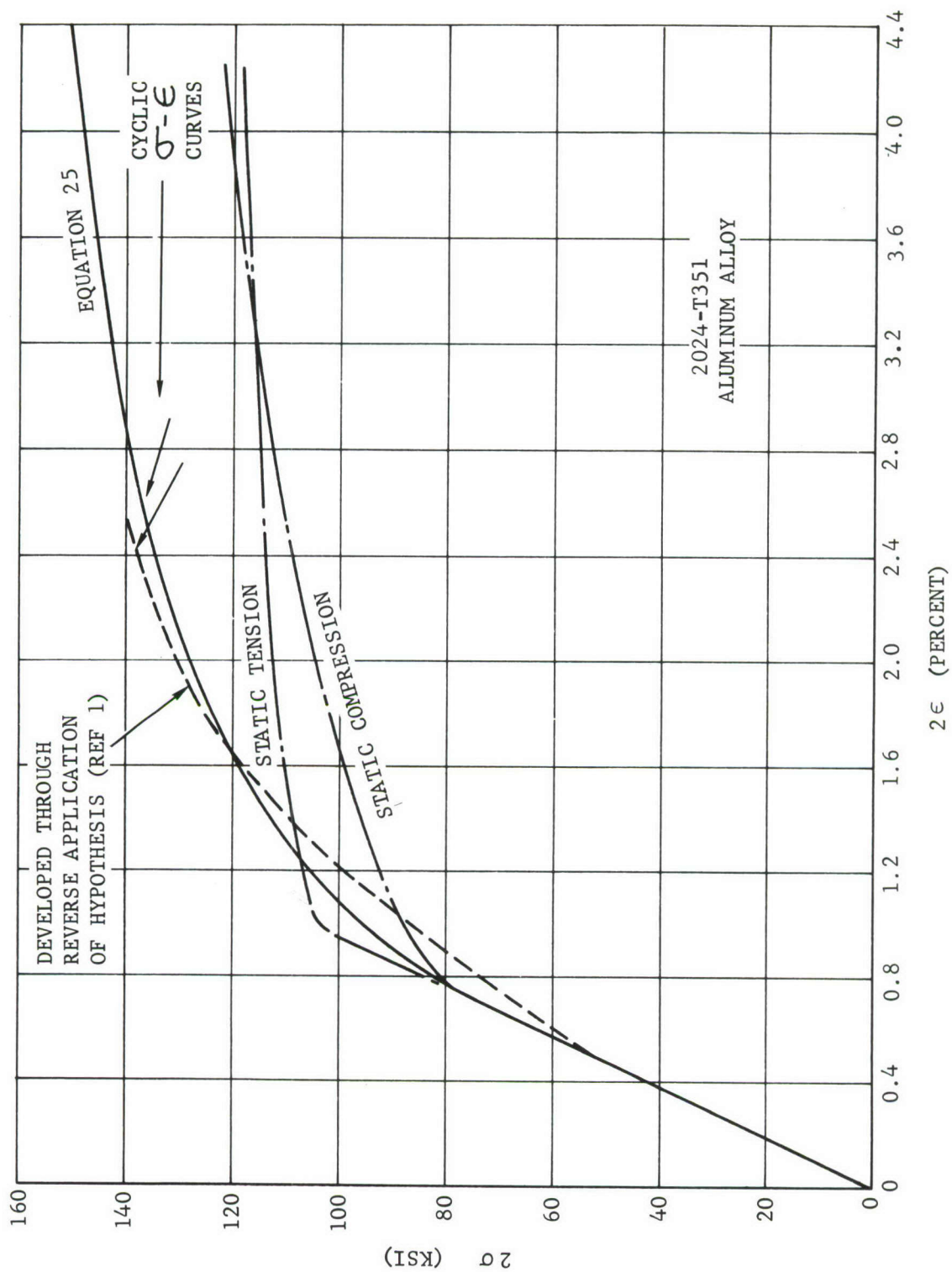


FIGURE 47. COMPARISON BETWEEN HYPOTHESIZED CYCLIC STATE USING LONG-LIFE
FATIGUE DATA AND THE THEORETICAL CYCLIC STATE

two sets of fatigue data employed in the comparison were not gathered from precisely the same heat of material, type of specimen, or experimental set-up. The long-life S-N data employed in the development of the dashed cyclic curve was obtained from References (30) and (31). Similar close agreement can be displayed for 2014-T6 aluminum alloy and SAE 4130 and 4340 steels, but reliable comparative data was not available for the other materials.

6.3.2 COMPARISON OF CYCLIC STRESS-STRAIN CURVE WITH ENVELOPE CURVE

It should be noted that both coordinates in Figure 47 have been expanded to double size. This has been done purposely to bring all curves in Figure 47 to the same stress and strain levels as those of Figure 46. It should be apparent, then, that the envelope curve for 2024-T351 aluminum alloy in Figure 46 has been simply moved to Figure 47. In the new position of the latter figure the curve becomes a double-size, cyclic stress-strain curve. In the former figure, envelope curves were plotted against stress-range ($\Delta\sigma$) and strain-range ($\Delta\epsilon$), whereas in the latter figure the cyclic stress-strain curves have been plotted against double amplitudes, 2σ and 2ϵ .

The difference between the definition of an envelope curve and a cyclic stress-strain curve is shown in Figure 48. As defined previously, the latter curve is the locus curve joining the tips of several hysteresis loops which remain symmetrical about the origin. The envelope curve, on the other hand, is the envelope of the stable hysteresis loops which have been shifted to a common point at peak compression (See Figure 35 and Section 5.2.4). Due to the original symmetry of the loops about the origin, the shifting of the loops to a common peak-compression point will produce an envelope curve that is double the size of the cyclic stress-strain curve provided superposition also occurs for the outer traces of the several loops. Dolan (Reference 24) and Snowden and Wilsdorf (Reference 25) have presented experimental evidence showing that superposition of outer traces does occur when peak compression is fixed. Furthermore, Halford (References 32 and 33) has presented a mathematical development showing that the outer traces of separate loops (envelope curve) have identically the same function as the cyclic stress-strain curve, except that the cyclic stress-strain curve is less by a scale factor of 2. Also, Halford noted that the accuracy of his mathematical development hinged on the constancy of the strain-hardening exponent, m/n , between the several loops and the cyclic stress-strain curve. Experimental results verified that m/n was essentially constant for conditions leading to fatigue life near the transition-life (equal elastic and plastic strain-range components for the loops). As indicated earlier, (Section 6.1) this is the "analog" region where secondary effects are minimized and close correspondence exists between microscopic and macroscopic processes. Therefore, the constancy of m/n (or its microstructural counterpart) can be assumed throughout the fatigue range at the microscopic level.

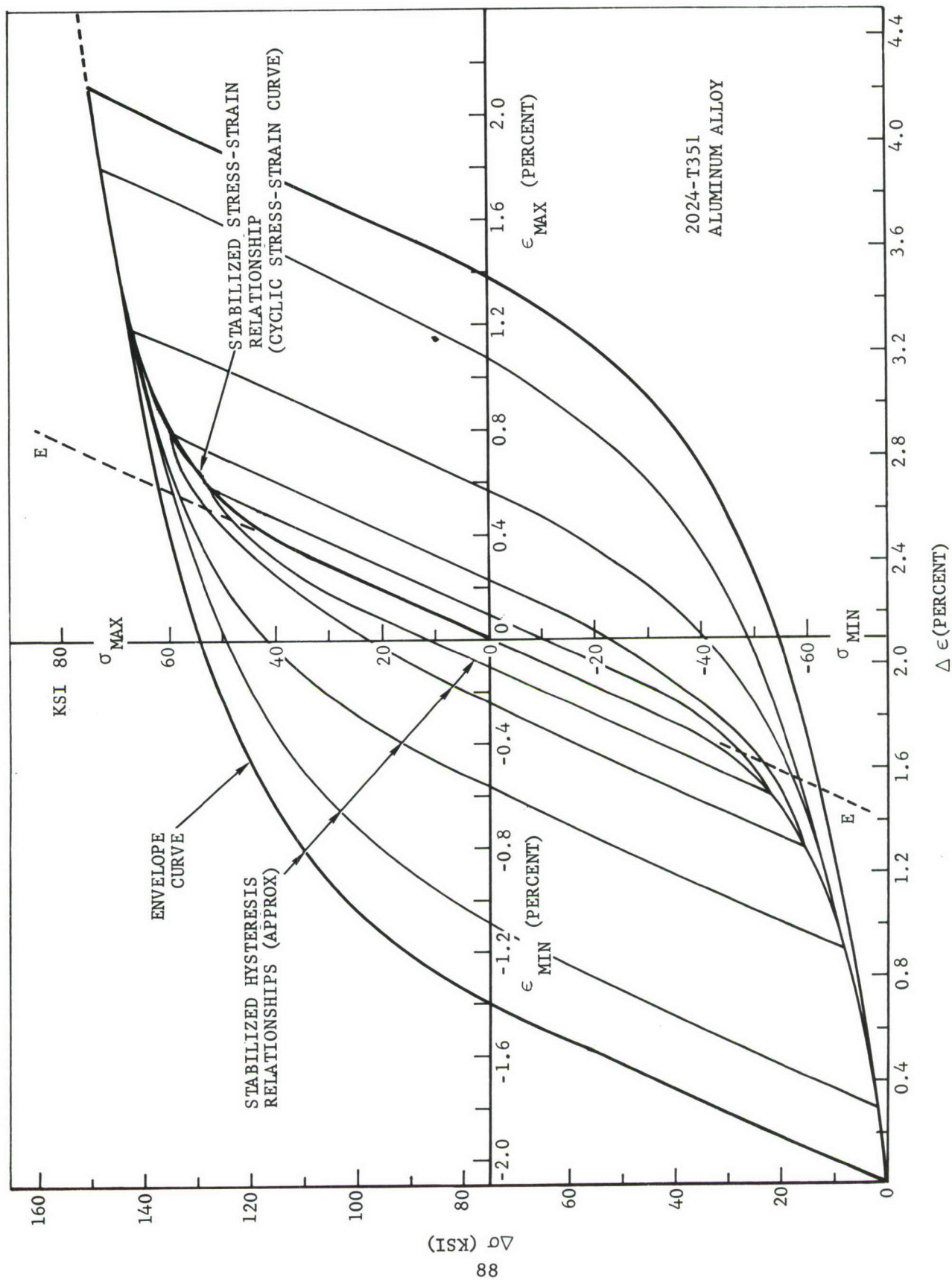


FIGURE 48. THE RELATIONSHIP BETWEEN THE ENVELOPE CURVE AND THE CYCLIC STRESS-STRAIN CURVE

SECTION VII

PREDICTION OF MEAN STRESS EFFECT FROM CYCLIC STRESS-STRAIN CURVE

7.1 MEAN VALUE EFFECTS AT SHORT-LIFE

In an earlier section (Section 6.1) it was emphasized that at each end of the fatigue range a region exists within which mean-stress (or mean-strain) effects are very significant. In the low-cycle region, $N_f \leq 100$, where materials are subjected to large excursions of plastic strain, failure occurs before the cyclic state is reached. Even though an abundance of plastic flow is present for relaxing the mean stress that accompanies a given mean strain, full relaxation cannot occur before the mean stress has accelerated the low-cycle failure process. The low-cycle (large strain) failure mechanism is known to be primarily a tensile mode of cracking often referred to as the Stage II mechanism (References 34 and 35). This failure mechanism does not await stabilization; in fact, it has been confirmed for a wide variety of materials (Reference 16) that the Stage II crack propagation occupies at least 75 percent of the life in low-cycle fatigue. Therefore, specimens which have an initial mean stress and which are tested at sufficiently high strains to cause failure in less than 100 cycles, or so, will show a mean-stress effect. When mean stress (or mean strain) is initially zero, the Stage II failure process can be shown (References 16 and 36) to agree with the crack-propagation law that forms the basis of the so called Manson-Coffin power-law relationship (Equation 6). This, of course, means that in passing from the region of Stage I crack propagation (slip plane failure mechanism) to the region of Stage II processes the cyclic stress-strain relation is unaffected at the micro-structural level. These findings justify the extension of the macroscopically obtained power-law relations ($R_\epsilon = -1$) through the ill-defined* low-cycle region ($N_f < 100$) so as to intercept the static test data at $N_f = 1/4$ or 1.

As far as predicting the mean-strain effect on fatigue life below 100 cycles, the following equation has been suggested (Reference 23) as a good approximation to experimental data,

$$N_f = [(\epsilon_f - \epsilon_o) / \Delta\epsilon]^2 \quad (28)$$

When mean strain, ϵ_o , is zero, Equation (28) reduces to

$$N_f = (\epsilon_f / \Delta\epsilon)^2 \quad (29)$$

*ill-defined is used with reference to the uncertainties clouding the very low cycle data resulting from specimen buckling, difficult measurements of applicable stresses and strains, etc.

which corresponds to the power-law relationship of Equation (6) where $C_1 = \epsilon_f$ and $\Delta\epsilon_p = \Delta\epsilon$. The first of these equalities is a good approximation regardless of the magnitude of N_f and the second is also a reasonably good approximation at $N_f < 100$.

No attempt has been made in this report to directly derive an equation having the form of Equation (28) from the cyclic stress-strain curve. However, even though the hysteresis conditions are rapidly varying with each cycle in the low-life range, the cyclic state curve may offer a base-line for the formulation of a more precise mean-strain equation whose range of validity is unrestricted.

7.2 MEAN VALUE EFFECTS AT LONG-LIFE

In the long-life region of fatigue, say $N_f > 10^4$, the plastic-strain components for most materials during stable hysteresis are found to be near imperceptible at the macroscopic level. A shortage of plastic flow is, thus, emphasized and it is found that even small initial mean stresses cannot be erased by relaxation. Therefore, at $R \neq -1$, both constant strain-range cycling and constant stress-range cycling produce mean-stress effects.

In the long-life region of fatigue the material reaches the cyclic state during the early percent of the fatigue life; therefore, unlike low-life fatigue, the cyclic stresses and strains are of stable magnitudes throughout the critical period of crack propagation.* For the $R_\sigma = R_\epsilon = -1$ conditions, the narrow hysteresis loops remain symmetrical about the origin and the relationship between stress- and strain-range is expressed by the envelope curve. In addition, the symmetry of the cyclic stress-strain curve about the origin (see Figure 48) also provides a direct relationship between the peak (positive and negative) stresses and strains.

When the stress ratio, R_σ , or strain ratio, R_ϵ , is greater than -1.0, the utility of the cyclic stress-strain curve can be extended, as outlined in Reference 1, to give the effect of mean stress on fatigue life. That is, the cyclic stress-strain relationship, according to the previously expressed hypothesis, can be employed in the same manner as the widely used mean-stress relationships** which are of the form,

$$\left(\frac{\sigma_a}{\sigma_e}\right)^p + \left(\frac{K \sigma_m}{\sigma_{ult}}\right)^q = 1 \quad (30)$$

where σ_a = amplitude of alternating stress

*Stage I crack propagation is the process active in long-life fatigue (Reference 34).

**These relationships include Modified Goodman, Soderberg, Gerber and Ellipse equations.

- σ_e = endurance limit (amplitude) for completely reversed cycling. Generally defined as maximum stress to give life of 10^7 cycles.
- σ_m = mean stress
- σ_{ult} = ultimate stress (nominal) from static tension test
- p and q = exponents, equal to either 1 or 2, depending on relationship.

Generally, the mean-stress relationship of Equation (30) is expected to furnish a "built-in" conservatism for design purposes. This would not, of course, be true for the predictions resulting from the use of the cyclic stress-strain curve as a substitute. Here, accuracy in predicting test results is the criterion.

A brief review of the mechanics of using a cyclic stress-strain curve in the prediction of mean-stress effects is facilitated by Figure 49. In the figure are shown the static and cyclic stress-strain curves and the strains relating to either constant stressing or constant straining of a given material. According to the hypothesis, the stable loop, AB, will be established by cycling between stress levels $A\sigma$ and $B\sigma$ such that the maximum stress, $A\sigma$, yields at the microstructural level to the stable point A on the cyclic stress-strain curve. Simultaneous with the strain adjustment at the peak stress, a cyclical permanent set, $B\sigma B$, at the microstructural level will occur whereby point B is attained. The movement of $A\sigma$ to A and $B\sigma$ to B is the result of unidirectional deformations* occurring at the microstructural level simultaneous with the alternating deformation. After the stable loop position is reached, all unidirectional deformation ceases with the reversible straining, $\Delta\epsilon$, remaining throughout the greater part of the fatigue life.

The stable loop, AB, would also be achieved at the microstructural level under constant strain-range cycles between maximum and minimum strains, $A\epsilon$ and $B\epsilon$, respectively. In this case, however, stress level $A\epsilon$ would reach level A on the cyclic curve through strain softening. Simultaneous with the adjustment at the maximum strain, the stress level B would be reached at the minimum strain such that point B becomes compatible with both the strain requirement and the "elastic hysteresis" passing through A. Again, after the stable loop has been achieved (with the peak stress lying on the cyclic stress-strain curve), the reversible straining, $\Delta\epsilon$, would continue through the greater part of the fatigue life.

The discussion given in the above two paragraphs relative to deformations and the cyclic curve has purposely emphasized the microstructural viewpoint. In the long-life fatigue region ($N_f > 10^4$) it appears that this view is necessary since the long-life fatigue region lies outside the "analog region" and macroscopic measurements can no longer be expected to reflect microscopic

*See recent publication by Wood (Reference 37) in which he discusses unidirectional deformation at the microstructural level while specimens are undergoing reversible deformations at the macroscopic level.

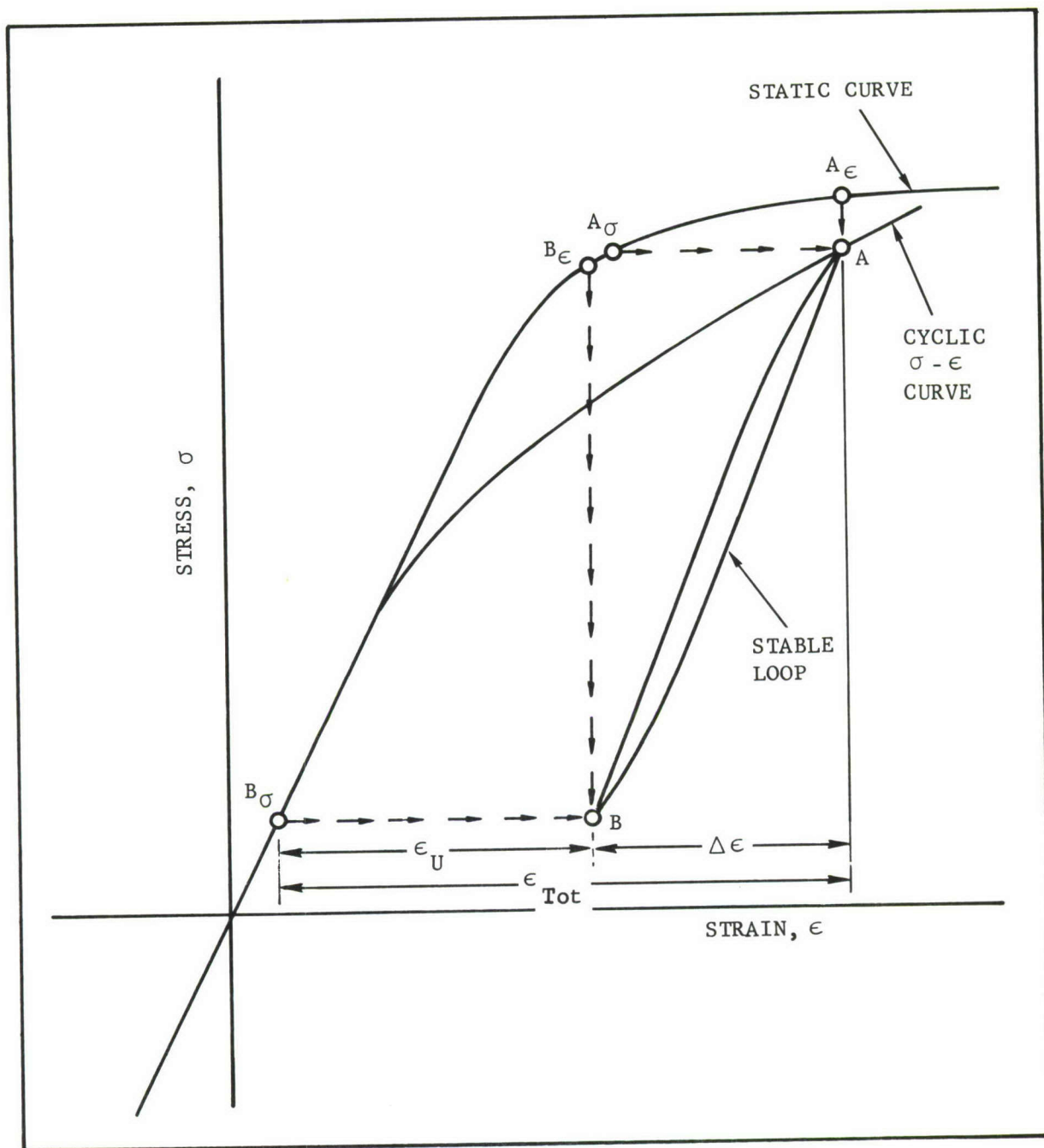


FIGURE 49. THE CYCLIC STRESS-STRAIN CURVE AND RELATED STRAINS

behavior. Nevertheless, the mechanics of using the cyclic stress-strain curve, once it has been developed from a test series within the "analog region," is the same at either the macroscopic or microscopic level. These procedures are discussed in the following paragraphs.

Under either constant straining or constant stressing, it has been considered in the development of the hypothesis that the cyclic state is reached before significant damage has been incurred. Also, after the cyclic state has been established, it has been considered that the peaks of the stable loop and its position relative to the cyclic stress-strain curve offers a measure of the two principal contributors to fatigue damage. The first of these measurements is afforded by the cyclical permanent set, ϵ_U , which is defined as the irrecoverable strain measured between the lower extreme of the stable hysteresis loop and the cyclic stress-strain curve. In Figure 49 the cyclical permanent set is identified. On the microstructural level the permanent set is considered to offer a measure of the permanent disorientation occurring in grains or "structural cell-formations" (Reference 37) within the polycrystalline aggregate.

The second contributor to fatigue damage can be measured directly as the alternating strain, $\Delta\epsilon$, taking place as the stable loop is traversed. The crucial feature of the alternating strain is that it proceeds to intensify the defects or damage from the disorientation as measured by the cyclical permanent set. The summation of the two strain measurements (permanent set plus alternating) was, then, considered to establish a critical total of strain. This total of strain (or limiting strain) is identified as ϵ_{Tot} in Figure 49. It should be noted that ϵ_{Tot} is measured from the cyclic curve, and it depicts the total of strain (or range of stabilized deformation) that has been considered in the hypothesis to uniquely determine the fatigue life. That is, the cyclic stress-strain curve can be used to establish all ranges of stress which will produce the same fatigue life.

In order to employ the cyclic curve in the above fashion to generate $\sigma-N_f$ curves (S-N curves) for all values of mean stress, it is necessary to have one relationship giving the variation of fatigue life with range of stress. This can best be in the form of a single $\sigma-N_f$ curve determined from actual fatigue data at a convenient mean stress or stress ratio. The need for the single $\sigma-N_f$ curve lies in the fact that it is necessary to know at least one range of stress producing a given fatigue life. This range of stress enables the total strain, ϵ_{Tot} , causing failure in the given number of cycles to be determined from the cyclic stress-strain curve as indicated in Figure 49. Finally, this value of total strain can be used with the cyclic curve to establish all other ranges of stress giving the same fatigue life.

In the event that a $\sigma-N_f$ curve is unavailable, the total strain versus fatigue-life relationship (Equation 11) could be substituted and employed in the long-life fatigue region as an $R\epsilon = R\sigma = -1$ curve. However, in the development of Equation (11) the possible existence of an endurance limit

strain has not been included. Therefore, it is important for many materials to introduce in the $\Delta\epsilon$ - N_f equation a provision for the existence of an endurance limit. For this purpose, Manson (Reference 18) has presented procedures for introducing the endurance limit by means of the equation,

$$N_f = A(\Delta\epsilon - \Delta\epsilon_{end})^\gamma \quad (31)$$

where,

A is of the order of $\epsilon_f^{-1/n}$
 γ is of the order of $1/n$

The result of using the cyclic stress-strain curve in combination with an available fatigue curve to obtain the fatigue curves at other values of R is shown in Figure 50. The fatigue data for 2024-T3 aluminum alloy shown in this figure were obtained from References (30) and (31). The fatigue curve at R = -1 which appeared to be the more accurately defined was taken as the given fatigue curve.

By the procedure given in detail in Reference (1) and in Appendix B of this report, the R = -1 curve was used to establish the ranges of stress and limiting strains (from cyclic stress-strain curve) that produce failure at convenient intervals of fatigue life, say 10^8 , 10^7 , 10^6 , 10^5 , and 10^4 cycles. Each limiting strain, in turn, was employed with the cyclic curve to establish other ranges of stress corresponding to the selected intervals of fatigue life. From these ranges of stress and the related values of σ_{max} and mean-stress, a plot of constant life lines against σ_{max} and σ_{mean} was generated to assist in the determination of σ_{max} for each required value of R and fatigue life.

The fatigue curves in Figure 50 for R = -0.6 through 0.5 are the end-result of the above procedure. Fortunately, fatigue data were available from References (30) and (31) for these additional values of R, thus providing a means of checking the accuracy of the hypothesis underlying the method. Although the cyclic stress-strain curve was determined from circular cross-section test specimens and the data points in Figure 50 were determined from sheet specimens supported by guide plates, the predictions offered by the application of the hypothesis are very good. It should be noted that the tensile yield strength and tensile ultimate of the 2024-T3 and 2024-T351 aluminum alloys were identical.

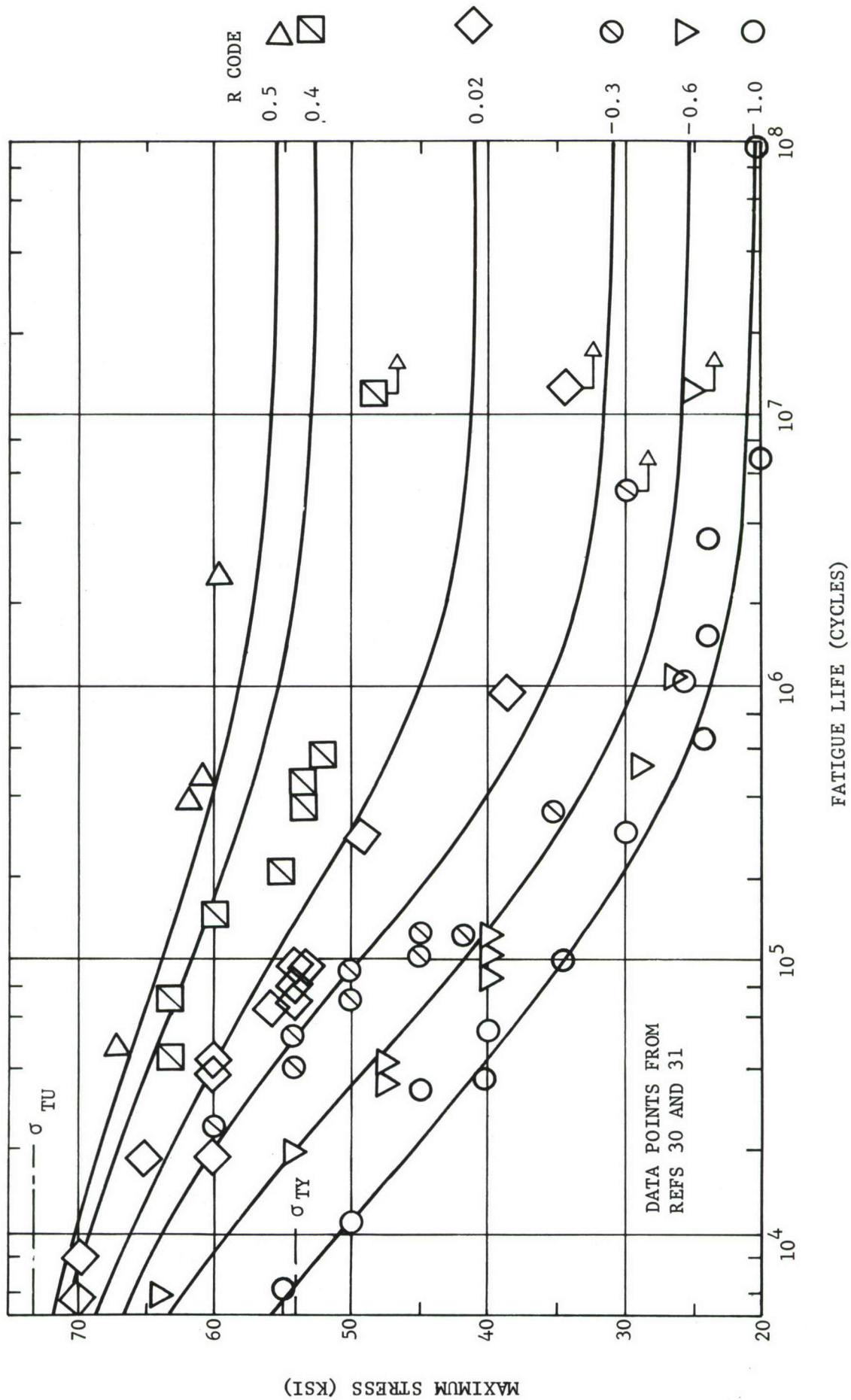


FIGURE 50. FATIGUE CURVES FOR 2024-T3 ALUMINUM ALLOY

Figure 51 presents data points taken from Reference (30) for SAE 4130 steel with superimposed fatigue curves derived from a cyclic stress-strain curve in conjunction with the $R = -1$ curve. In this instance the cyclic curve was developed from data taken from Reference (9). These latter data are shown in Figure 52 with the power-law relationships that were used to define the cyclic stress-strain curve. As before, the data taken from the two references were gathered from round bar specimens, Reference (9), and sheet specimens, Reference (30), but the predictions are still very good. The difference between the static tension properties of the hard 4130 steel, Reference (9), and the normalized 4130 steel, Reference (30), is misleading in that the hard material softens* during cycling to very near the same cyclic state as that of the normalized material.

In a similar manner, intermediate- to long-life fatigue data on SAE 4340 steel from Reference (38) and short- to intermediate-life fatigue data from Reference (9) have been combined to further evaluate the predictions of the hypothesis. The comparison between test data and the predictions derived from the cyclic state are shown in Figure 53. The data from Reference (9) and the power-law relationships used in the definition of the cyclic stress-strain curve are shown in Figure 54. Again, the differences existing between the static material properties as given in the two references did not reflect the close similarity of the cyclic state exhibited by various hardened conditions of the SAE 4340 steel. A typical cyclic state for hardened SAE 4340 steel is given in Reference (9).

The cyclic stress-strain curves for the four materials tested in the present program and reported herein, plus the SAE 4130 and 4340 steels employed in the comparisons, are presented in Figure 55. In view of the fact that development of the fatigue curves for any value of R is dependent only upon the relative magnitudes of the limiting strains (total strains, ϵ_{Tot}) as measured from the cyclic stress-strain curve, the cyclic curves have been normalized such that the alternating strain**at $N_f = 10^7$ cycles is assigned the value of unity. This normalizing expedient has been used in the presentation of curves in Figure 55. In this figure it should be noted that the normalized strains constitute a measure of the damage index, $\gamma(\sigma)$. The value of the damage index relating to the endurance limit*** (fatigue limit) of the 2024-T3 aluminum alloy displayed in Figure 50 is given by $\gamma(\sigma_{\text{end}}) = 0.91$. The corresponding values of $\gamma(\sigma_{\text{end}})$ for SAE 4130 and 4340 (Figures 51 and 53, respectively) are 0.57 and 1.05, respectively. Since these indices are single amplitude values, essentially indefinite fatigue life would be expected as long as $\gamma(\sigma_{\text{max}}) - \gamma(\sigma_{\text{min}}) \leq 2\gamma(\sigma_{\text{end}})$. It should be noted that the damage index is a negative value if obtained for a compressive stress.

*See comparison between cyclic and virgin tensile stress-strain curves of Reference (9).

**One-half the value found from Equation (11) without consideration of an endurance limit strain.

***Single amplitude of stress at $R = -1$ for $N_f = 10^7$ cycles.

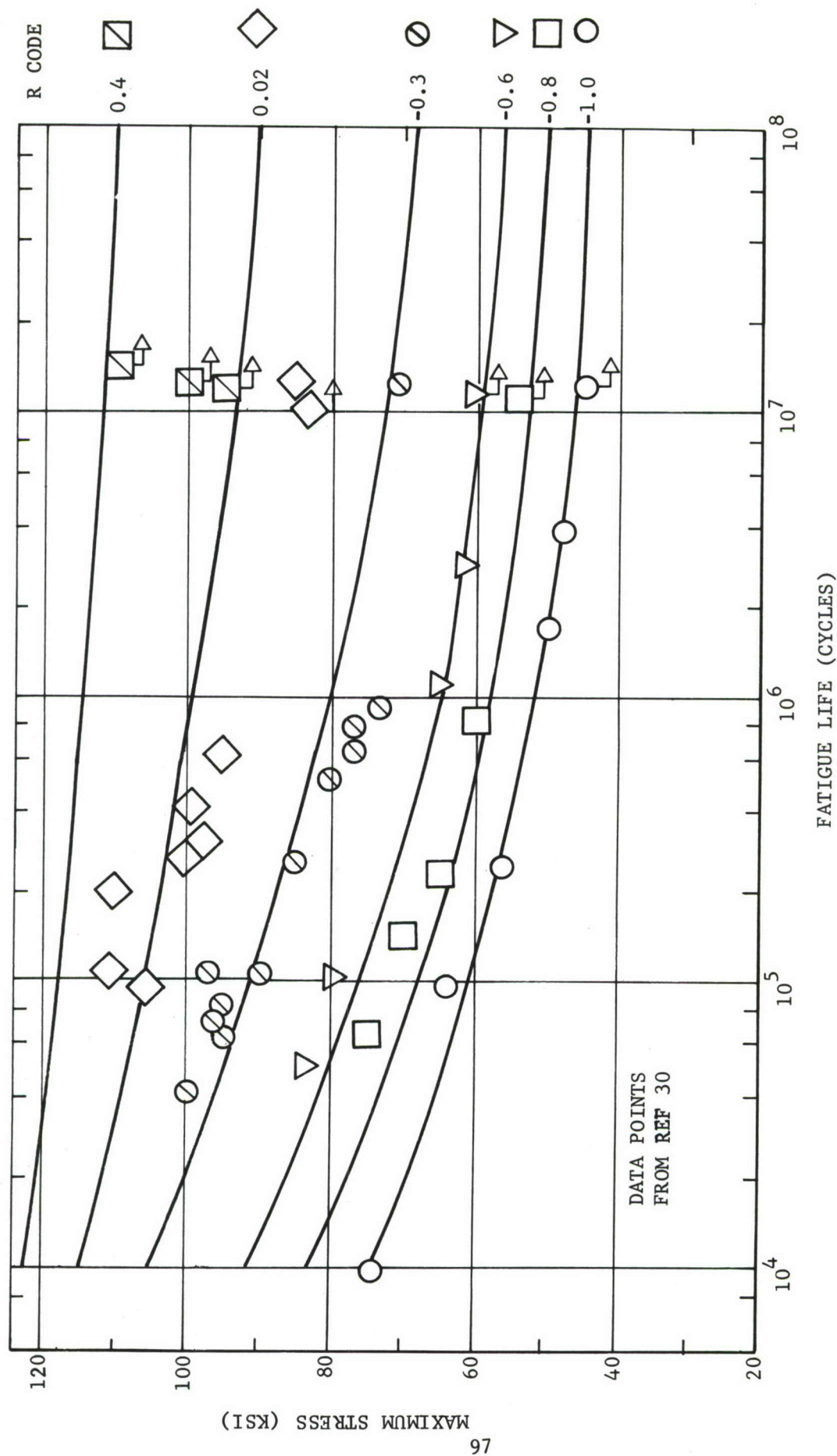


FIGURE 51. FATIGUE CURVES FOR NORMALIZED SAE 4130 STEEL

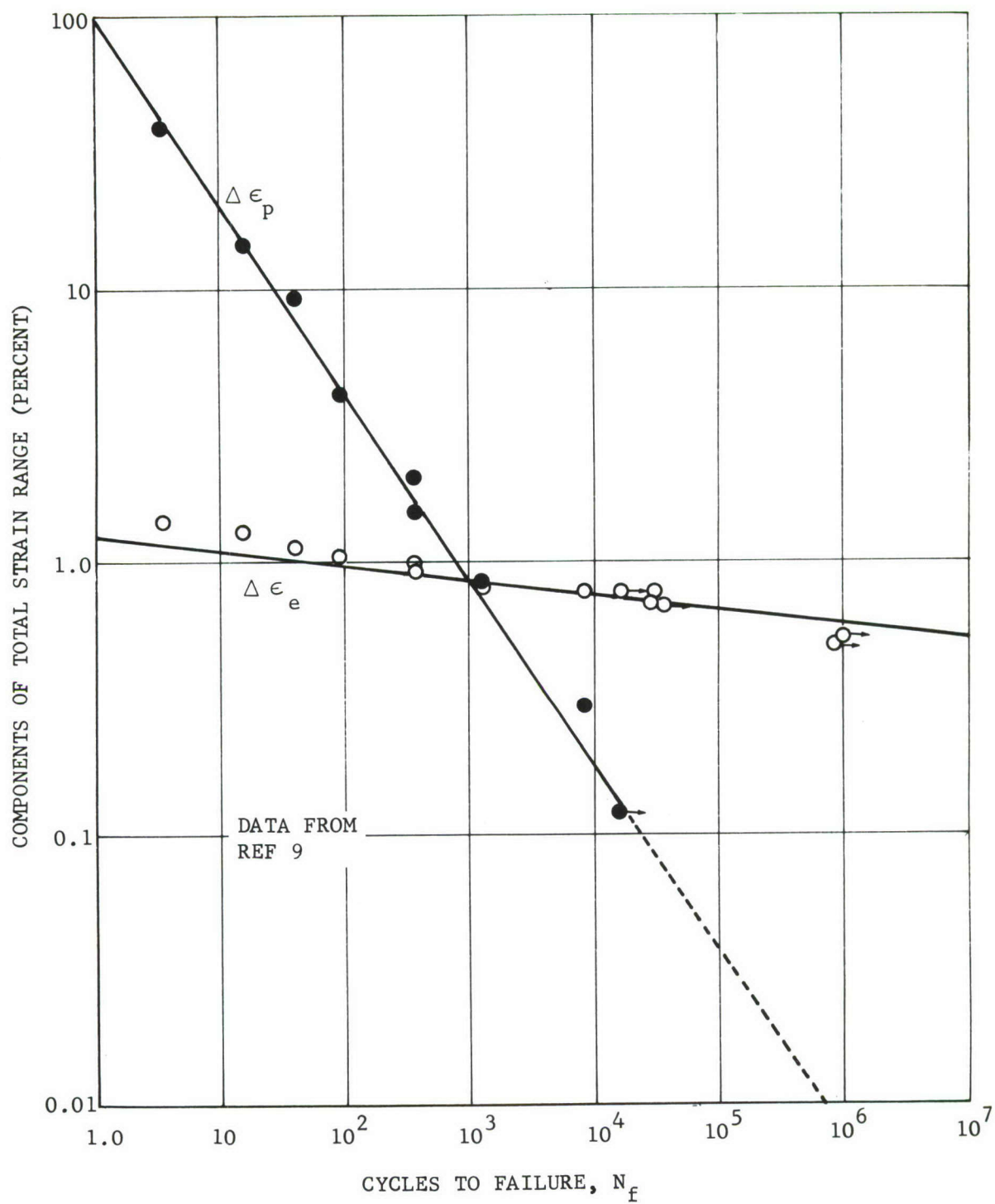


FIGURE 52. COMPONENTS OF TOTAL STRAIN RANGE DURING FATIGUE OF HARD AISI 4130 STEEL

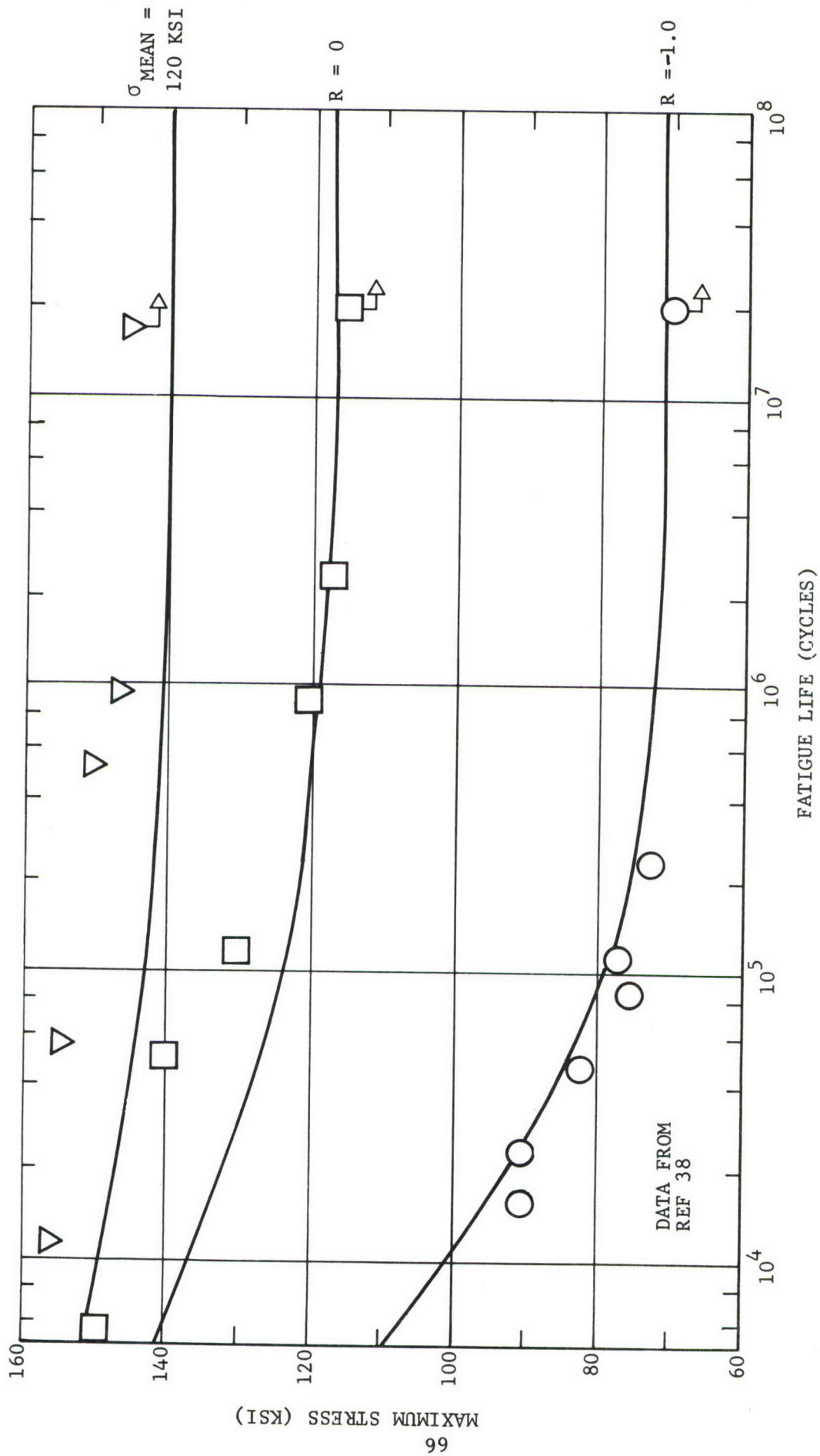


FIGURE 53. FATIGUE CURVES FOR SAE 4340 STEEL

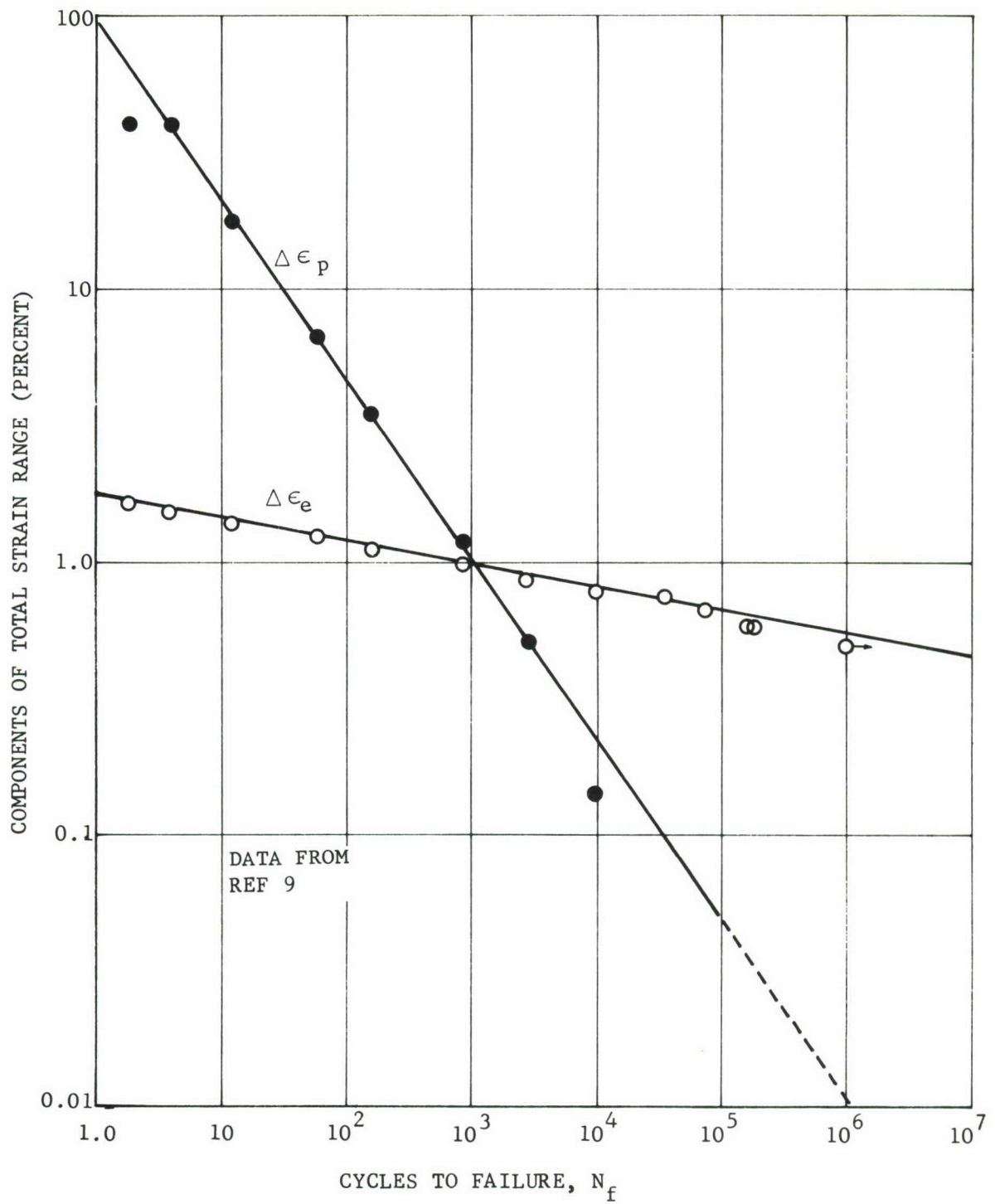


FIGURE 54. COMPONENTS OF TOTAL STRAIN RANGE DURING FATIGUE OF HARD AISI 4340 STEEL

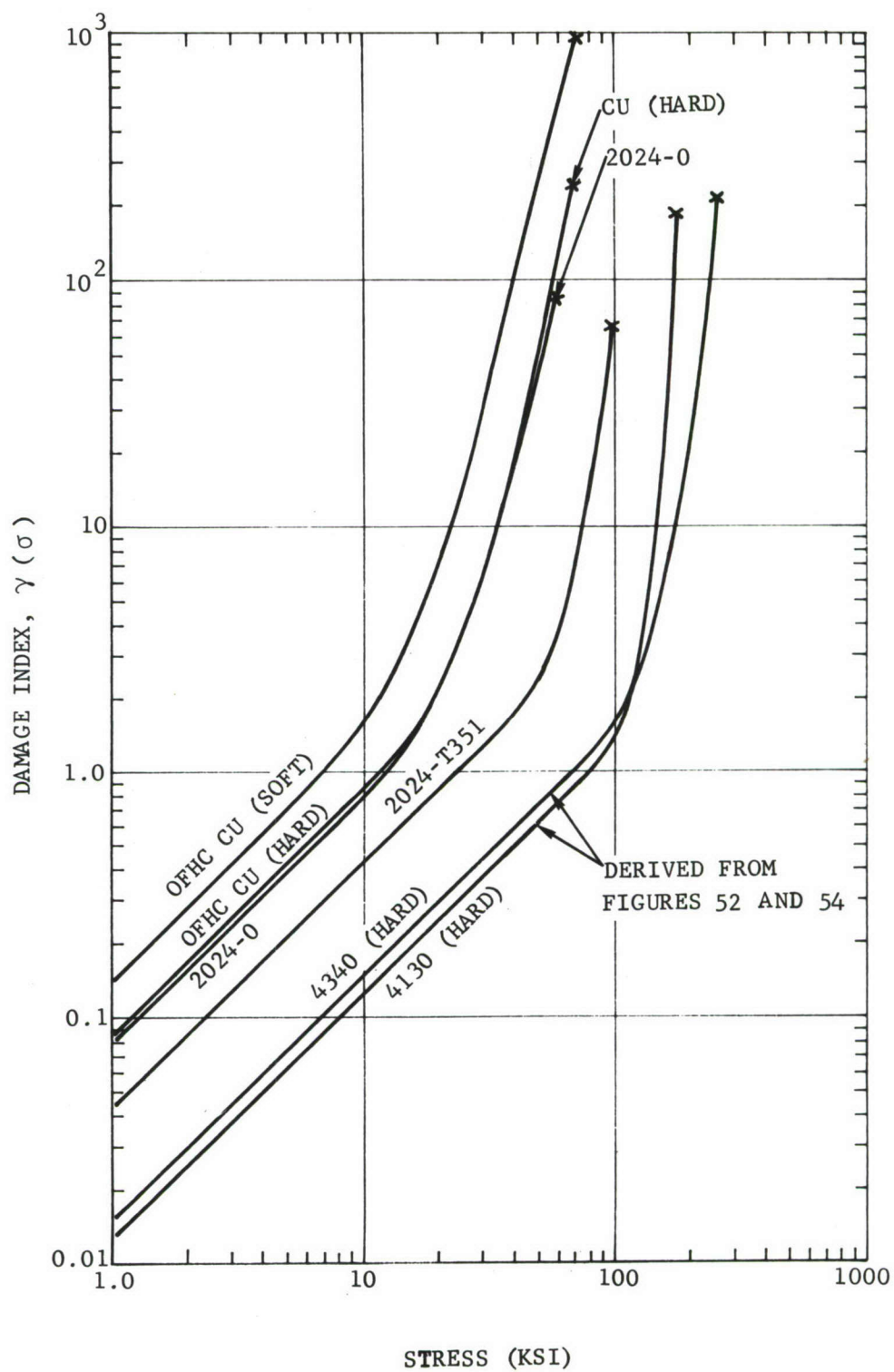


FIGURE 55. NORMALIZED CYCLIC STRESS-STRAIN CURVES

SECTION VIII

EFFECTS OF VARIABLE AMPLITUDE STRAINING

8.1 RESPONSE TO DUAL LEVEL STRAIN AMPLITUDES

The discussions presented in the foregoing sections of this report have emphasized the fundamental behavior of materials during the application of constant ranges of load or strain. Since these constant-level loading conditions are seldom experienced by materials within actual structures, it is also important to have basic information as to the response of materials when abrupt changes are made in the applied strain amplitudes. A brief study of such material behavior was made in this program on the annealed and hard conditions of copper which display work-hardening and work-softening characteristics, respectively, during cyclic straining. The resulting information gives some insight as to the effect of changes in amplitudes of cyclic strain-ranges on these materials.

The responses shown by annealed copper and hard copper, when the applied strain-range is abruptly changed, are shown in Figures 56, 57, and 58. For each of the dual-level tests depicted in the figures, the abrupt change to the second test level was made after the material had stabilized at the initial level.

The result of increasing by a factor of two the applied strain-range on initially annealed copper is given in Figure 56. Here, the induced stress limits give a measure of the hardening that has taken place in the material during the cycles of strain. The test on the annealed copper began at the 1-level and the hardening progressed, as a function of N , as shown by the solid lines representing the limits of the induced stress. The initially applied strain-range was 0.47 percent which remained constant through the 3000th cycle (or, one-third the expected fatigue life at this level). As noted by the figure, the strain-hardening had reached saturation by the 200th cycle at this initial strain level. At the beginning of the 3001st cycle the strain range was abruptly increased to 1.00 percent with the lower strain limit being held at approximately zero. In attaining the higher maximum strain level the first 1/4 cycle after the 3000th cycle carried the material along a stress-strain path that was below that of the cyclic stress-strain curve shown earlier in Figure 46. However, the additional hardening at the higher test level (2-level) soon carried the material very near the cyclic curve. The additional hardening at the second level is noted in Figure 56 by the related solid lines.

The upper and lower dashed lines in Figure 56 indicate the path that would have been taken by the induced stresses if the strain-range had been held constant at 1.00 percent throughout the test. The horizontal portion of the

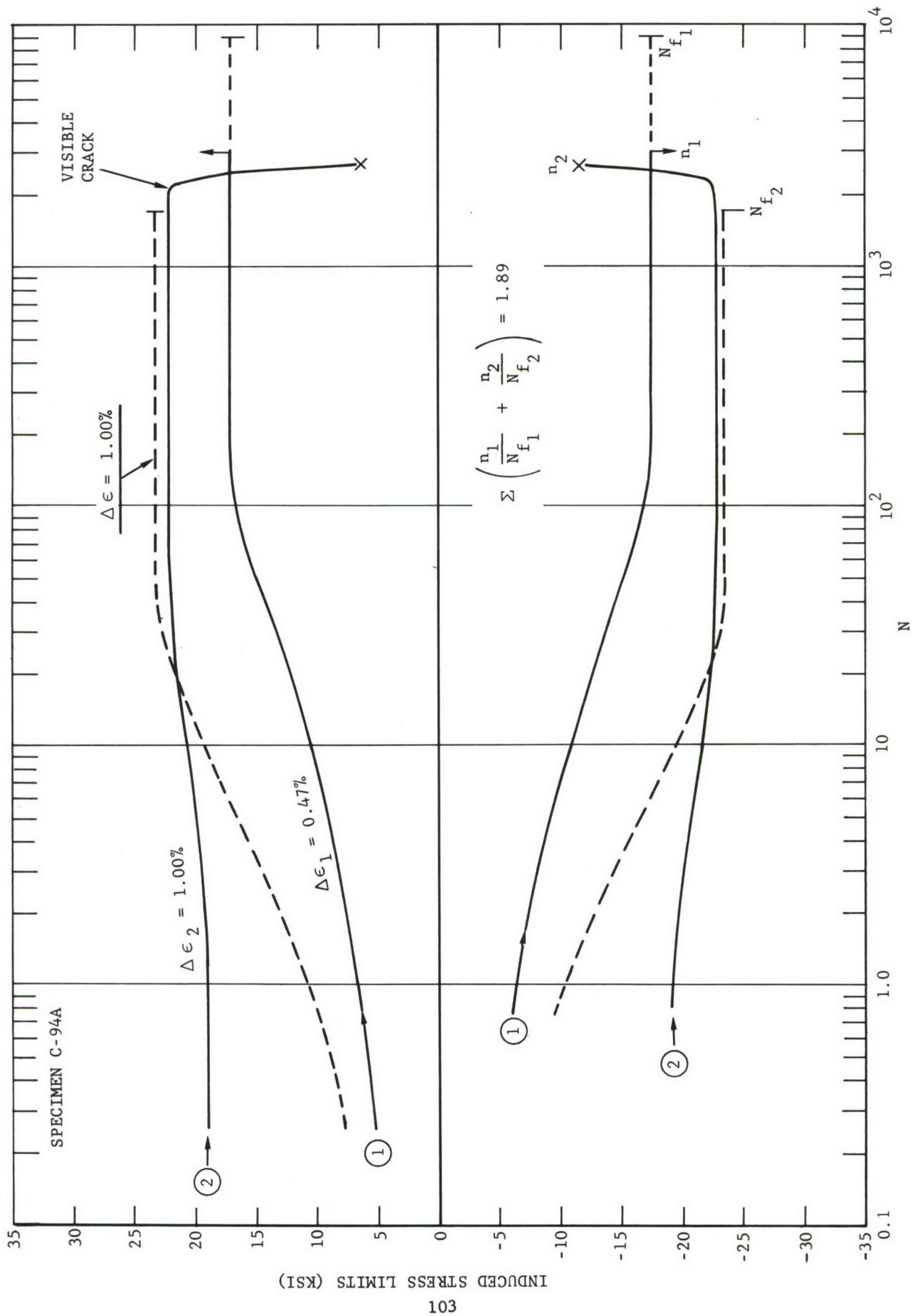


FIGURE 56. STRESS LIMIT VARIATIONS FOR ANNEALED COPPER DURING CYCLES OF LOW-HIGH MAGNITUDES OF CONSTANT STRAIN RANGE ($R_\epsilon \approx 0$)

two dashed lines defines the range of stress employed with the constant strain-range of 1.00 percent to give a point on the cyclic stress-strain envelope curve. Therefore, since the induced strain-range given by the dashed lines is not quite reached by the 2-level solid lines, neither is the cyclic stress-strain curve reached by the stabilized conditions at the 2-level. This deviation between the levels of saturation hardening exhibited for the single-level test and the second-level of the dual-level test are not unexpected results. That is, the work-hardening introduced in the initially annealed copper by the prior cycles at the first-level would be expected to create a new hardness of copper (as well as, possibly, a damaged copper) upon which the second-level of strain-range would be applied and held constant to failure. Thus, the annealed copper after prior cycles at the first-level would display a saturation hardness level that is compatible with the cyclic-state of the newly created condition of copper. Furthermore, depending on the percentage of fatigue-life expended at the first level, the newly created condition of copper would be expected to be more or less a function of an induced change in hardness than a function of induced damage from cracks initiated and propagated at the initial level.

The data presented in Figure 56 show that the fatigue-life of the initially annealed copper, when subjected to cycles of 1.00 percent strain-range, is actually improved by prior cycles at the 0.47 percent strain-range. Again, this is not an unexpected result if it is considered that the prior cycles have actually created a material that is not precisely comparable to the initially annealed material whose stress response is given by the dashed curve. If a new condition of copper has been created by the first-level test, then the fatigue characteristics of this new material must be described by a new set of power-law relationships.

Qualitatively, the improvement in fatigue-life at one strain-range level by prior cycles at another strain-range level can be explained by reviewing the role played by coefficients, C_1 and C_2 , and the exponents, m and n , in Equation (11). It should be apparent that a particular set of these constants can be identified with a given material, and if the material undergoes basic changes the applicable power-law constants will also change. In particular, it can be observed in Figures 41 and 43 that straining processes which harden copper have the effect of reducing the value of the fracture ductility and the engineering strain at tensile fracture. Also, the slope of the total strain-range curve is less for the harder copper. Thus, if the effect of prior cycles is primarily that of increasing hardness, then two simultaneous effects on the total strain-range curve will be produced, namely, a translation downward due to the reduction of ductility and a counter-clockwise rotation due to the reduction in slope. In combination, these effects may produce a total strain-range curve for the newly created material that displays better fatigue characteristics for a given strain-range than the annealed copper in a single-level test.

In Figure 57, the results of a similar set of dual-level strain-range tests are shown for annealed copper. Here, however, the larger strain-range has

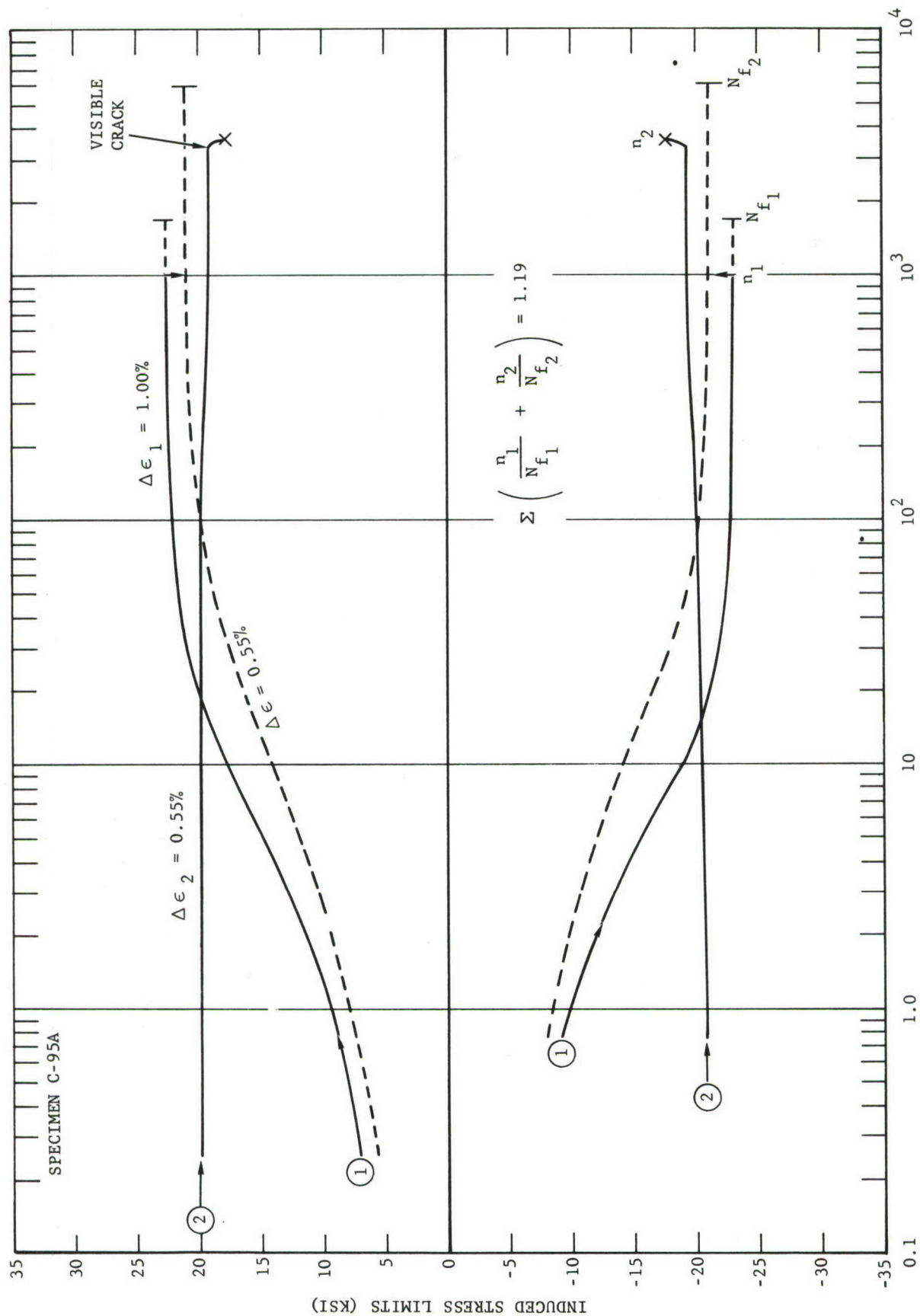


FIGURE 57. STRESS LIMIT VARIATIONS FOR ANNEALED COPPER DURING CYCLES OF HIGH-LOW MAGNITUDES OF CONSTANT STRAIN RANGE ($R_\epsilon \approx 0$)

been applied first. As indicated by the 1-level, a strain-range of 1.00 percent was applied to the initially annealed copper for 1000 cycles (59 percent of the expected fatigue life at this level). Saturation hardening was reached at this initial level by the 200th cycle. At the beginning of the 1001st cycle, the strain-range was abruptly lowered to 0.55 percent with the lower strain limit being held constant at approximately zero. As cycles of the lower strain-range were applied, a slight softening was observed. The softening is displayed in the figure by the slight reduction in induced strain-range at the 2-level. Again, similar to the data in Figure 56, the saturation-hardness at the second-level did not coincide with the level shown by the dashed line for single-level testing at the same strain-range. As in the dual-level test of Figure 56, the difference in saturation hardness levels appears to be a strain history effect which has introduced a new hardness of copper whose behavior is not directly comparable to that of the annealed material.

The failure data presented in Figure 57 show that the prior cycles at the 1-level have caused a reduction in fatigue life at the 2-level. This result is more satisfying to intuition, and it is also more compatible with the cumulation of damage at several levels as proposed by the Palmgren-Miner method (Reference 41). Nevertheless, regardless of the effect of prior cycles, the fatigue life at the second-level appears to be amenable to the explanation given earlier in which hardness changes require alterations of the constants in the fatigue equation. In this instance, a rather large reduction of ductility and a small decrease of slope (log-log power-law plot) for the new hardness of copper had the combined effect of reducing the fatigue characteristics at the second level of the test.

Dual-level test results on initially hard copper are shown in Figure 58. The first level of applied strain-range (0.73 percent) was cycled for 580 cycles or 21 percent of the fatigue life expected if this range were held constant to failure. Beginning with the 581st cycle the strain-range was abruptly increased to the second level at 1.33 percent. As noted in the figure, very little additional softening was measured after the shift to the higher range of strain. The saturation softness level reached during the second level of cyclic strains was only slightly below that reached by a single-level test at 1.33 percent strain-range (see dashed line). This result may indicate that the cyclic stress-strain curve for the newly created copper (resulting from the stress history of prior cycles) has a stress-strain point that is closely common to the cyclic stress-strain curve for the initially hard copper.

The failure data shown in Figure 58 show that the prior cycles at the first-level have increased the fatigue resistance at the second-level by about 36 percent. The same qualitative arguments presented earlier for explaining the effect of prior cycles on the fatigue resistance of initially annealed copper appears equally applicable to the above results on initially hard copper.

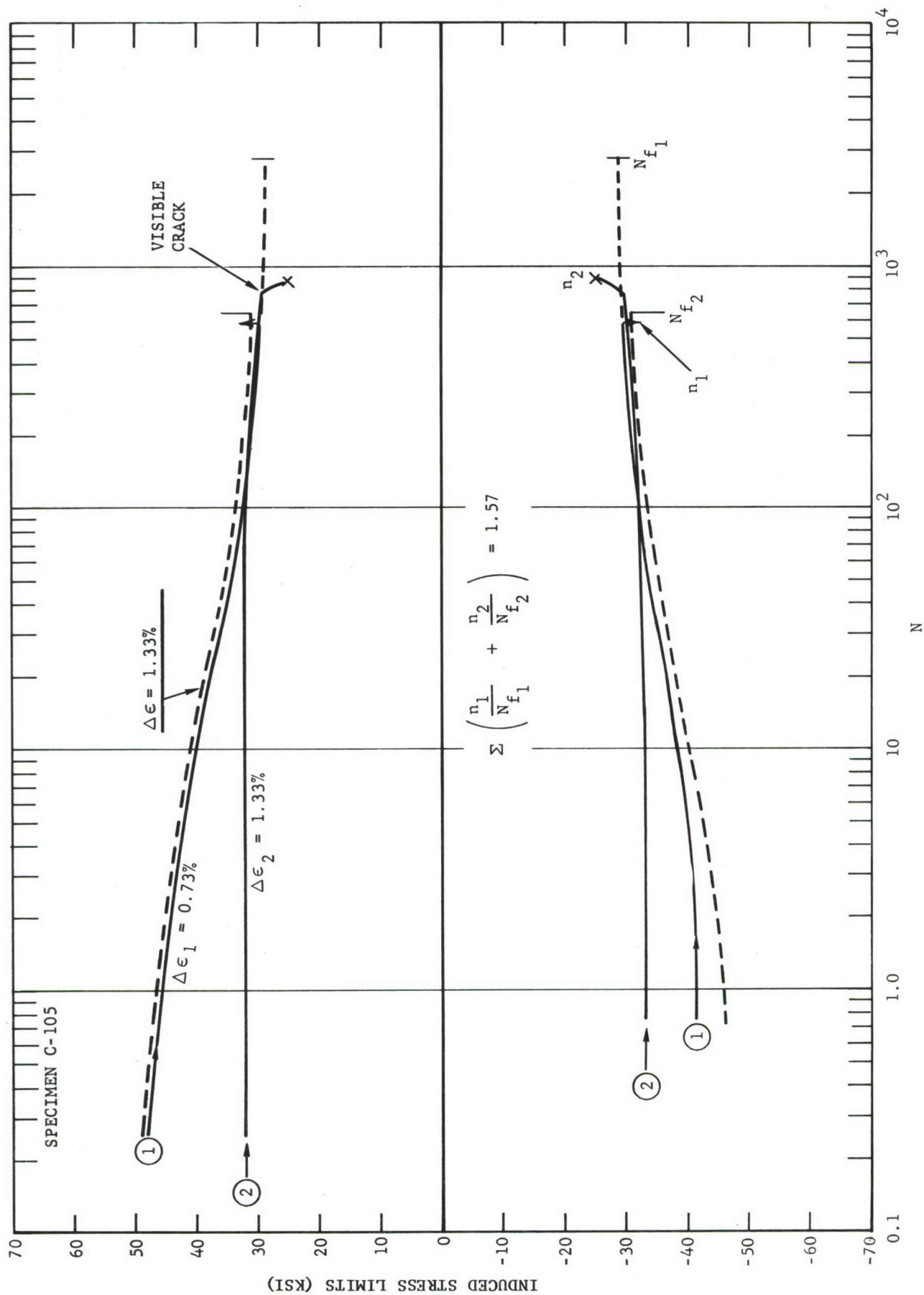


FIGURE 58. STRESS LIMIT VARIATIONS FOR HARD COPPER DURING CYCLES OF LOW-HIGH MAGNITUDES OF CONSTANT STRAIN RANGE ($R_\epsilon \approx 0$)

8.2 CUMULATIVE FATIGUE DAMAGE DURING MULTI-LEVEL LOADING

From all the published cumulative damage theories available today, only the simple Palmgren-Miner rule, (Reference 41) has found wide application. The extensive use of the method stems not only from its simplicity, but other theories have not yet succeeded in gaining more confidence with respect to their reliability.

The basic hypothesis of the Palmgren-Miner rule may be stated as follows: Assume a material or structure is subjected to a cyclic loading for only n_1 cycles although this level of cyclic loading would have eventually produced failure in N_{f1} cycles. Under these conditions the rule states that a fraction of the total fatigue life of the structure equal to n_1/N_{f1} will have been consumed. If the structure were then subjected to another level of loading for n_2 cycles, for which N_{f2} cycles would have produced failure, then an additional fraction of the total fatigue life equal to n_2/N_{f2} would be consumed. The step-wise consumption of fatigue life in this manner is then considered to be cumulative such that

$$\sum_i \left(\frac{n_i}{N_{fi}} \right) = 1 \quad (32)$$

The Palmgren-Miner rule is not compatible with more than one independent damage parameter, therefore its validity from a physical point of view is questionable. Nevertheless, Shanley (Reference 15) has employed typical crack-growth curves to give some physical basis for the rule. As Shanley points out, the accumulation of damage need not be linear in applying this rule, although the "cycle ratios" are added linearly. The rule assumes that there is no interaction effect from the order in which the strain (or stress) ranges are applied. This, of course, is incompatible with some experimental results which have shown large effects which depend on the ordering of the loadings. Nevertheless, the vast majority of experiments which have applied the rule to fatigue data obtained under variable amplitude loadings have shown that the summation of the cycle ratios, $\sum n_i/N_{fi}$, produces values that fall between 0.5 and 2.0. And, it is important to note that the majority of results involving typical structural members (riveted joints, wing structures, notched specimens, etc.) showed conservative values for the summation (i.e., > 1). The seemingly large spread in results (0.5 to 2.0) obtained by the Palmgren-Miner rule should not, however, label the method as being inaccurate. First, it is necessary to define what is meant by "accurate" in this instance. Schijve, (Reference 42) has reviewed experiments on cumulative damage, and he has concluded that life predictions within a factor of 2 may be regarded as good estimates from the technical point of view. That is, the summation of the cycle ratios may vary between 0.5 and 2.0 and still be considered very good. This conclusion by Schijve needs some qualification, however, since a summation

provided by Equation (32) which lies between 0.5 and 2.0 for fatigue tests performed at only a few levels would indicate that the method is valueless. As an example, if a dual-level test series were to show a summation of "cycle ratios" equal to, or near, 2.0, then this would indicate that even though 99.9 percent of the fatigue life may have been consumed at the first level, approximately 100 percent of the fatigue life was still available at the second level. Such a result would, of course, completely invalidate Miner's rule. Therefore, for the summation of the "cycle ratios" to vary between 0.5 and 2.0 and still be considered a satisfactory test of Miner's rule, a large number of test levels must be involved in the test-series.

The Palmgren-Miner rule has been applied to the very simple dual-level test-series described in Figures 56, 57, and 58. On the face of these figures the summation of the "cycle ratios" has been shown to be 1.89, 1.19, and 1.57, respectively. Thus, Miner's rule would have been very inadequate for predicting the cumulative fatigue life in the first and third test-series.

As stated in Section 8.1, the changes in hardness and the associated changes in ductility that accompany abrupt changes in applied strain levels appears to have an important influence on fatigue life during dual-level tests within the low-life fatigue region. Under these conditions, the "material change" that takes place during a switch in the applied strain level evidently introduces a new fatigue equation, and before Miner's rule can be accurately applied, this new equation must be identified.

SECTION IX

CONCLUSIONS

The following conclusions appear justified from the combined observations of the present program and the related results from the referenced investigations.

9.1 EXPERIMENTAL PROCEDURES

The one-inch gage length specimen employed in this investigation, from which axial strains were measured directly, offers an excellent means of obtaining hysteresis and fatigue data in the range of fatigue life $10^2 < N_f < 10^4$. The specimen is not recommended, however, for tests in which fatigue life is less than 10^2 cycles due to the possibility of buckling at $R = -1$, even under fixed-ended conditions.

The detrimental effect of knife-edge marks from an extensometer can be easily eliminated through the use of a thin adhesive pad bonded at the gage point locations.

The mechanical extensometer is a reliable and accurate device for sensing cyclic strains in the low- to intermediate-life fatigue range.

Hysteresis measurements and fatigue-life determinations below 10^4 cycles are best obtained through constant strain-range testing with $R_\epsilon = -1$, thus giving effective control over the large deformations.

No measurable temperature-rise was noted in the tests described herein; therefore, for low-speed testing such measurements do not appear to offer promise for detecting fatigue-mechanisms or energy dissipation unless extremely sensitive schemes are employed.

9.2 PHENOMENOLOGICAL OBSERVATIONS

The range of stress or strain over which Poisson's ratio changes from a value near $1/3$ to the plastic value of $1/2$ can be very large depending on the "knee" of the static stress-strain curve.

For highly ductile materials, true fracture strain or fracture ductility can be in error by 50 percent if determined solely from measurements of final fracture diameter. More properly, fracture should be considered to have occurred when failure is reached at the neck axis as indicated by an abrupt drop in the true stress during the tensile test.

The Bridgman "correction factors" for stress distribution at the neck of tensile specimens are not significant for most engineering materials;

therefore, such refinements in the determination of stress levels offers very little improvement in correlating the elastic component of the fatigue equation with the tensile test.

Hardness readings do not appear to offer a sufficiently accurate means for correlating either uniform hardness or localized hardness with fatigue.

Cyclic creep can be expected to be significant in most materials during constant load-range testing for which fatigue failure occurs below, or near, 10^3 cycles.

Cyclic creep strain versus peak true stress converges on the true-stress-true strain power-law relationship during the primary stage of the process. During the secondary and tertiary stages of cycle-induced creep, the true stress-true strain relationship is closely followed.

When the cyclic creep process carries the material to strains in the P_{\max} region of the true stress-true strain curve, neck-down instability is imminent.

Cyclic creep is cycle-dependent rather than time-dependent.

Cyclic creep is produced by gradually accumulating elongations which arise from applications of cyclic loads. These elongations are predictable and are known to be of second-order and irreversible.

Cyclic creep does not alter the shape of the hysteresis loop significantly during the constant load test; both maximum and minimum peaks of the loop creep in equal amounts.

Materials with compression yield strengths lower than the tensile yield strength can be expected, as a result of the Bauschinger Effect, to creep into compression to some degree during the initial cycles.

Saturation hardening or softening of materials is best exhibited through constant strain-range testing.

During the cyclic strain hardening or softening process, stress levels adjust to a complete reversal position provided sufficient plastic strain is available in the cycle.

In very low cycle, constant strain-range fatigue, below 100 cycles or so, the hardening or softening process is clouded by the failure process; that is, failure generally occurs before saturation.

A definite mean-strain effect exists below $N_f \approx 100$ cycles; and, above $N_f \approx 10^4$ cycles, both a mean-strain and mean-stress effect exists. Between these fatigue ranges the mean value effect is virtually non-existent.

Specimen buckling during the fatigue test can be cycle dependent. That is, once a critical ratio, σ_c/E_{tan} , (as measured from an unstable hysteresis loop) is reached, buckling appears to occur.

Fatigue cracks were not visually detectable during constant strain-range testing until very near the last two or three percent of the fatigue life was reached. Generally, the presence of a crack was first noted by the abrupt change in the induced stress (load) level shown on the recording.

9.3 DATA CORRELATIONS AND FUNDAMENTAL RELATIONSHIPS

The cyclic-state relationship can be determined without carrying specimens to failure in fatigue.

The cyclic-state relationship can be determined from the outer trace of a particular hysteresis loop.

The cyclic-state relationship can be determined by constant load- or constant strain-range testing; however, data from the former tests may be difficult to reduce due to cyclic creep effects.

The relationships between $\Delta\epsilon_p$ versus N_f and $\Delta\epsilon_e$ versus N_f are power-law relationships extending from $1 \leq N_f \leq \infty$ only if the strain is completely reversed.

The cyclic stress-strain envelope curve and the cyclic stress-strain curve differ by a scale factor of 2.

From the tests on the four materials described herein, the average value for the slope of the elastic- and plastic-component lines versus fatigue life are -0.11 and -0.59. These agree almost exactly with Manson's proposed values of -0.12 and -0.6, respectively.

When fracture ductility, D_f , is plotted at $N_f = 1/4$ cycle, the power-law correlation between fatigue data and the tensile test, as hypothesized by Coffin, are confirmed provided the fatigue data reduction employs longitudinal strains defined as conventional engineering strains ($\epsilon = \Delta l/l_0$).

When fracture ductility, D_f , is plotted at $N_f = 1$ cycle, the power-law correlation between fatigue data and the tensile test is dependent on fatigue data reduction which employs longitudinal strains derived, through the assumption of plastic incompressibility, from measurements of diametral strain.

The power-law relationship which expresses the plastic component of the fatigue equation can be correlated with the tensile test when the conventional engineering strain ($\epsilon = \Delta l/l_0$) at tensile failure is plotted at $N_f = 1$ cycle and conventional engineering strains are employed in the fatigue data reduction.

The cyclic state at the microstructural level can be reflected onto the macroscopic level by means of constant strain-range tests performed within an "analog region" of fatigue-life. The stable hysteresis loops developed within the "analog region" also become "analogs" in that their outer traces described the cyclic stress-strain curve.

The existence of a stabilized locus curve (cyclic stress-strain curve) as proposed by Younger, (Reference 1), has been verified by data obtained within the "analog region" of fatigue.

The limiting-strain hypothesis presented by Younger, (Reference 1), and the cyclic stress-strain curve have been employed to accurately predict the effect of mean stresses in long-life fatigue.

Fatigue failure below 10^4 cycles resulting from cumulative effects at several strain-range levels appears governed by ductility variations induced by the shifts in applied strains as well as the changes in the rate of crack growth.

The Palmgren-Miner rule is unsatisfactory for predicting the number of cycles to failure for annealed or hard OFHC copper during dual-level tests leading to failure below 10^4 cycles.

REFERENCES

1. D. G. Younger, "A Fatigue Failure Hypothesis Based Upon Stabilized Unidirectional Slip," *Proceedings ASTM*, Vol. 58, pp 576-595, 1958.
2. J. Dubuc, "Plastic Fatigue Under Cyclic Stress and Cyclic Strain With a Study of the Bauschinger Effect," *Doctorate Thesis*, Department of Strength of Materials, Ecole Polytechnique, Universite de Montreal, Vol. I, pp 37-40, January 1961.
3. R. V. Baud, "Fillet Profiles for Constant Stress," *Product Engineering*, p 133, April 1934.
4. P. W. Bridgman, Studies in Large Plastic Flow and Fracture, McGraw-Hill Book Company, New York, 1952.
5. P. W. Bridgman, "The Stress Distribution at the Neck of a Tension Specimen," *Transactions, ASM*, Vol. 32, p 553, 1944.
6. N. H. Polakowski and A. Palchoudhuri, "Softening of Certain Cold-Worked Metals Under the Action of Fatigue Loads," *Proceedings ASTM*, Vol. 54, 701-716, 1954.
7. L. C. Lidstrom and B. J. Lazan, "Effect of Fatigue Stress History on Elasticity Properties and Stress Distribution Under Rotating Bending," *WADC-TR 56-122*, August 1956.
8. L. F. Coffin, Jr. and J. F. Tavernelli, "The Strain Cycling and Fatigue of Metals," *Transactions AIME*, Vol. 215, pp 794, 1959.
9. R. W. Smith, M. H. Hirschberg, and S. S. Manson, "Fatigue Behavior of Metals Under Strain Cycling in Low and Intermediate Life Range," *NASA TN D-1574*, April 1963.
10. D. G. Younger, "Some Unidirectional Cyclic Stress-Strain Studies of 17S-T Aluminum Alloy," *MS Thesis*, Department of Engineering Mechanics, University of Texas, June 1950.
11. F. R. Tuler, "Cyclic Stress-Strain Behavior of OFHC Copper," *MS Thesis*, Department of Theoretical and Applied Mechanics, University of Illinois, 1962. See also TAM Report No. 239, March 1963.
12. S. S. Manson, "Behavior of Materials Under Conditions of Thermal Stress," *Heat Transfer Symposia*, University of Michigan Engineering Research Institute, pp 9-75. Also published as *NACA TN 2933*, 1954.
13. L. F. Coffin, Jr., "A Study of Cyclic-Thermal Stresses in a Ductile Metal," *Transactions, ASME*, Vol. 76, pp 931-950, 1954.

REFERENCES (Continued)

14. J. F. Tavernelli and L. F. Coffin, Jr., "Experimental Support for Generalized Equation Predicting Low Cycle Fatigue," Transactions, ASME, Journal of Basic Engineering, Vol. 84, No. 4, pp 533-537, December 1962.
15. F. R. Shanley, "Discussion of Methods of Fatigue Analysis," Proceedings, Symposium on Fatigue of Aircraft Structures, WADC TR 59-507, pp 182-206, August 1959.
16. R. C. Boettner, C. Laird, and A. J. McEvily, Jr., "Crack Nucleation and Growth in High Strain-Low Cycle Fatigue," Ford Motor Company, Scientific Laboratory, TN SL 64-50, July 1964.
17. S. S. Manson, "Discussion of Paper (Reference 14, above) on Experimental Support for Generalized Equation Predicting Low Cycle Fatigue," Transactions, ASME, Journal of Basic Engineering, Vol. 84, No. 4, pp 537-541, December 1962.
18. S. S. Manson, "Fatigue: A Complex Subject - Some Simple Approximations," The William H. Murray Lecture, presented at 1964 SESA Annual Meeting, Cleveland, Ohio, October 28-30, also published in Experimental Mechanics, pp 193-226, July 1965.
19. S. S. Manson, "Thermal Stresses in Design, Part 19 - Cyclic Life of Ductile Materials," Machine Design, July 7, 1960.
20. S. I. Liu, and G. Sachs, "The Flow and Fracture Characteristics of the Aluminum Alloy 24ST After Alternating Tension and Compression," Transactions, AIMME, Metals Division, p 193, 1949.
21. P. P. Benham, "Axial-Load and Strain-Cycling Fatigue of Copper at Low Endurance," Journal Institute of Metals, Vol. 89, pp 328-338, 1961.
22. R. D. D'Amato, and R. De Boer, "A Study of the Relationships Between Notched and Unnotched Specimens of 2024 Aluminum Alloy in the Low-Cycle Fatigue Regime," WADC TN 59-2, May 1959.
23. G. Sachs, W. W. Gerberich, V. Weiss, and J. V. LaTorre, "Low-Cycle Fatigue of Pressure-Vessel Materials," Proceedings ASTM, Vol. 60, pp 512-529, 1960.
24. T. J. Dolan, "Non-Linear Response Under Cyclic Loading Conditions," presented at the Ninth Midwest Mechanics Conference, 16 August 1965.
25. K. V. Snowden and H. H. F. Wilsdorf, "A Study of the Behavior of Dislocations and Their Interaction With Other Lattice Defects Under Conditions of Alternating Stress," Aerospace Research Laboratories Report, ARL 63-114, July 1963.

REFERENCES (Continued)

26. O. H. Basquin, "The Exponential Law of Endurance Tests," Proceedings ASTM, Vol. 10, pp 625-630, 1910.
27. E. M. Eden, W. N. Rose, and D. L. Cunningham, "The Endurance of Metals," Proceedings IME (AIME), p 839, 1911.
28. H. F. Moore, and J. B. Kommers, The Fatigue of Metals, McGraw-Hill Book Company, Inc., New York, New York, 1927.
29. L. Bairstow, "The Elastic Limits of Iron and Steel Under Cyclical Variations of Stress," Philosophical Transactions, Royal Society, London, Vol. 210, 1910.
30. H. J. Grover, S. M. Bishop, and L. R. Jackson, "Axial-Load Fatigue Tests on Unnotched Sheet Specimens of 24S-T3 and 75S-T6 Aluminum Alloys and SAE 4130 Steel," NACA TN 2324, March 1951.
31. W. Illg, "Fatigue Tests on Notched and Unnotched Sheet Specimens of 2024-T3 and 7075-T6 Aluminum Alloys and of SAE 4130 Steel With Special Consideration of the Life Range from 2 to 10,000 Cycles," NACA TN 3866, December 1956.
32. G. R. Halford, "Plastic Strain Energy Analysis of Torsional Low Cycle Fatigue," MS Thesis, Department of Theoretical and Applied Mechanics, University of Illinois, 1961.
33. G. R. Halford and J. Morrow, "Low Cycle Fatigue in Torsion," Proceedings ASTM, Vol. 62, pp 695-707, 1962.
34. P. J. E. Forsythe, "Fatigue Damage and Crack Growth in Aluminum Alloys," Acta Metallurgica, Vol. 11, pp 703-715, July 1962.
35. C. Laird, and G. C. Smith, "Crack Propagation in High Stress Fatigue," Philosophical Magazine, Vol. 7, pp 847-857, 1962.
36. J. C. Grosskreutz, "A Theory of Stage II Fatigue Crack Propagation," AFML-TR-64-415, March 1965.
37. W. A. Wood, "Experimental Approach to Basic Study of Fatigue," Department of Civil Engineering and Engineering Mechanics, Columbia University, Technical Report No. 24, August 1965.
38. W. J. Trapp, "Elevated Temperature Fatigue Properties of SAE 4340 Steel," WADC TR 52-325, Part 1, December 1952.

REFERENCES (Continued)

39. W. Johnson and P. B. Mellor, Plasticity for Mechanical Engineers, D. Van Nostrand Company, Ltd., 1962.
40. A. M. Freudenthal and M. Ronay, "Second Order Effects in Dissipative Media," Proceedings of The Royal Society, Series A, No. 1428, Vol. 292, May 1966. (This reference is out of sequence in the text. See pages 21 and 38.)
41. M. A. Miner, "Cumulative Damage in Fatigue," Journal of Applied Mechanics, ASME, Vol. 12, No. 3, September 1945.
42. J. Schijve, "The Estimate of the Fatigue Performance of Aircraft Structures," National Aeronautical Research Institute, Amsterdam, Report No. MP-212 (Paper No. 52), June 1962.

APPENDIX A

RELATIONSHIP BETWEEN DIAMETRAL AND AXIAL STRAINS*

In performing uniaxial cyclic fatigue testing on specimens of circular cross-section, it is not uncommon to determine the axial strains and stresses from experimental axial load and diametral strain measurements. In this procedure, however, it is necessary to have a relation among axial strain, diametral strain, and axial load in order to calculate the axial strain from the diametral strain. The following is a derivation of such a relationship.

It is assumed that the material under consideration is isotropic and behaves in the manner of a theoretical elastic-plastic material. The basic equations defining the relations among strain increments and stress increments of an isotropic elastic-plastic material are found in many texts on plasticity. For example, Reference (39) is cited. Increments, or rates, of stress and strain are conveniently denoted by a dot over the respective quantity, although differentiation with respect to time need not be involved. Thus, in a cylindrical coordinate system, $\{X, R, \theta\}$, the infinitesimal increments of axial stress and strain, $d\sigma_x$ and $d\epsilon_x$, would be denoted as follows, for example.

$$d\sigma_x \equiv \dot{\sigma}_x \qquad d\epsilon_x \equiv \dot{\epsilon}_x \qquad (A-1)$$

The total increment of each strain component consists of an elastic part and a plastic part, which may be denoted by superscripts E and P, respectively. The elastic parts of strain increments are related to the stress increments by the usual stress-strain relations of three dimensional elasticity for an isotropic material, expressed in incremental form. Then, in the cylindrical coordinate system, the direct stress and strain rates (extension or compression) on the coordinate axes are related by

$$\dot{\epsilon}_x = \frac{1}{E} [\dot{\sigma}_x - \nu (\dot{\sigma}_R + \dot{\sigma}_\theta)] + \dot{\epsilon}_x^P \qquad (A-2)$$

$$\dot{\epsilon}_R = \frac{1}{E} [\dot{\sigma}_R - \nu (\dot{\sigma}_\theta + \dot{\sigma}_x)] + \dot{\epsilon}_R^P \qquad (A-3)$$

$$\dot{\epsilon}_\theta = \frac{1}{E} [\dot{\sigma}_\theta - \nu (\dot{\sigma}_x + \dot{\sigma}_R)] + \dot{\epsilon}_\theta^P \qquad (A-4)$$

where E is Young's elastic modulus and ν is Poisson's ratio. Similar relations exist among shear stresses and strains. It is seen that the

*Appendix A has been prepared by Dr. H. M. Berkowitz, Advanced Structures Development Department, Aeronutronic Division, Philco Corporation.

elastic portion of the strain increments are given by the terms involving the stress-rates $\dot{\sigma}_x$, $\dot{\sigma}_R$, and $\dot{\sigma}_\theta$ in Equations (A-2) through (A-4).

It is usual to assume that volumetric compressibility effects in elastic-plastic flow are purely elastic. Thereby, the volumetric plasticity is assumed to be incompressible. This incremental volumetric plasticity relation among the plastic strain increments is thus

$$dV^P = \dot{\epsilon}_x^P + \dot{\epsilon}_R^P + \dot{\epsilon}_\theta^P = 0 \quad (A-5)$$

The plastic strain increments are assumed to be related to the stresses by the Prandtl-Reuss flow rules, which assume that the plastic strain increments are always in the same relative proportions as the stress deviators. These stress deviators are the shear stresses and the differences between the direct stress components and the mean direct stress, q . q itself represents a state of hydrostatic stress and produces no plastic deformations. These relations, considering only the direct stresses and strains, are

$$\dot{\epsilon}_x^P : \dot{\epsilon}_R^P : \dot{\epsilon}_\theta^P = (\sigma_x - q) : (\sigma_R - q) : (\sigma_\theta - q) \quad (A-6)$$

where

$$q = \frac{1}{3}(\sigma_x + \sigma_R + \sigma_\theta) \quad (A-7)$$

Completing the formulation of the plastic relations by imposing yield surface conditions to relate the stresses and plastic strain increments during plastic flow is not required here. Such conditions characterize the material behavior, such as ideal elastic-plastic, work hardening, or work softening, and can relate quantities as a function of loading history. This is left open in the derivation. Thus, all that has been assumed is that:

- (a) Strains consist of elastic plus plastic portions;
- (b) Straining is plastically incompressible;
- (c) Plastic strain increments are in the same proportion as the stress deviators.

Let it now be assumed that the state of stress is ideally uniaxial. Thus, shear stresses vanish and coordinate directions become principal directions (in the $\{X, R, \theta\}$ system) when the uniaxial state is considered to be given by

$$\sigma_x = \sigma \quad \sigma_R = \sigma_\theta = 0 \quad (A-8)$$

Equation (A-7) then gives

$$q = \frac{1}{3} \sigma \quad (\text{A-9})$$

Equation (A-6) then yields the relations

$$\dot{\epsilon}_R^P = \dot{\epsilon}_\theta^P \quad (\text{A-10})$$

$$\dot{\epsilon}_x^P = -2\dot{\epsilon}_\theta^P \equiv -2\dot{\epsilon}_R^P \quad (\text{A-11})$$

It is seen that Equations (A-10) and (A-11) satisfy Equation (A-5) identically. Equations (A-8), (A-10), and (A-11) reduce Equations (A-2) through (A-4) to

$$\dot{\epsilon}_x = (\dot{\sigma}/E) - 2\dot{\epsilon}_\theta^P \quad (\text{A-12})$$

$$\dot{\epsilon}_\theta = -(\nu\dot{\sigma}/E) + \dot{\epsilon}_\theta^P \quad (\text{A-13})$$

$$\dot{\epsilon}_R = \dot{\epsilon}_\theta \quad (\text{A-14})$$

Eliminating $\dot{\epsilon}_\theta^P$ between Equations (A-12) and (A-13) yields the sought after relation

$$\dot{\epsilon}_x = \frac{(1-2\nu)}{E} \dot{\sigma} - 2\dot{\epsilon}_\theta \quad (\text{A-15})$$

It is noted that Equation (A-14) shows the equivalence of radial strain increment ($\dot{\epsilon}_R$) and hoop strain increment ($\dot{\epsilon}_\theta$), so that either may be termed diametral strain. Equation (A-15) relates the whole axial strain increment, $\dot{\epsilon}_x$, to the axial stress increment, $\dot{\sigma}$, and the whole diametral strain increment, $\dot{\epsilon}_\theta$. Equation (A-15) may now be integrated by following the loading from an initial to a final state in order to relate the changes in strains, $\Delta\epsilon_x$ and $\Delta\epsilon_\theta$, to changes in stress, $\Delta\sigma$, during this finite loading process. The integration yields

$$\Delta\epsilon_x = \frac{(1-2\nu)}{E} \Delta\sigma - 2\Delta\epsilon_\theta \quad (\text{A-16})$$

Equation (A-16) thus applies for changes between any two states during an ideal uniaxial loading process, and relates the whole strains (total of elastic plus plastic strains) and stress without distinguishing elastic and plastic parts.

Now consider the case of cyclic loading between two diametral strain limits, or "peaks." Assume that at any instant during the cycling that the axial stress increment is opposite in sense (tension or compression) to the sense

of diametral strain increment (extension or contraction), and that limiting (peak) axial stresses occur at limiting diametral strains. From these assumptions, Equation (A-15) thus implies that axial stress and strain increments are in phase (same sense) and that "peak" axial strains occur simultaneously with "peak" axial stresses and "peak" diametral strains (if the assumptions apply from the onset of loading). If the absolute magnitude of any diametral strain range, axial strain range, and axial stress range are simultaneously $\Delta\epsilon^d$, $\Delta\epsilon^l$, and $\Delta\sigma^l$, respectively, then Equation (A-16) relates these as

$$\Delta\epsilon^l = \frac{(1-2\nu)}{E} \Delta\sigma^l + 2\Delta\epsilon^d \quad (\text{A-17})$$

Equation (A-17) has been derived under only the two assumptions concerning the cyclic loading process stated in the paragraph preceding Equation (A-17). Limit values (peaks) of a given strain, or the stress, can both have the same sense. It is essentially only assumed that axial stress and strain are in phase with each other and the negative of the diametral strain. It is easily seen that Equation (A-17) can be recast into an equation relating amplitudes of variation of the strains and stress about some mean values by defining the limit values of the strains and stress during a half cycle as follows:

$$\epsilon_\theta = \epsilon_m^d - \epsilon_a^d \quad (\text{A-18})$$

$$\epsilon_x = \epsilon_m^l + \epsilon_a^l \quad (\text{A-19})$$

$$\sigma = \sigma_m + \sigma_a \quad (\text{A-19})$$

Equations (A-18) through (A-20) thus relate the amplitudes of variation to the ranges as follows:

$$\Delta\epsilon^d = 2\epsilon_a^d \quad (\text{A-21})$$

$$\Delta\epsilon^l = 2\epsilon_a^l \quad (\text{A-22})$$

$$\Delta\sigma^l = 2\sigma_a \quad (\text{A-23})$$

The remaining quantities in Equations (A-18) through (A-20) are mean strains and stress during a half cycle. In terms of the amplitudes of the cyclic range, Equation (A-17) becomes

$$\epsilon_a^l = \frac{(1-2\nu)}{E} \sigma_a + 2\epsilon_a^d \quad (\text{A-24})$$

Equations (A-17) or (A-24) can be expressed in a variety of alternate forms. For example, using only Equation (A-22) in Equation (A-17) yields

$$\epsilon_a^{\ell} = \frac{(1-2\nu)}{2E} \Delta\sigma^{\ell} + \Delta\epsilon^d \quad (\text{A-25})$$

If it is now additionally assumed that the mean strains and stress in Equations (A-18) through (A-20) are all null, Equations (A-24) or (A-25) are seen to relate amplitudes of fully reversed stress and strain cycles.

It has not been previously stipulated whether the stress and strain quantities in the previous relations are "engineering" quantities or "true" quantities. The terms "engineering" or "true" will be defined in the following.

At first, consider that stresses in the above derivations are defined as engineering stresses. These are defined by the relation

$$\sigma = P/A_0 \quad (\text{A-26})$$

where A_0 is the initial cross-section area of the test specimen and P is an applied load. Then, during a peak-to-peak half cycle of loading, it follows that

$$\Delta\sigma^{\ell} = (\Delta P)/A_0 \quad (\text{A-27})$$

where ΔP is the absolute magnitude of the applied load range. Then, if engineering stress is assumed, with as yet unqualified strains, the cyclic relation Equation (A-25) becomes

$$\epsilon_a^{\ell} = \left(\frac{1}{2} - \nu\right) \frac{\Delta P}{EA_0} + \Delta\epsilon^d \quad (\text{A-28})$$

True stress is defined as

$$\sigma = P/A \quad (\text{A-29})$$

where A is the instantaneous cross-section area of the test specimen. In terms of true stress, it follows that

$$\Delta\sigma^{\ell} = \Delta(P/A) \quad (\text{A-30})$$

Assuming true stress but as yet still unqualified strains, Equation (A-25) becomes

$$\epsilon_a^{\ell} = \frac{\left(\frac{1}{2} - \nu\right)}{E} \Delta(P/A) + \Delta\epsilon^d \quad (\text{A-31})$$

Equation (A-31) reduces to Equation (A-28) under the assumption that A is approximately equivalent to A_0 , so that replacing A by A_0 in Equation (A-31) introduces negligible error. This implies small strains of the cross-section.

In establishing the theory of elastic-plastic materials, the theoretical plasticity conditions are usually established from consideration of empirical relations among "true" stresses and "true" strains. For axially symmetric conditions, the instantaneous true axial and true hoop strain increments are defined by

$$\dot{\epsilon}_x = \frac{d\ell}{\ell} \quad (\text{A-32})$$

$$\dot{\epsilon}_\theta = \frac{dR}{R} \quad (\text{A-33})$$

where ℓ and R are the instantaneous length and radial position of some material element initially of length ℓ_0 and at radius R_0 . Considering this element to be unstrained in its initial state, Equations (A-32) and (A-33) can be integrated to yield the true strains, ϵ_x and ϵ_θ .

$$\epsilon_x = \ln(\ell/\ell_0) \quad (\text{A-34})$$

$$\epsilon_\theta = \ln(R/R_0) \quad (\text{A-35})$$

The engineering strains, e_x and e_θ , are defined conventionally by the relations

$$e_x = (\ell - \ell_0)/\ell_0 \quad (\text{A-36})$$

$$e_\theta = (R - R_0)/R_0 \quad (\text{A-37})$$

Combining Equations (A-34) and (A-35) with (A-36) and (A-37) relates the true strains to engineering strains.

$$\epsilon_x = \ln(1 + e_x) \quad (\text{A-38})$$

$$\epsilon_\theta = \ln(1 + e_\theta) \quad (\text{A-39})$$

If the area of a circular region of deformed radius R is defined as A , and in the initial state, when $R = R_0$, is defined as A_0 , then

$$A = \pi R^2 \quad (\text{A-40})$$

$$A_0 = \pi R_0^2 \quad (\text{A-41})$$

Equation (A-35) then becomes

$$\epsilon_{\theta} = \frac{1}{2} \ln(A/A_0) \quad (A-42)$$

In a state of ideal uniaxial loading, σ , from an unstressed and unstrained state, Equation (A-16) then relates the various strain measures at any instant as

$$\epsilon_x = \frac{(1-2\nu)}{E} \sigma - 2\epsilon_{\theta} \quad (A-43)$$

Consider the stress σ as the true stress, defined by Equation (A-29). This is common practice for theoretical plasticity. Designate engineering stress by S . Equation (A-24) can now be recast in a variety of forms by using previous relations.

$$\epsilon_x = (1-2\nu) \frac{P}{AE} + \ln(A_0/A) \quad (A-44)$$

$$\ln(1+e_x) = (1-2\nu) \frac{P}{AE} + \ln(A_0/A) \quad (A-45)$$

$$\ln(1+e_x) = (1-2\nu) \frac{S}{E} \left(\frac{A_0}{A}\right) + \ln(A_0/A) \quad (A-46)$$

A common measure for engineering strain is the approximation

$$e_x = \frac{A_0}{A} - 1 \quad (A-47)$$

It is seen that Equation (A-47) is exact only if the material is elastically incompressible ($\nu = 1/2$). Equation (A-47) is otherwise valid as an approximation only if

$$\left| (1-2\nu) \frac{P}{AE} \right| \ll \left| \ln(A_0/A) \right| \quad (A-48)$$

where $| |$ designates absolute magnitude. It is thus seen that if $\nu \neq 1/2$, Equation (A-47) will not necessarily be valid for very small engineering strains.

For small engineering strains, $|e_x| \ll 1$ and $|e_{\theta}| \ll 1$, Equation (A-37) indicates that $|R-R_0| \ll R_0$ and therefore $|A_0/A| \doteq 1$. Also, Equations (A-38) and (A-39) give as approximations

$$\epsilon_x \doteq e_x \quad |e_x| \ll 1 \quad (A-49)$$

$$\epsilon_{\theta} \doteq e_{\theta} \quad |e_{\theta}| \ll 1 \quad (A-50)$$

Equation (A-43) then may be approximated as a relation among engineering stress and strains

$$e_x = \frac{(1-2\nu)}{E} S - 2e_\theta \quad |e_x| \ll 1, |e_\theta| \ll 1 \quad (A-51)$$

It follows that for approximately zero mean engineering stress and engineering strain cycling, Equation (A-24) is valid in terms of engineering stress and strain amplitudes, with only a few percent relative error in prediction of e_a^L , if e_a^d is 0.15 or less. That is

$$\left. \begin{aligned} e_a^L &\doteq \left(\frac{1}{2} - \nu\right) \frac{\Delta P}{A_0 E} + \Delta e^d \\ \Delta e^d &= 2e_a^d \end{aligned} \right\} e_a^d \leq 0.15 \quad (A-52)$$

All the foregoing relations have been achieved under the assumption of ideal uniaxial tension. If the state of stress is a superposition of uniaxial tension plus hydrostatic tension at a given point, as is the case resulting from Bridgman's analysis (Reference 4) of stress in a tensile specimen, then an elastic-plastic analysis proceeds as above, starting from the assumptions

$$\sigma_x = F + P \quad \sigma_R = \sigma_\theta = P \quad (A-53)$$

Equations (A-10) and (A-11) again follow, leading to an equation similar to Equation (A-15)

$$\dot{e}_x = \frac{(1-2\nu)}{E} (\dot{F} + 3\dot{P}) - 2\dot{e}_\theta \quad (A-54)$$

All other relations derived above then also follow, but with σ replaced by $(F + 3P)$.

APPENDIX B

PROCEDURE FOR USING THE CYCLIC STRESS-STRAIN CURVE TO ESTABLISH THE EFFECT OF STRESS RATIO IN LONG-LIFE FATIGUE

The procedure for using the cyclic stress-strain curve to establish the effect of stress ratio, R , on S-N data beyond 10^4 cycles is outlined in the following paragraphs. For this purpose the development of the 2024-T3 aluminum alloy fatigue curves shown in Figure 50 (for which $R > -1$) will be employed as an example.

As indicated in Section 7.2, the data that are essential to the evaluation of the stress-ratio effect are (1) the cyclic stress-strain curve determined from low-life fatigue tests and (2) an S-N curve for one convenient value of R which traverses the long-life fatigue region. These requirements are fulfilled by the normalized cyclic stress-strain curve for 2024-T351 presented in Figure 55 and the S-N curve for $R = -1$ given in Figure 50. The object, of course, is to employ this information to obtain the five other S-N curves shown in the latter figure.

The following tabulated values for stresses and related range of damage indices have been determined from the S-N curve ($R = -1$) and the cyclic stress-strain curve by choosing convenient intervals for N_f .

$\frac{N_f}{8}$	σ_{\max}	σ_{\min}	$\Delta\sigma$	$\Delta[\gamma(\sigma)]$
10^8	20.5 KSI	-20.5 KSI	41.0 KSI	2(0.89)
10^7	21.0	-21.0	42.0	2(0.91)
10^6	23.0	-23.0	46.0	2(1.00)
10^5	34.5	-34.5	69.0	2(1.50)
10^4	51.0	-51.0	102.0	2(2.53)

As stated by the corollary to the "limiting strain" hypothesis (Section 6.1), the above values of $\Delta[\gamma(\sigma)]$ can be used with the cyclic stress-strain curve to establish all other ranges of stress giving the same related fatigue life. The value of $\Delta[\gamma(\sigma)]$ when $R = -1$ determines ϵ_{Tot} , thus, for each selected fatigue life, N_f , the corresponding value of limiting strain, ϵ_{Tot} , is established.

The next step is to consider each fatigue life, N_f , separately so as to determine analytically or graphically, several ranges of stress from the cyclic curve which display the same value of the limiting strain. As an example, for the 2024-T3 aluminum alloy, the following tabulation of stresses can be established at $N_f = 10^8$ for which $\epsilon_{\text{Tot}} = 2(0.89) = 1.78$.

$$N_f = 10^8, \epsilon_{Tot} = 1.78$$

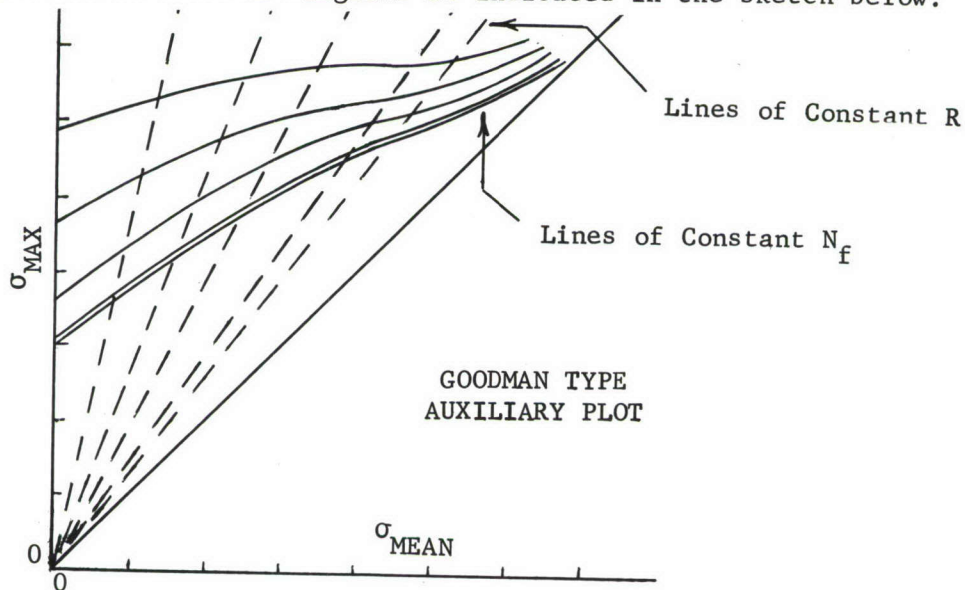
σ_{max}	$\gamma(\sigma_{max})$	$\gamma(\sigma_{min})^*$	σ_{min}	σ_{mean}^{**}
20.5 KSI	0.89	-0.89	-20.5 KSI	0.0 KSI
30.0	1.30	-0.48	-11.0	9.5
35.0	1.51	-0.27	- 6.2	14.4
40.0	1.78	0.00	0.0	20.0
45.0	2.10	+0.32	+ 7.3	26.2
50.0	2.45	+0.67	+15.5	32.8
55.0	3.00	+1.22	+28.5	41.8
60.0	3.90	+2.12	+46.0	53.0
65.0	5.00	+3.22	+56.5	60.8
70.0	6.70	+4.92	+65.0	67.5

$$* \gamma(\sigma_{min}) = \gamma(\sigma_{max}) - \epsilon_{Tot}$$

$$**\sigma_{mean} = \frac{1}{2} (\sigma_{max} + \sigma_{min})$$

The values of σ_{max} and σ_{mean} in the above table will produce a fatigue life of $N_f = 10^8$. Next, this process should be repeated for the other selected values of N_f , namely, 10^7 , 10^6 , 10^5 , and 10^4 , to find the corresponding sets of σ_{max} and σ_{mean} values.

After the above stress values have been determined for each fatigue life, a plot can be made of σ_{max} versus σ_{mean} for constant values of N_f to give the familiar set of Goodman Diagrams as indicated in the sketch below.



The above plots are employed for the purpose of obtaining the combinations of σ_{\max} and σ_{mean} for each value of R specified in Figure 50, namely, $R = -0.6, -0.3, 0.02, 0.4,$ and 0.5 . Lines of constant R represented by dashed lines have been superimposed on the sketch to show the manner of properly selecting σ_{\max} for each N_f and specified R . The values of σ_{\max} versus N_f for these constant values of R are then plotted as in Figure 50 to show the effect of stress ratio in long-life fatigue.

UNCLASSIFIED

Security Classification

DOCUMENT CONTROL DATA - R&D

(Security classification of title, body of abstract and indexing annotation must be entered when the overall report is classified)

1. ORIGINATING ACTIVITY (Corporate author) Aeronutronic Division, Philco Corporation Ford Road, Newport Beach, California 92663		2a. REPORT SECURITY CLASSIFICATION Unclassified	
		2b. GROUP None	
3. REPORT TITLE THE CYCLIC STATE OF MATERIALS AND THE RELATIONSHIP TO MECHANICAL PROPERTIES AND FATIGUE			
4. DESCRIPTIVE NOTES (Type of report and inclusive dates) Final Report covering period April 1965 through August 1966			
5. AUTHOR(S) (Last name, first name, initial) YOUNGER, DEWEY G., JR.			
6. REPORT DATE November 1966		7a. TOTAL NO. OF PAGES 140	7b. NO. OF REFS 42
8a. CONTRACT OR GRANT NO. AF 33(615)-2539		9a. ORIGINATOR'S REPORT NUMBER(S) Aeronutronic Publication No. U-3670	
b. PROJECT NO. 1467			
c. Task No. 146704		9b. OTHER REPORT NO(S) (Any other numbers that may be assigned this report)	
d. BPSN 5(6146704-62405334)		AFFDL-TR-66-125	
10. AVAILABILITY/LIMITATION NOTICES This document is subject to special export controls and each transmittal to foreign governments or foreign nationals may be made only with prior approval of AFFDL(FDTR), Wright-Patterson Air Force Base, Ohio 45433.			
11. SUPPLEMENTARY NOTES		12. SPONSORING MILITARY ACTIVITY Structures Division, Flight Dynamics Laboratory, RTD, WPAFB, Dayton, Ohio	
13. ABSTRACT This report contains the results of an experimental and theoretical study relating to the stabilized cyclic state of materials. The objectives accomplished in the program were (a) the experimental verification of the important role played by the cyclic state in fatigue. (b) The correlation of virgin material properties with the cyclic stress-strain curve for four materials (2024-0 and 2024-T351 aluminum alloy plus annealed and hard OFHC copper), and (c) the application of the cyclic stress-strain curve to fatigue analysis. Both constant load-range and constant strain-range fatigue tests up to fatigue-lives of 10^4 cycles were performed under axial loading conditions at speeds of 3 to 15 cycles/minute. Specimens were of circular cross-section with a one-inch gage length and longitudinal strain measurements were made with a dual-range mechanical extensometer. Power-law relationships were developed from the elastic and plastic components of stabilized strains, and these were related to true fracture stress and failure strain. Both <u>cyclic stress-strain envelope curves</u> and <u>cyclic stress-strain curves</u> were developed and employed in fatigue analyses to predict the effect of mean stresses on the fatigue life. A brief series of dual-level cumulative fatigue tests were performed in the low-life fatigue region and the validity of the Palmgren-Miner rule was questioned.			

DD FORM 1 JAN 64 1473

UNCLASSIFIED

Security Classification

14.	KEY WORDS	LINK A		LINK B		LINK C	
		ROLE	WT	ROLE	WT	ROLE	WT
	FATIGUE OF METALS						
	CYCLIC STATE						
	MATERIALS BEHAVIOR						
	FAILURE MECHANISM						
	FATIGUE TESTING						
	STRESS						
	STRAIN						
	THEORETICAL MECHANICS						
	CRACK PROPAGATION						
	CUMULATIVE FATIGUE						

INSTRUCTIONS

1. **ORIGINATING ACTIVITY:** Enter the name and address of the contractor, subcontractor, grantee, Department of Defense activity or other organization (*corporate author*) issuing the report.

2a. **REPORT SECURITY CLASSIFICATION:** Enter the overall security classification of the report. Indicate whether "Restricted Data" is included. Marking is to be in accordance with appropriate security regulations.

2b. **GROUP:** Automatic downgrading is specified in DoD Directive 5200.10 and Armed Forces Industrial Manual. Enter the group number. Also, when applicable, show that optional markings have been used for Group 3 and Group 4 as authorized.

3. **REPORT TITLE:** Enter the complete report title in all capital letters. Titles in all cases should be unclassified. If a meaningful title cannot be selected without classification, show title classification in all capitals in parenthesis immediately following the title.

4. **DESCRIPTIVE NOTES:** If appropriate, enter the type of report, e.g., interim, progress, summary, annual, or final. Give the inclusive dates when a specific reporting period is covered.

5. **AUTHOR(S):** Enter the name(s) of author(s) as shown on or in the report. Enter last name, first name, middle initial. If military, show rank and branch of service. The name of the principal author is an absolute minimum requirement.

6. **REPORT DATE:** Enter the date of the report as day, month, year; or month, year. If more than one date appears on the report, use date of publication.

7a. **TOTAL NUMBER OF PAGES:** The total page count should follow normal pagination procedures, i.e., enter the number of pages containing information.

7b. **NUMBER OF REFERENCES:** Enter the total number of references cited in the report.

8a. **CONTRACT OR GRANT NUMBER:** If appropriate, enter the applicable number of the contract or grant under which the report was written.

8b, 8c, & 8d. **PROJECT NUMBER:** Enter the appropriate military department identification, such as project number, subproject number, system numbers, task number, etc.

9a. **ORIGINATOR'S REPORT NUMBER(S):** Enter the official report number by which the document will be identified and controlled by the originating activity. This number must be unique to this report.

9b. **OTHER REPORT NUMBER(S):** If the report has been assigned any other report numbers (*either by the originator or by the sponsor*), also enter this number(s).

10. **AVAILABILITY/LIMITATION NOTICES:** Enter any limitations on further dissemination of the report, other than those

imposed by security classification, using standard statements such as:

- (1) "Qualified requesters may obtain copies of this report from DDC."
- (2) "Foreign announcement and dissemination of this report by DDC is not authorized."
- (3) "U. S. Government agencies may obtain copies of this report directly from DDC. Other qualified DDC users shall request through _____."
- (4) "U. S. military agencies may obtain copies of this report directly from DDC. Other qualified users shall request through _____."
- (5) "All distribution of this report is controlled. Qualified DDC users shall request through _____."

If the report has been furnished to the Office of Technical Services, Department of Commerce, for sale to the public, indicate this fact and enter the price, if known.

11. **SUPPLEMENTARY NOTES:** Use for additional explanatory notes.

12. **SPONSORING MILITARY ACTIVITY:** Enter the name of the departmental project office or laboratory sponsoring (*paying for*) the research and development. Include address.

13. **ABSTRACT:** Enter an abstract giving a brief and factual summary of the document indicative of the report, even though it may also appear elsewhere in the body of the technical report. If additional space is required, a continuation sheet shall be attached.

It is highly desirable that the abstract of classified reports be unclassified. Each paragraph of the abstract shall end with an indication of the military security classification of the information in the paragraph, represented as (TS), (S), (C), or (U).

There is no limitation on the length of the abstract. However, the suggested length is from 150 to 225 words.

14. **KEY WORDS:** Key words are technically meaningful terms or short phrases that characterize a report and may be used as index entries for cataloging the report. Key words must be selected so that no security classification is required. Identifiers, such as equipment model designation, trade name, military project code name, geographic location, may be used as key words but will be followed by an indication of technical context. The assignment of links, rules, and weights is optional.